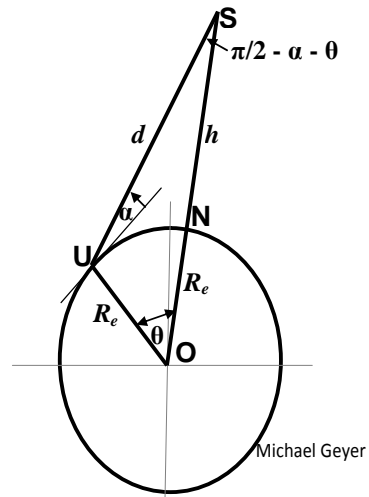


# GEOMETRIC ANALYSIS OF AN OBSERVER ON A SPHERICAL EARTH AND AN AIRCRAFT OR SATELLITE

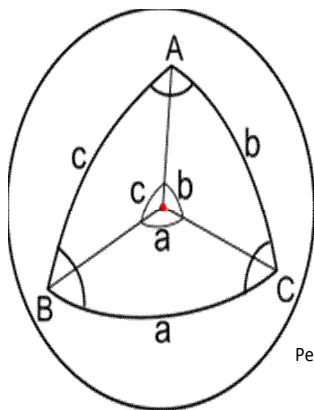
Michael Geyer



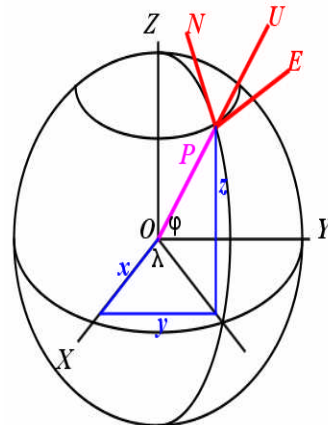
Federico Rostagno



Michael Geyer



Peter Mercator



nosco.com

## Project Memorandum — September 2013

DOT-VNTSC-FAA-13-08

Prepared for:

**Federal Aviation Administration  
Wake Turbulence Research Program**



U.S. Department of Transportation  
Research and Innovative Technology Administration  
John A. Volpe National Transportation Systems Center

**Volpe**

## TABLE OF CONTENTS

<b>1. INTRODUCTION.....</b>	<b>1</b>
1.1 Basic Problem and Solution Approach.....	1
1.2 Vertical Plane Formulation .....	2
1.3 Spherical Surface Formulation .....	3
1.4 Limitations and Applicability of Analysis.....	4
1.5 Recommended Approach to Finding a Solution.....	5
1.6 Outline of this Document .....	6
<b>2. MATHEMATICS AND PHYSICS BASICS .....</b>	<b>8</b>
2.1 Exact and Approximate Solutions to Common Equations .....	8
2.1.1 The Law of Sines for Plane Triangles.....	8
2.1.2 The Law of Cosines for Plane Triangles.....	8
2.1.3 Solution of a Quadratic Equation .....	9
2.1.4 Computing Inverse Trigonometric Functions .....	9
2.1.5 Expansions of arcsin, arccos and arctan for Small Angles .....	11
2.1.6 Surface Area on a Sphere .....	11
2.2 Shape of the Earth .....	11
2.2.1 WGS-84 Ellipsoid Parameters.....	11
2.2.2 Radii of Curvature Defined in Literature .....	12
2.2.3 Vincenty’s Algorithm for the Direct and Indirect Problems of Geodesy.....	14
2.3 Altitude-Related Matters .....	14
2.3.1 Accounting for User Altitude.....	15
2.3.2 Conditions for Unblocked US LOS.....	15
2.3.3 Different Notions of Altitude .....	16
<b>3. SOLUTION TO VERTICAL PLANE FORMULATION.....</b>	<b>18</b>
3.1 Mathematical Problem and Solution Taxonomy.....	18
3.1.1 Mathematical Formulation .....	18
3.1.2 Taxonomy of Solution Approaches.....	18
3.1.3 Detailed Geometry.....	19
3.2 Computing Geocentric Angle .....	20
3.2.1 Altitude and Elevation Angle Known – Basic Method.....	20
3.2.2 Altitude and Elevation Angle Known – Alternative Method.....	21
3.2.3 Altitude and Slant Range Known .....	21
3.2.4 Elevation Angle and Slant Range Known .....	22
3.3 Computing Elevation Angle.....	22
3.3.1 Altitude and Geocentric Angle Known .....	22
3.3.2 Altitude and Slant Range Known .....	23
3.3.3 Geocentric Angle and Slant Range Known.....	23
3.4 Computing Slant Range .....	23
3.4.1 Altitude and Geocentric Angle Known .....	23
3.4.2 Altitude and Elevation Angle Known .....	24
3.4.3 Geocentric Angle and Elevation Angle Known .....	24

<b>3.5</b>	<b>Computing Altitude .....</b>	<b>24</b>
3.5.1	Slant Range and Geocentric Angle Known.....	24
3.5.2	Slant Range and Elevation Angle Known.....	25
3.5.3	Elevation Angle and Geocentric Angle Known.....	25
<b>3.6</b>	<b>Example Applications.....</b>	<b>25</b>
3.6.1	Example 1: En Route Radar Coverage.....	26
3.6.2	Example 2: Aircraft Instrument Approach Procedure.....	29
3.6.3	Example 3: Satellite Visibility of/from Earth .....	31
<b>4.</b>	<b>SOLUTION TO SPHERICAL SURFACE FORMULATION.....</b>	<b>33</b>
<b>4.1</b>	<b>Basics of Spherical Trigonometry .....</b>	<b>33</b>
4.1.1	Historical Perspective.....	33
4.1.2	Application to Navigation .....	33
4.1.3	Resources Available on the Web.....	34
4.1.4	Key Formulas .....	35
4.1.5	Taxonomy of Problems Involving Spherical Triangles.....	37
4.1.6	Taxonomy of Spherical Surface Formulation Problems .....	38
<b>4.2</b>	<b>Solving the Indirect Problem of Geodesy .....</b>	<b>39</b>
4.2.1	Computing the Geocentric Angle.....	39
4.2.2	Computing the Azimuth Angles of the Connecting Arc .....	40
<b>4.3</b>	<b>Solving the Direct Problem of Geodesy .....</b>	<b>41</b>
4.3.1	Computing the Satellite Latitude.....	41
4.3.2	Computing the Satellite Longitude.....	42
4.3.3	Computing the Azimuth of the Connecting Arc at the Satellite.....	42
<b>4.4</b>	<b>Solving a Modified Version of the Direct Problem: Satellite Longitude Known .....</b>	<b>43</b>
4.4.1	Computing the Satellite Latitude.....	43
4.4.2	Computing the Geocentric Angle.....	43
4.4.3	Computing the Azimuth of the Connecting Arc at the Satellite.....	44
<b>4.5</b>	<b>Solving a Modified Version of the Direct Problem: Satellite Latitude Known .....</b>	<b>44</b>
4.5.1	Computing the Azimuth of the Connecting Arc at the Satellite.....	44
4.5.2	Computing the Satellite Longitude.....	45
4.5.3	Computing the Geocentric Angle.....	45
<b>4.6</b>	<b>Latitude Extremes of a Great Circle.....</b>	<b>46</b>
<b>4.7</b>	<b>Example Applications.....</b>	<b>47</b>
4.7.1	Example 1, Continued: En Route Radar Coverage .....	47
4.7.2	Example 2, Continued: Aircraft Instrument Approach Procedure .....	49
4.7.3	Example 3, Continued: Satellite Visibility of/from Earth.....	50
4.7.4	Example 4: Great Circle Flight Route .....	51
4.7.5	Example 5: Radar Display Coordinate Transformations .....	53
<b>5.</b>	<b>VECTOR APPROACH TO A UNIFIED 3D SOLUTION .....</b>	<b>56</b>
<b>5.1</b>	<b>Vector and Coordinate Frame Definitions.....</b>	<b>56</b>
5.1.1	Earth-Centered Earth-Fixed (ECEF) Coordinate Frame .....	56
5.1.2	Local-Level Coordinate Frame at User's Position .....	57
5.1.3	User and Satellite Positions in User's Local-Level Frame .....	58
<b>5.2</b>	<b>Solving the Indirect Problem of Geodesy .....</b>	<b>59</b>
5.2.1	Geocentric Angle from Latitudes and Longitudes, by Vector Dot Product.....	59
5.2.2	Geocentric Angle from Latitudes and Longitudes, by Vector Cross Product.....	60
5.2.3	Path Azimuth Angles, from Latitudes and Longitudes .....	60

<b>5.3</b>	<b>Corollaries of the Indirect Problem Solution.....</b>	<b>61</b>
5.3.1	Latitude Extremes of a Great Circle.....	61
5.3.2	Locus of Points on a Great Circle .....	62
<b>5.4</b>	<b>Computing Satellite Elevation Angle and Slant Range.....</b>	<b>62</b>
5.4.1	Solution for Elevation Angle from Altitude and Geocentric Angle.....	63
5.4.2	Solution for Slant Range from Altitude and Geocentric Angle .....	63
<b>5.5</b>	<b>Solving the Direct Problem of Geodesy .....</b>	<b>63</b>
<b>6.</b>	<b>SPHERICAL EARTH APPROXIMATION ACCURACY .....</b>	<b>65</b>
6.1	Evaluation Methodology and Scenarios .....	65
6.2	Spherical Earth Model Azimuth Error .....	66
6.3	Methodology for Determining Spherical Earth Model Distance Error .....	66
6.4	Distance Errors for Three Methods of Computing the Effective RoC.....	68
6.5	Improving the Effective RoC by a 3-Point Parabolic Fit.....	70
6.6	Experiments in Further Improving Path Length Accuracy .....	73
<b>7.</b>	<b>REFERENCES.....</b>	<b>76</b>

## LIST OF FIGURES

<b>Figure 1</b>	Vertical Plane Containing Points <b>U</b> , <b>O</b> , <b>N</b> and <b>S</b> .....	2
<b>Figure 2</b>	Spherical Surface Containing <b>U</b> and <b>S</b> .....	3
<b>Figure 3</b>	Increase in Solution Complexity with Number of Problem Variables .....	5
<b>Figure 4</b>	Principal Values of arcsin and arccos Functions .....	9
<b>Figure 5</b>	Ellipsoidal Earth’s Radii of Curvature, Normalized to Semi-Major Axis .....	13
<b>Figure 6</b>	Problem Geometry for LOS <b>US</b> Tangent to the Earth’s Surface .....	16
<b>Figure 7</b>	Illustrating Different Notions of Altitude .....	17
<b>Figure 8</b>	Detailed Geometry for Vertical Plane Formulation.....	19
<b>Figure 9</b>	Aircraft Minimum Visible HAT vs. Range for Three Radar HAT Values .....	28
<b>Figure 10</b>	Approach Plate: LPV Procedure to MCI Runway 19L.....	30
<b>Figure 11</b>	Fraction of Earth Visible vs. Satellite Altitude.....	32
<b>Figure 12</b>	Example Spherical Triangle .....	33
<b>Figure 13</b>	Spherical Triangle for Navigation .....	33
<b>Figure 14</b>	Illustrating the Taxonomy of Spherical Triangle Problems.....	37
<b>Figure 15</b>	Sine, cosine and versine related to the unit circle.....	39
<b>Figure 16</b>	Aircraft Altitude Visibility Contours for the North Truro, MA, Radar System .....	49
<b>Figure 17</b>	WAAS Satellite Visibility Contours for 5 deg Mask Angle.....	51
<b>Figure 18</b>	Latitude/Longitude Coordinates of Paths Connecting BOS and NRT for Spherical- Earth Approximation and Vincenty’s Ellipsoidal-Earth Algorithm .....	53
<b>Figure 19</b>	Effect of Displaying a Target’s Slant Range .....	54
<b>Figure 20</b>	Separation (Slant Range Correction) Error for Tangent Plane Radar Display .....	55
<b>Figure 21</b>	Vector Technique Coordinate Frames of Interest.....	57
<b>Figure 22</b>	Histogram of Differences in Airport-Airport Azimuth Angles between Spherical and Ellipsoidal Earth Models .....	67
<b>Figure 23</b>	Path Length Errors for Spherical-Earth Model vs. Actual Path Lengths, for Three- Point NN Determination of Effective RoC.....	69
<b>Figure 24</b>	Airport-Airport Great-Circle Paths Having the Largest Errors in Calculated Lengths, for a Spherical-Earth Model and Three-Point NN Determination of the Effective RoC.....	70
<b>Figure 25</b>	Airport-Airport Calculated Path Length Error for Spherical-Earth Model vs. Latitude Change over the Path, for Three-Point PF Determination of the Effective RoC....	72
<b>Figure 26</b>	Great-Circle Path Having the Largest Error in Calculated Length, for a Spherical-Earth Model and Three-Point PF Determination of the Effective RoC.....	73
<b>Figure 27</b>	Airport-Airport Calculated Path Length Errors for Spherical-Earth Model vs. Latitude Change over the Path, for Three Methods of Determining the Effective RoC .....	74

## LIST OF TABLES

<b>Table 1</b>	Geocentric Angle $\theta$ and Its Cosine and Tangent Functions, near $\theta = 0$ .....	10
<b>Table 2</b>	Specified and Computed Fix Altitudes for MCI Runway 19L LPV Approach .....	29
<b>Table 3</b>	Taxonomy of Spherical Surface Mathematical Problems .....	38
<b>Table 4</b>	Computed Fix Coordinates for MCI Runway 19L LPV Approach .....	50
<b>Table 5</b>	CONUS Airports Used in Analysis.....	65
<b>Table 6</b>	International Airports Used in Analysis.....	65
<b>Table 7</b>	Absolute Value of Difference in Calculated Airport-Airport Path Azimuth Angles for Spherical and Ellipsoidal Earth Models .....	66
<b>Table 8</b>	Absolute Value of Relative Difference in Calculated Distances (Percent) for Spherical- Earth Model and Three Methods of Determining the Effective RoC .....	68
<b>Table 9</b>	Ten Airport Pairs Having the Largest Error in Calculated Path Length, for a Spherical- Earth Model and Three-Point NN Determination of the Effective RoC.....	70
<b>Table 10</b>	Percentage Error in Calculated Airport-Airport Path Lengths, for Spherical-Earth Model and Two Methods of Weighting Three Computed RoCs .....	71
<b>Table 11</b>	Ten Airport Pairs Having the Largest Error in Calculated Path Length, for a Spherical-Earth Model and Three-Point PF Determination of the Effective RoC .....	72
<b>Table 12</b>	Error Statistics for Five Airport Pairs Having Predominately North-South Paths for Spherical-Earth Model and Three Methods of Determining the Effective RoC .....	74
<b>Table 13</b>	Error Statistics for Five Airport Pairs Having Predominately East-West Paths for Spherical-Earth Model and Three Methods of Determining the Effective RoC .....	75

## 1. INTRODUCTION

### 1.1 *Basic Problem and Solution Approach*

This memorandum contains a large amount of technical detail. However, in significant contrast, it addresses an easily-understood and fundamental need in surveillance and navigation systems analysis — quantifying the geometry of two locations relative to each other and to a spherical earth. Here, geometry simply means distances and angles. Sometimes, distances are the lengths of straight lines; in other cases they are the lengths of arcs on the earth's surface. Similarly, angles may be measured between lines on a plane or between lines on a spherical surface.

Because the earth has an established latitude/longitude coordinate system, the approach that first comes to mind is to address this situation as a three-dimensional problem and use vector analysis. However, the approach preferred here is that, to simplify and clarify the analysis process, the three-dimensional problem should be re-cast as two separate two-dimensional problems:

- **Vertical Plane Formulation** (Section 1.2 and Chapter 3)<sup>\*</sup> — This analysis considers the vertical plane containing the two locations of interest and the center of the earth. The two locations are unconstrained vertically, although one altitude must be known. Plane trigonometry is the natural analysis tool for this problem. Latitudes and longitudes are not involved, which is its biggest limitation.
- **Spherical Surface Formulation** (Section 1.3 and Chapter 4) — This analysis — which is sometimes called great-circle navigation — only considers two locations on the surface of a spherical earth. Spherical trigonometry is a natural analysis tool in this setting, and latitudes and longitudes are inherent in this method. A significant limitation of this analysis is that altitudes cannot be accounted for.

These separate two-dimensional analyses can generally be performed in the above sequence, with the result that the limitations of each are overcome. The two-2D formulation is preferable to a one-3D formulation because it provides better insight into the solution — which reduces computational errors and improves the analyst's ability to understand and explain results. Also, since scalar quantities are involved, calculations can be done with a spread sheet; specialized vector-matrix software is not needed.

For historical and practical reasons<sup>†</sup>, in this document the two locations of interest are labeled **U** (for user) and **S** (for satellite). However, these are only labels, and have no relevance to application of the analysis; other labels, such as “1” and “2” would be equally valid. Generally, for surveillance applications, one location will be associated with a sensor and the other will be associated with a target — e.g., a ground-based radar and aircraft target. For navigation

---

<sup>\*</sup> Terminology: 1. Chapter; 1.1 Section; 1.1.1 Subsection.

<sup>†</sup> Historical: these notes were begun many years ago, for a project involving satellites. Practical: The Microsoft Word equation editor does not have a global change capability.

applications, the two locations are usually associated with the beginning and ending points of a flight segment (e.g., an instrument approach to a runway) or an entire flight (e.g., Boston to Tokyo).

While not preferred, Chapter 5 is devoted to the vector approach to a unified solution. Most problems can be solved by either the two-2D or one-3D approach. However, some useful equations can only be derived by one approach. More importantly, when addressing a new situation to which the solution is not apparent, it is wise to have as many techniques available as possible. Also, there are multiple software packages available for navigation analyses that use the vector approach.

### 1.2 Vertical Plane Formulation

Figure 1 depicts a typical vertical-plane analysis scenario involving: an earth-based “user” **U**; a satellite **S** above a spherical earth; the satellite nadir point, **N**; and the center of the earth, **O**. All four locations (modeled as points) are in the plane of the paper. Points **O**, **N** and **S** form a straight line. These points have no special relationship with the earth's spin axis. Since a “snapshot” analysis is involved, no assumptions are made regarding the satellite’s trajectory.

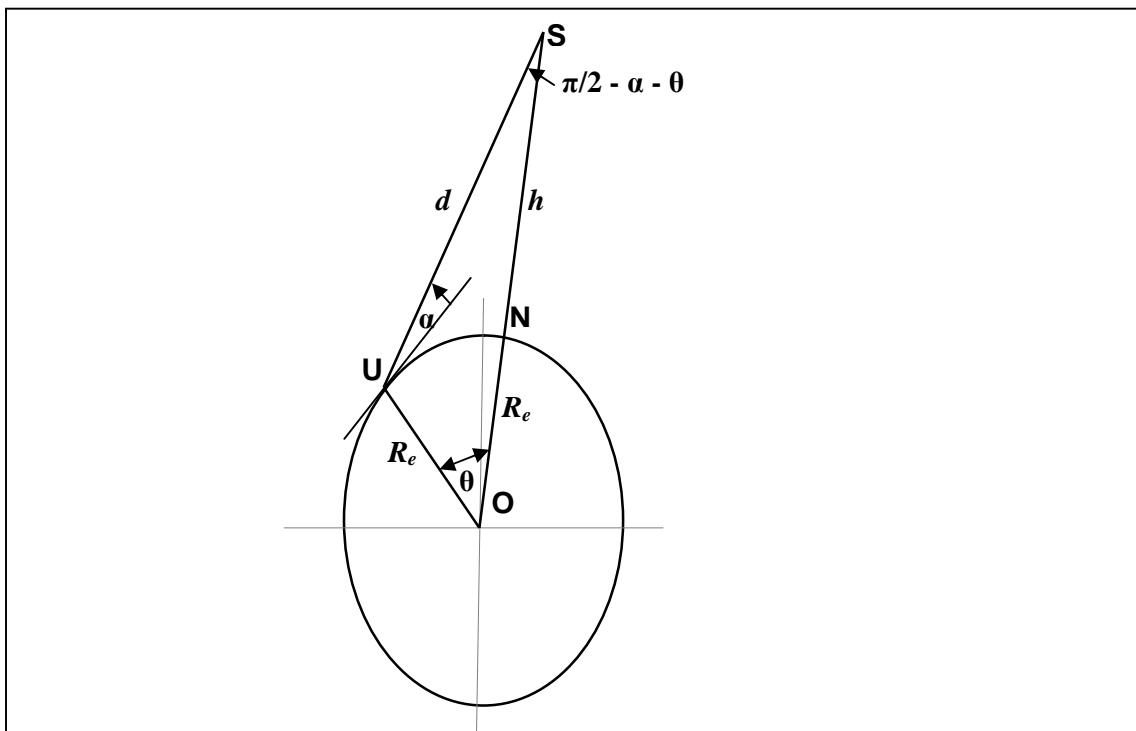


**Figure 1** Vertical Plane Containing Points **U**, **O**, **N** and **S**

In Figure 1, three linear distances are of interest:

- $R_e$  Earth radius (length of **OU** and **ON**)
- $h$  Satellite altitude above the earth (length of **NS**)
- $d$  User-satellite slant range (length of **US**).

And two angles are of interest:

- $\alpha$  Satellite elevation angle relative to the user's horizon (may be positive or negative)
- $\theta$  Geocentric angle between the user and satellite nadir (is always positive).

The earth radius  $R_e$  is always assumed to be known.

There are four variables associated with this formulation:  $h$ ,  $d$ ,  $\alpha$  and  $\theta$ . Any two must be known, and the remaining two can be found (six possible groupings). Subsection 2.3.1 shows how to relax the restriction of **U** being on the earth's surface, to its having a known altitude. Chapter 3 details the full set of 12 possible equations for this formulation.

Of these four variables, the geocentric angle  $\theta$  (which is equivalent to distance along the earth's surface) is also a variable in the spherical surface formulation. It serves as the mechanism for relating the two formulations — i.e., for transferring a solution to the vertical plane formulation into the spherical surface formulation. The other three variables ( $h$ ,  $d$  and  $\alpha$ ) are related to the altitude of **S** above the earth's surface and have no role in the spherical surface formulation.

### 1.3 Spherical Surface Formulation

The left-hand side of Figure 2 depicts the earth's familiar latitude/longitude grid. Although the earth is three-dimensional, restricting attention to the surface results in a two-dimensional analysis formulation. The right-hand side shows **U** and **S** on the earth's surface and the seven variables involved in a two-location problem on a sphere:

- the latitude/longitude, respectively, of **U** ( $L_U, \lambda_U$ ) and of **S** ( $L_S, \lambda_S$ )
- the geocentric angle  $\theta$  between **U** and **S**; and
- the azimuth angles  $\psi_{S/U}$  and  $\psi_{U/S}$  of the great circle arc connecting **U** and **S**.

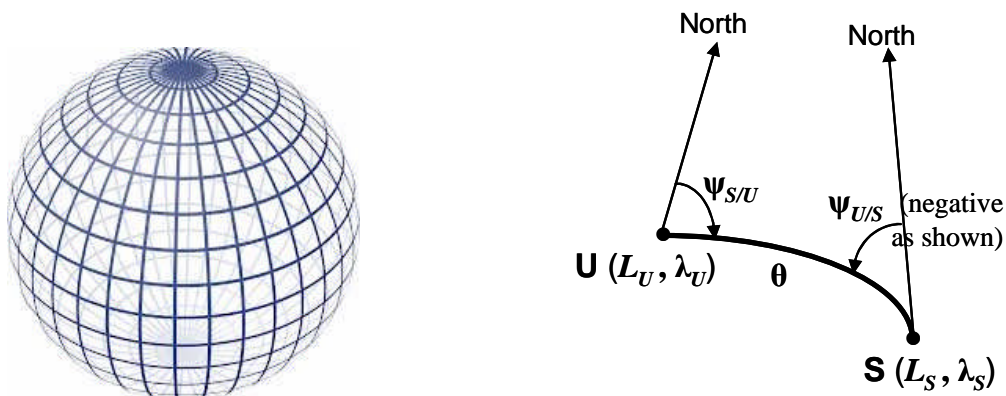


**Figure 2** Spherical Surface Containing **U** and **S**

Generally, four of these seven variables must be known, from which the other three can be computed. There are 35 possible groupings of known/unknown variables, which can be reduced to 16 unique and fully solvable mathematical problems (Subsection 4.1.6). These result in 48 equations for unknown variables. However, in contrast with the approach taken vertical plane formulation (i.e., exhaust all possible groupings), a more selective approach is adopted for the spherical-earth formulation. Attention is limited to the groupings of highest interest, and a solution roadmap is provided for the remaining cases.

In geodesy<sup>\*</sup>, analyses involving two groupings of known/unknown variables occur so frequently that the groupings have been named:

- **Direct** (or *first*) problem<sup>†</sup> of geodesy: (a) Given the coordinates  $(L_U, \lambda_U)$  of **U** on the earth's surface, the geocentric angle  $\theta$  between **U** and **S**, and azimuth angle  $\psi_{S/U}$  of a geodesic path starting at **U** and ending at **S** on the surface; (b) Find the coordinates  $(L_S, \lambda_S)$  of the end point **S**, and the path azimuth angle at the end point  $\psi_{U/S}$ .
- **Indirect** (or *second*, or *inverse*) problem of geodesy: (a) Given the coordinates,  $(L_U, \lambda_U)$  and  $(L_S, \lambda_S)$ , of points **U** and **S** on the earth's surface, (b) Find the geocentric angle  $\theta$  connecting **U** and **S**, and the azimuth angles (relative to north),  $\psi_{U/S}$  and  $\psi_{S/U}$ , of the path at each end.

Solution equations are only provided for the direct and indirect problems of geodesy, and small variations thereon, in Chapters 4 and 5.

#### 1.4 Limitations and Applicability of Analysis

Regardless of whether the scalar “two-2D” or vector “one-3D” mathematical approach is employed, the methodology addressed by this memorandum has inherent limitations in its applicability due to these simplifying assumptions:

- **Static Scenarios** — Scenarios analyzed are “snapshots” — i.e., motion of an aircraft or satellite is not explicitly involved. A sequence of locations may be considered, but the notions of velocity or time as mechanisms for relating those points are not utilized.
- **Spherical Earth** — Modeling the earth as a sphere (rather than as an ellipsoid) is much easier to deal with analytically and is adequate for many applications. (Chapter 6 quantifies this approximation and provides a method to improve it.)
- **Great Circle Flight Paths** — All trajectories of aircraft and satellites are great circles. That is, they lie in a vertical plane that contains the center of the earth.
- **Terrain/Obstacles Ignored** — Except for the earth, obstacles that could block the signal path between the user **U** and satellite **S** locations are not addressed.

---

<sup>\*</sup> Geodesy is the study of the earth (e.g., its shape, gravity field, and magnetic field); geometric geodesy includes study of distances and angles between points on its surface.

<sup>†</sup> Note the academic/mathematical use of the word “problem” in the narrow sense of a specific grouping of known and unknown variables. This memorandum also uses “problem” in the broader sense of a situation to be analyzed.

Engineering analyses have been characterized thusly: “There are exact solutions to approximate problems, and approximate solutions to exact problems. But there are no exact solutions to exact problems”.<sup>\*</sup> The techniques described herein fall into the first category — exact solutions to approximate problems.

The simplifications employed herein are often made in authoritative documents that address similar navigation and surveillance areas — e.g., Ref. 1 and 2. These techniques are well suited to analysis of vehicle routes (navigation) and navigation and surveillance sensor coverage.

### 1.5 Recommended Approach to Finding a Solution

The problem of analyzing the geometry of two points and a sphere is conceptually simple. And the mathematics involved in its solution are simple as well (as will be seen, they primarily involve trigonometry). Nevertheless, finding a solution can be complex, because of the number of variables/equations involved. This is an aspect of “the curse of dimensionality”. As the number of variables in a situation grows, the number of possible groupings of known/unknown variables and the associated number of solution equations explodes.

Figure 3 illustrates the “curse of dimensionality, in a worst-case sense, for the problem addressed herein. The combination of the vertical plane and spherical surface formulations involves a total of 10 variables. If treated as a single set, such a formulation could result in over 200 groupings and 1,200 equations. By taking account of the symmetry of the spherical surface formulation, the number of equations can be reduced but will still exceed 500. This is simply too many possibilities to address in a memorandum, or likely consider in an organized manner.

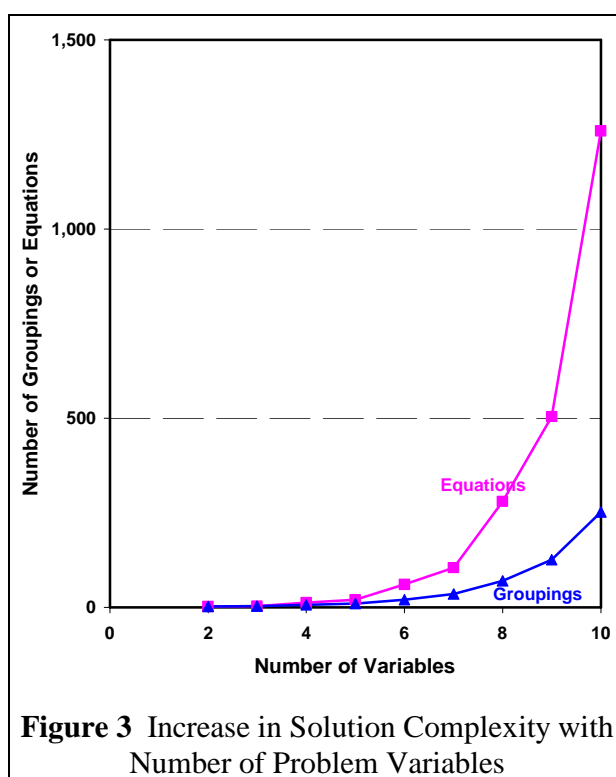


**Figure 3** Increase in Solution Complexity with Number of Problem Variables

The recommended approach in a problem involving two points and the earth (often, one point is fixed and the other is varied over a route or area) is to

<sup>\*</sup> Conveyed by Prof. Donald Catlin (Univ. of Mass. Amherst, Mathematics Dept.), who attributed it to Prof. Lotfi Zadeh (Univ. of Calif. Berkley, Electrical Engineering Dept.).

- Partition the overall problem into two separate problems that can be addressed, in sequence, by the vertical plane and spherical surface formulations
- Identify the known/unknown variables for the vertical plane problem
- Using the Table of Contents, find the solution equations for the unknown variables in Chapter 3 (i.e., treat Chapter 3 as a reference or “cookbook”).
- Evaluate the equations and transfer the value for the geocentric angle  $\theta$  to the next step
- Identify the known/unknown variables for the spherical surface formulation
- Using Subsection 4.1.6, find the appropriate problem case
- For the most common four cases, evaluate the pertinent solution equations that are provided in Chapter 4
- For less common cases, derive the solution equations using the roadmap in Subsections 4.1.4 to 4.1.6, then evaluate them.

## **1.6 Outline of this Document**

Chapter 1 (this one) describes the basic problem addressed by this memorandum and outlines the method of its solution. Chapter 2 is mathematical in nature, and is included to make this document more self-contained. It has sections on: the solution of direct and inverse trigonometric equations (including their approximations); the WGS-84 ellipsoid model for the earth; removing the restriction of  $\mathbf{U}$  to the earth’s surface; and the concepts of altitude that are used in aviation.

Chapters 3 and 4, in combination, detail the recommended solution to the basic task addressed by this memorandum. Chapter 3 addresses the vertical plane problem described in Section 1.2. The 12 possible equations that may be needed to solve this formulation are derived. An effective way to utilize this material is as “cookbook” where equations can be found when needed. The last section presents three example problems that can be solved by the methods described therein. Chapter 4 addresses solution of the spherical surface formulation described in Section 1.3. The first section is a brief introduction to spherical trigonometry, which is generally not well known. It includes a taxonomy of spherical triangle problems and a roadmap to their solution. The next sections provide solutions to the indirect and direct problems of geodesy, and two alternatives to the direct problem. The last section revisits the three example applications at the end of Chapter 3, and provides more complete solutions. It also includes two additional example applications.

Chapter 5 addresses the solution to the basic task addressed by this memorandum using three-dimensional vector analysis. It is shown that almost all of the equations derived by plane trigonometry and spherical trigonometry in combination can also be derived by vector analysis. Chapter 6 addresses the accuracy of the spherical earth approximation relative to the WGS-84 ellipsoid. It quantifies the accuracy and demonstrates that it can be improved in most situations.

While the focus of this memorandum is describing an approach to solving mathematical problems, it is instructive to see how this approach can be applied to problems that might occur in practice. The examples presented at the ends of Chapters 3 and 4 address:

- Air Traffic Control (ATC) radar coverage (North Truro, MA, ARSR-4/ATCBI-6 is the specific case)
- Aircraft precision approach procedure design (RNAV (GPS) to KMCI runway 19L is the specific case)
- Satellite visibility of/from the Earth (WAAS is the specific case)
- Aircraft trajectory between two points on the earth (Boston – Tokyo is the specific case)
- ATC radar display coordinate transformations (terminal and en route are the specific cases).

## 2. MATHEMATICS AND PHYSICS BASICS

### 2.1 Exact and Approximate Solutions to Common Equations

#### 2.1.1 The Law of Sines for Plane Triangles

For future reference, the law of sines applied to the plane triangle **UOS** in Figure 1 yields

$$\frac{\sin(\theta)}{d} = \frac{\sin\left(\frac{\pi}{2} + \alpha\right)}{R_e + h} = \frac{\sin\left(\frac{\pi}{2} - \alpha - \theta\right)}{R_e} \quad \text{Eq 1}$$

which reduces to

$$\frac{\sin(\theta)}{d} = \frac{\cos(\alpha)}{R_e + h} = \frac{\cos(\alpha + \theta)}{R_e} \quad \text{Eq 2}$$

In Eq 2, the left-center equality,

$$(R_e + h)\sin(\theta) = d \cos(\alpha) \quad \text{Eq 3}$$

relates all five quantities of interest in a simple way.

The left-right equality in Eq 2 is equivalent to

$R_e \sin(\theta) = d \cos(\alpha + \theta)$	Eq 4
----------------------------------------------	------

This expression relates: one side variable, **d**; and the two angle variables **α** and **θ**.

Similarly, the center-right equality in Eq 1 is equivalent to

$R_e \cos(\alpha) = (R_e + h) \cos(\alpha + \theta)$	Eq 5
------------------------------------------------------	------

This expression relates: one side variable, **h**; and the two angle variables **α** and **θ**.

#### 2.1.2 The Law of Cosines for Plane Triangles

For future reference, the law of cosines is applied to the plane triangle **UOS** in Figure 1. When the angle at **O** is used, the result is

$d^2 = R_e^2 + (R_e + h)^2 - 2R_e(R_e + h)\cos(\theta)$	Eq 6
---------------------------------------------------------	------

When the law of cosines is applied using the angle at **U**, the result is

$(R_e + h)^2 = R_e^2 + d^2 - 2R_e d \cos\left(\frac{\pi}{2} + \alpha\right)$	Eq 7
------------------------------------------------------------------------------	------

Each of these equations relates the two side variables, **d** and **h**, and one angle variable. Eq 6 involves **θ** and Eq 7 involves **α**.

### 2.1.3 Solution of a Quadratic Equation

In some instances, a quadratic equation similar to the following must be solved

$$Ax^2 + Bx + C = 0 \quad \text{Eq 8}$$

The algebraic solution is

$$x = \frac{-B \pm \sqrt{B^2 - 4AC}}{2A} \quad \text{Eq 9}$$

We cannot have imaginary roots, so  $B^2 > 4AC$ . In many instances, (a) the positive root is sought (since lengths cannot be negative), and (b)  $B^2 > |4AC|$ . For these situations:

$$x = \frac{-B + \sqrt{B^2 - 4AC}}{2A}$$

$$x = \frac{B}{2A} \left( \frac{1}{2}D - \frac{1}{8}D^2 + \frac{1}{16}D^3 - \frac{5}{128}D^4 + \frac{7}{256}D^5 - \frac{21}{1024}D^6 \pm \text{etc.} \right) \quad \text{where } D = \frac{-4AC}{B^2} \quad \text{Eq 10}$$

$$x \rightarrow -\frac{C}{B} \quad \text{as } \frac{4AC}{B^2} \rightarrow 0$$

### 2.1.4 Computing Inverse Trigonometric Functions

Intrinsic to navigation analysis is the calculation of angles — e.g., satellite elevation angle,  $\alpha$ , and geocentric angle,  $\theta$  (Figure 1) using an inverse trigonometric function. In performing this calculation, two concerns should be borne in mind: (1) numerical ill-conditioning and (2) ambiguous solutions. These conditions generally do not arise simultaneously — numerical ill-conditioning occurs near sine or cosine function values of  $\pm 1$ , or angles of  $0, \pi/2, \pi$ , etc. Ambiguous solutions generally arise when the approximate value of the angle is not known. The equations provided in the following chapters attempt to address these concerns, but every situation may not be anticipated.

Concerning numerical ill-conditioning: Both the sine and cosine functions have angular arguments for which the function's (a) value is non-zero (specifically,  $\pm 1$ ), and (b) derivative is zero — see Figure 4. Thus, changes in the angular argument result in significantly smaller changes in the function value which may be subject to truncation or roundoff.

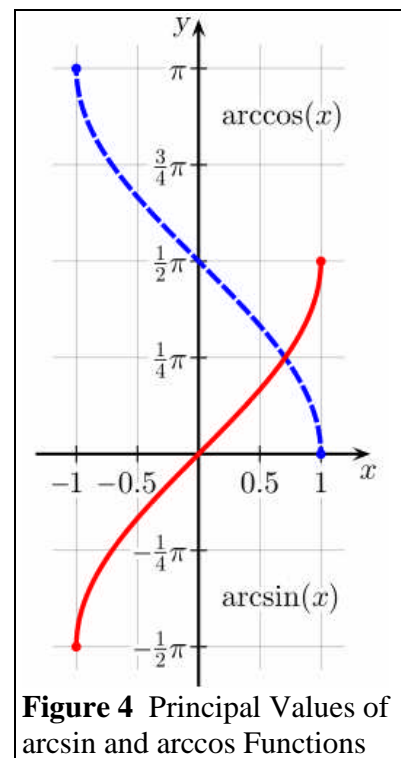


**Figure 4** Principal Values of arcsin and arccos Functions

Table 1 below illustrates this concern for the geocentric angle computed from the arc cosine function. For example, if five decimal digits are used for angles and trigonometric functions, the minimum detectable cosine function change corresponds to between 10 NM and 30 NM. A remedy is to employ the sine or tangent function rather than the cosine function. Unlike the cosine function, the sine and tangent functions (a) increase monotonically from a zero value for a zero angle, and (b) have a positive derivative value near zero angle. In Table 1, the last column indicates that for distances up to approximately 70 NM, the tangent function has a minimum of a two decimal place numerical advantage over the cosine function. The same behavior occurs for the sine function near  $\pi/2$ .

**Table 1** Geocentric Angle  $\theta$  and Its Cosine and Tangent Functions, near  $\theta = 0$

$\theta$ (rad)	$\theta$ (deg)	$R_e \cdot \theta$ (NM)	$\cos(\theta)$	$1 - \cos(\theta)$	$\tan(\theta)$	$\tan(\theta) /$ $1 - \cos(\theta)$
0.00000	0.000	0.000	1.00000	0.00000	0.00000	—
0.00001	0.001	0.034	1.00000	0.00000	0.00001	2.0E+05
0.00003	0.002	0.103	1.00000	0.00000	0.00003	6.7E+04
0.00010	0.006	0.344	1.00000	0.00000	0.00010	2.0E+04
0.00030	0.017	1.031	1.00000	0.00000	0.00030	6.7E+03
0.00100	0.057	3.438	1.00000	0.00000	0.00100	2.0E+03
0.00300	0.172	10.313	1.00000	0.00000	0.00300	6.7E+02
0.01000	0.573	34.378	0.99995	0.00005	0.01000	2.0E+02
0.03000	1.719	103.134	0.99955	0.00045	0.03001	6.7E+01
0.10000	5.730	343.780	0.99500	0.00500	0.10033	2.0E+01

A method for recasting an ill-conditioned equation for  $\cos(\theta)$ , which dates to the middle of the first millennium, is shown in Eq 11 immediately below. To be effective, the quantity under the radical must be further manipulated to eliminate the subtraction of nearly equal quantities.

$$\text{Given } \cos(\theta) = f(\alpha, d, h; R_e) \text{ where } f(\alpha, d, h; R_e) \approx 1$$

$$\text{And } \cos(\theta) \equiv 1 - 2 \sin^2\left(\frac{\theta}{2}\right)$$

$$\text{Thus } \sin\left(\frac{\theta}{2}\right) = \sqrt{\frac{1}{2} - \frac{1}{2} f(\alpha, d, h, R_e)}$$

Eq 11

Concerning ambiguous solutions: Trigonometric functions are periodic, so inverse trigonometric functions can result in multiple angles. To address this issue: (a) when making a computation, take account of the expected range of values for the angle involved — e.g.,  $\alpha$  generally varies between  $\pm\pi/2$ , so the arc sine or arc tangent functions are preferable to the arc cosine function; (b) utilize half-angle formulas when possible (as immediately above), since they double the range of angles that can be computed uniquely; and (c) when possible, use a four-quadrant (two argument) arc tangent function, which requires finding both the sine and cosine of the angle involved.

### 2.1.5 Expansions of arcsin, arccos and arctan for Small Angles

In the analysis that follows, a common situation is the need to compute the inverse of a trigonometric function for an argument such that the resulting angle will be close to 0 — e.g.,  $\theta = \arcsin(x)$ ,  $\theta = \arccos(1 - x)$  or  $\theta = \arctan(x)$ , where  $x$  is close to 0.

First, it is well known (Ref. 3) that

$$\arcsin(x) = x + \frac{1}{6}x^3 + \frac{3}{40}x^5 + \frac{5}{112}x^7 + \text{etc.} \quad \text{Eq 12}$$

A Taylor series expansion of  $\arccos(1 - x)$  is not available, due to its lacking a derivative at  $x = 0$ . However, more general power series (often called Frobenius) expansions are available; thus, utilizing Eq 11 and Eq 12:

$$\arccos(1 - x) = 2 \arcsin\left(\sqrt{\frac{x}{2}}\right) = \sqrt{2}x^{1/2} + \frac{\sqrt{2}}{12}x^{3/2} + \frac{3\sqrt{2}}{160}x^{5/2} + \frac{5\sqrt{2}}{896}x^{7/2} + \text{etc.} \quad \text{Eq 13}$$

Lastly, from Ref. 3:

$$\arctan(x) = x - \frac{1}{3}x^3 + \frac{1}{5}x^5 - \frac{1}{7}x^7 + \text{etc.} \quad \text{Eq 14}$$

### 2.1.6 Surface Area on a Sphere

The surface area of the sphere with radius  $R_e$  is  $4\pi(R_e)^2$ . The surface area enclosed by a circle on the surface of that sphere is

$$A = 2\pi(R_e)^2[1 - \cos(\theta)] \quad \text{Eq 15}$$

Here  $\theta$  is the half-angle of the cone, with apex at the center of the sphere, whose intersection with the surface forms the circle under discussion. Using Figure 1, the cone would be formed by rotating sector **ONU** about line **ON**.

## 2.2 Shape of the Earth

### 2.2.1 WGS-84 Ellipsoid Parameters

While the assumption of spherical earth having radius  $R_e$  is fundamental to this analysis, the accepted model for the shape of the earth is not a sphere, but an oblate spheroid (ellipse rotated about its minor axis). The World Geodetic Survey 1984 (WGS-84) fundamental model parameter are the ellipsoid's semi-major axis,  $a$ , and the flattening  $f$ . Their numerical values are

- $a \equiv 6,378,137$  m (WGS-84)
- $f \equiv 1 / 298.257,223,563$  (WGS-84)

In the U.S., the foot is the most common unit of distance. As a result of the International Yard and Pound Agreement of July 1959, the international foot is defined to be equal to exactly 0.3048 meter. Thus

- $a = 20,925,646.3$  ft (WGS-84)

Flattening of the ellipsoid is defined by

$$f = \frac{a-b}{a} \tag{Eq 16}$$

where  $b$  is the semi-minor axis. Numerically

- $b = (1-f)a = 6,356,752.3$  m = 20,855,486.6 ft (WGS-84)

In computations, the square of the eccentricity is frequently used in lieu of the flattening. Its definition and WGS-84 value are:

$$e^2 = \frac{a^2 - b^2}{a^2} = 2f - f^2 = f(2-f) \tag{Eq 17}$$

where

- $e^2 = 0.006,694,379,990,14$  (WGS-84)

In marine and aviation applications, the nautical mile (NM) is often used as the unit of distance. The international nautical mile was defined by the First International Extraordinary Hydrographic Conference, Monaco (1929) as exactly 1,852 meters. This definition was adopted by the United States in 1954. The international nautical mile definition, combined with the definition for the foot addressed above, result in there being 6,076.1155 feet in one nautical mile.

### 2.2.2 Radii of Curvature Defined in Literature

To approximate the ellipsoidal earth at a location on its surface by a sphere, two radii of curvature (RoCs) are commonly defined—the RoC in the meridian,  $R_{ns}$ , and the RoC in the prime vertical,  $R_{ew}$  (Ref. 4). These RoCs lie in orthogonal planes that include the normal (perpendicular line) to the surface of the ellipse. Their values are a function of the latitude  $L$  of the location involved

$R_{ns} = \frac{a(1-e^2)}{[1-e^2 \sin^2(L)]^{3/2}}$ $R_{ew} = \frac{a}{[1-e^2 \sin^2(L)]^{1/2}}$	Eq 18
--------------------------------------------------------------------------------------------------	-------

The earth's shape is — while not strictly a sphere — a sphere to 0.3%. The basis of this statement is that the earth's flattening is 0.00335281, or 0.34%. However, the RoCs defined by Eq 18 vary more widely. A plot of these quantities (Figure 5 below) shows that while  $R_{ew}$  in fact does change by about 0.34% between the Equator and a pole,  $R_{ns}$  changes by over 1%.

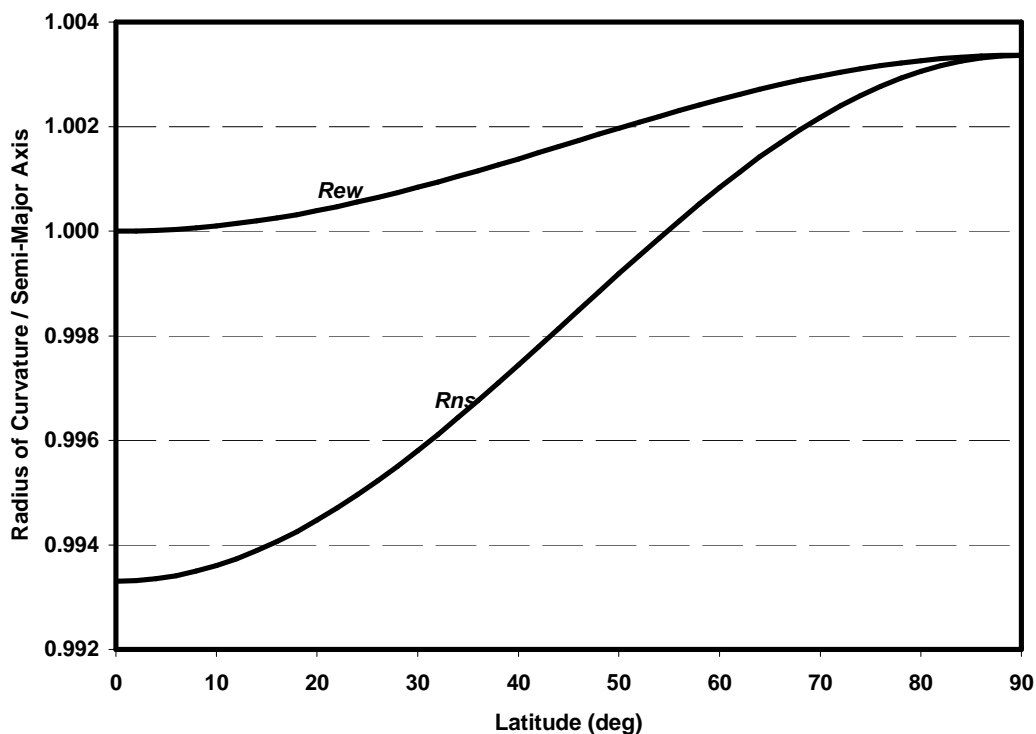


**Figure 5** Ellipsoidal Earth's Radii of Curvature, Normalized to Semi-Major Axis

The consequences of the behavior of  $R_{ew}$  and  $R_{ns}$  are that: (a) near the equator, at a given latitude, the effective RoC varies by almost 7% with the path's azimuth angle; (b) near the poles, at a given latitude, the effective RoC is almost insensitive to the path's azimuth angle; (c) for paths restricted to mid-latitudes, the effective RoC varies almost linearly with latitude and can be well characterized by the path end points; (d) for paths that cross the equator or pass over/near a pole, the effective RoC will have an interior minimum or maximum and its accurate characterization requires at least three points.

The RoC in an arbitrary plane that includes the normal to the ellipse and makes azimuth angle  $\psi$  with north is given by (Ref. 4)

$$R_{\psi} = \frac{1}{\frac{\cos^2(\psi)}{R_{ns}} + \frac{\sin^2(\psi)}{R_{ew}}} \quad \text{Eq 19}$$

When the latitudes/longitudes of **U** and **N** (or **S**) are known, the azimuth angle of the great circle connecting the points can be determined. Then Eq 18 and Eq 19 can be used to generate an estimate of  $R_e$  that is suited to a specific situation.

The average of  $R_\psi$  over  $0 \leq \psi \leq 2\pi$  (at a given latitude) is the Gaussian radius of curvature  $R_G$

$$R_G = \sqrt{R_{ns} R_{ew}} = \frac{a(1-f)}{1-e^2 \sin^2(L)} \quad \text{Eq 20}$$

In some applications, a global approximation to  $R_e$  (independent of latitude) may be sufficient — e.g., the arithmetic mean of the three semi-axes of the ellipsoid

$$R_{e,arith\ mean} = \frac{1}{3}(a + a + b) = \left(1 - \frac{1}{3}f\right)a \quad \text{Eq 21}$$

Thus

- $R_{e,arith\ mean} = 6,371,008.8 \text{ m} = 20,902,259.7 \text{ ft}$  (WGS-84)

When analyzing aircraft procedures for the FAA and other U.S. Government agencies with an aviation mission, the value of  $R_e$  to be used is defined in Ref. 1:

- $R_e = 20,890,537 \text{ ft}$  (U.S. TERPS)

### 2.2.3 Vincenty's Algorithm for the Direct and Indirect Problems of Geodesy

During the early 1970s, Thaddeus Vincenty\* revisited the issue of geodesics on an ellipsoid, and programmed a version of earlier mathematician's algorithms on a calculator. Given the available computing technology, his primary concern was minimizing the program's memory consumption. Accordingly, Vincenty developed an iterative algorithm, including versions for both the direct and indirect problems of geodesy (Ref. 5).

Due to its ease of coding, Vincenty's algorithm is now the most widely used method for computing geodesics on an ellipsoidal earth. The accuracy of Vincenty's algorithm is quoted as less than one millimeter, which has been independently validated by comparison with integration of the differential equations governing geodesic arcs on an ellipsoid (Ref. 6).

## 2.3 **Altitude-Related Matters**

The equations developed in Chapters 3 and 4 assume that (a) the user's location **U** is on the earth's surface, and (b) there is only one notion of "altitude" (vertical height above the earth's surface) involved. Subsections 2.3.1 and 2.3.2 show how to take account of a user altitude, and

---

\* Vincenty was working at the U.S. Defense Mapping Agency Aerospace Center, Geodetic Survey Squadron, Warren Air Force Base, in Wyoming.

Subsection 2.3.3 introduces different notions of vertical height above the earth's surface.

### 2.3.1 Accounting for User Altitude

In most situations of interest, there is no concern about the line-of-sight (LOS) between the User **U** (generally a sensor) and the Satellite (or aircraft) **S** being blocked by the earth's curvature. This is the case depicted in Figure 1. A method for determining the minimum elevation angle for which there is no LOS blockage is shown in Subsection 2.3.2.

Assuming that the user altitude  $h_U$  is known, when the LOS between **U** and **S** is unblocked, the equations presented in Chapters 3 and 4 can be used with these simple substitutions to take account of a non-zero user altitude:

- $R_e \rightarrow R_e + h_U$ , and
- $h \rightarrow h_S - h_U$  (where  $h_S$  is the satellite's altitude).

### 2.3.2 Conditions for Unblocked **US** LOS

The conditions for which the **US** LOS is unblocked can be determined using a diagram like Figure 6, which shows the LOS connecting the User **U** and Satellite **S** having a point of tangency **T** with the earth's surface. Generally, the primary variables involved in these analyses are the geocentric angle  $\theta$  and the user and satellite altitudes,  $h_U$  and  $h_S$ . Eq 22 applies to a situation when  $h_U$  and  $h_S$  are known and  $\theta$  is the unknown. (Observe that, if  $\theta$  is fixed, then  $h_U$  and  $h_S$  can be traded off — i.e., if one is increased, the other can be decreased.)

$\theta = \arccos\left(\frac{R_e}{R_e + h_U}\right) + \arccos\left(\frac{R_e}{R_e + h_S}\right)$	Eq 22
--------------------------------------------------------------------------------------------------	-------

To complete this analysis, when  $\theta$ ,  $h_U$  and  $h_S$  are known, the variables  $d$ ,  $\alpha_U$  and  $\alpha_S$ , can be found from

$d = R_e \tan(\theta_U) + R_e \tan(\theta_S)$ $\alpha_U = -\frac{\pi}{2} + \arcsin\left(\frac{R_e}{R_e + h_U}\right)$ $\alpha_S = -\frac{\pi}{2} + \arcsin\left(\frac{R_e}{R_e + h_S}\right)$	Eq 23
-----------------------------------------------------------------------------------------------------------------------------------------------------------------------------------------------	-------

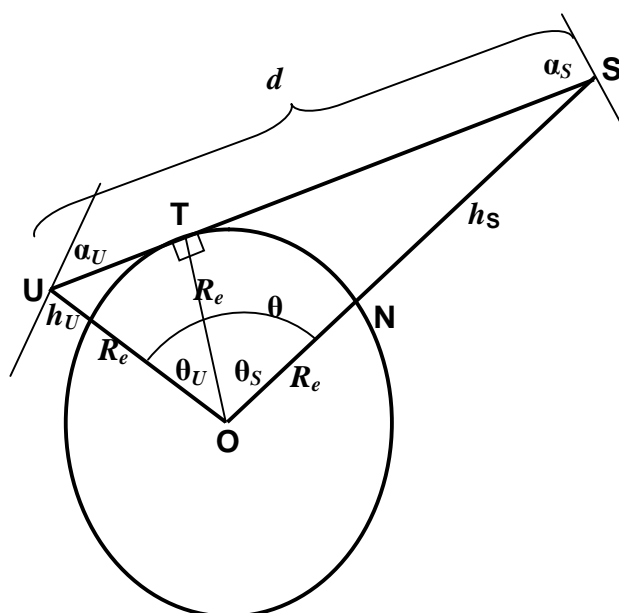


**Figure 6** Problem Geometry for LOS **US** Tangent to the Earth's Surface

While Eq 22 and Eq 23 reflect a common situation, the known and unknown quantities vary with application. An example is the siting an ATC radar, where  $h_S$  (minimum required coverage altitude) and  $\theta = \theta_U + \theta_S$  (distance between the location where the radar is to be installed and the outer boundary of the coverage region) are known. Then  $h_U$  is found using Eq 24, and  $d$ ,  $\alpha_U$  and  $\alpha_S$ , can be found from Eq 23.

$$\begin{aligned} \theta_S &= \arccos\left(\frac{R_e}{R_e + h_S}\right) \\ \theta_U &= \theta - \theta_S \\ h_U &= \left(\frac{1}{\cos(\theta_U)} - 1\right)R_e \end{aligned} \tag{Eq 24}$$

In addition to the above geometric considerations, the analyst should be aware that radar signal propagation paths, such as **US** in Figure 6, are subject to bending caused by changes in atmospheric density with altitude. A simple but commonly used method for modeling this phenomenon is discussed in Subsection 3.6.1.

### 2.3.3 Different Notions of Altitude

This memorandum is primarily mathematical, and — except for application examples — the equations in Chapters 3 and 4 involve only one notion of altitude: vertical geometric height above a spherical earth. However, when interpreting the results of calculations for applications,

the analyst must be aware that there are multiple notions (thus, meanings) of altitude. The differing notions are primary of concern in aviation, because aircraft (a) utilize barometric altimeters, but (b) must also maintain a vertical geometric distance above terrain. Figure 7 illustrates several notions of vertical distance above the earth, or “altitude”:

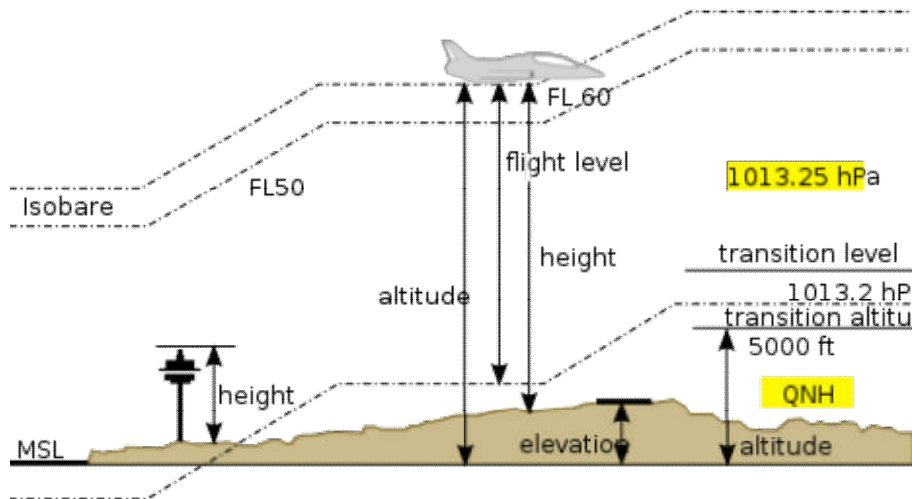


**Figure 7** Illustrating Different Notions of Altitude

- Height — or, better, Height Above Terrain (HAT) — is the vertical distance between an aircraft (or top of a structure on the ground) and the terrain beneath it
- Altitude — or, better, Altitude MSL (above Mean Sea Level) — is the vertical distance between an aircraft and mean sea level. Generally, aircraft use altitude MSL in terminal areas/at low altitudes. To do so, the aircraft’s altimeter is adjusted for the current local MSL pressure by applying the QNH\*, which is broadcast by a local airport.
- Flight Level — Vertical distance between an aircraft and the point below where the sea-level standard day pressure occurs (29.92 inches of mercury). In the U.S., flight levels are used above the transition altitude of 18,000 ft.†
- Elevation — Height of the terrain above MSL.

These definitions are reasonably standard, but are not universally used. Documents related to aircraft procedures are particularly carefully to adhere to these definitions.

\* QNH is not an acronym. It is one of a standardized collection of three-letter message encodings, all of which start with the letter "Q". They were initially developed for commercial radiotelegraph communication, and were later adopted by other radio services, especially amateur radio. Although created when radio used Morse code exclusively, Q-codes continued to be employed after the introduction of voice transmissions.

† The figure, from Wikipedia, was apparently drawn by a European, as it has (a) a lower transition altitude, and (b) the QNH quantified in hectopascals (hPa) rather than inches of mercury.

### 3. SOLUTION TO VERTICAL PLANE FORMULATION

#### 3.1 *Mathematical Problem and Solution Taxonomy*

##### 3.1.1 Mathematical Formulation

In mathematical terms, the basic objective of this chapter is to analyze the plane triangle **UOS** in Figure 1. As a plane triangle, it is fully described by its three sides and three interior angles (or quantities having a one-to-one relationship with these six quantities). However, since the interior angles of a plane triangle (quantified in radians) must sum to  $\pi$ , interest can be limited to two interior angles (or their one-to-one equivalents). Thus, any three of the five quantities  $R_e$ ,  $h$ ,  $d$ ,  $\alpha$ , and  $\theta$  can be selected independently (noting that at least one quantity will be a side), and the other two quantities will be uniquely determined. In this analysis,

- The angle having its vertex at the satellite **S** has a secondary role and is treated as a dependent variable.
- The earth's radius  $R_e$  is assumed to be a known parameter, rather than a variable.

Consequently, one purpose of this memorandum is to provide solutions for two of the four variables ( $h$ ,  $d$ ,  $\alpha$ ,  $\theta$ ) as a function of any two of the remaining variables (and the known parameter  $R_e$ ). Each group of three variables is related by one equation (provided in the next section) — thus a total of four equations mathematically define the geometric problem illustrated by Figure 1. Two equations (Eq 4 and Eq 5) are derived from the law of sines and involve two angle variables and one side variable. Two other equations (Eq 6 and Eq 7) are derived from the law of cosines and involve two side variables and one angle variable.

##### 3.1.2 Taxonomy of Solution Approaches

The preceding formulation — calculating one variable as a function of any two (of three possible) other variables — results in a total of 12 solutions. These solutions can be broken down into the following taxonomy, in approximate increasing order of complexity

- 2 angle variables and 1 distance variable involved; the distance variable is unknown — solution is based on the law of sines, and the most computationally complex operation is division — 2 cases
- 2 angle variables and 1 distance variable involved; an angle variable is the unknown — solution is based on the law of sines, and the most computationally complex operation is an inverse trigonometric function — 4 cases
- 1 angle variable and 2 distance variables involved; the angle variable is the unknown — solution is based on law of cosines, and the most computationally complex operation is an inverse trigonometric function — 2 cases

- 1 angle variable and 2 distance variables involved; the side opposite the angle is the unknown — solution is based on law of cosines, and the most computationally complex operation is a square root — 2 cases
- 1 angle variable and 2 distance variables involved; the distance variable adjacent to the angle is the unknown — solution is based on law of cosines, and the most computationally complex operation is solving a quadratic equation — 2 cases.

There are (usually more cumbersome) alternatives to the solution approaches outlined above. The first case addressed below, finding  $\theta$  from  $h$  and  $\alpha$ , provides an example.

### 3.1.3 Detailed Geometry

Figure 8 below is a more detailed depiction of the coordinate-free problem geometry shown in Figure 1. For each of the vertices of triangle **OUS** a line is constructed that intersects the opposite side (or an extension thereof) in a right angle. (The constructed lines are the same lines that are created in some proofs of the law of sines and law of cosines.) These intersection points are labeled **A**, **B** and **C**. Because triangle **OUS** is oblique, intersections points **B** and **C** are outside the perimeter of **OUS**. Each of the constructed lines results in the creation of two right triangles with the right angle at **A**, **B** or **C** (for example, line **OC** creates right triangles **OCU** and **OCS**). Figure 8 also introduces the chord **UN**, which is an example of the role of half-angles. Color-coded distances (violet) and angles (blue) associated with these new lines and points are also shown. Figure 8 provides a geometric interpretation some of the equations developed below.

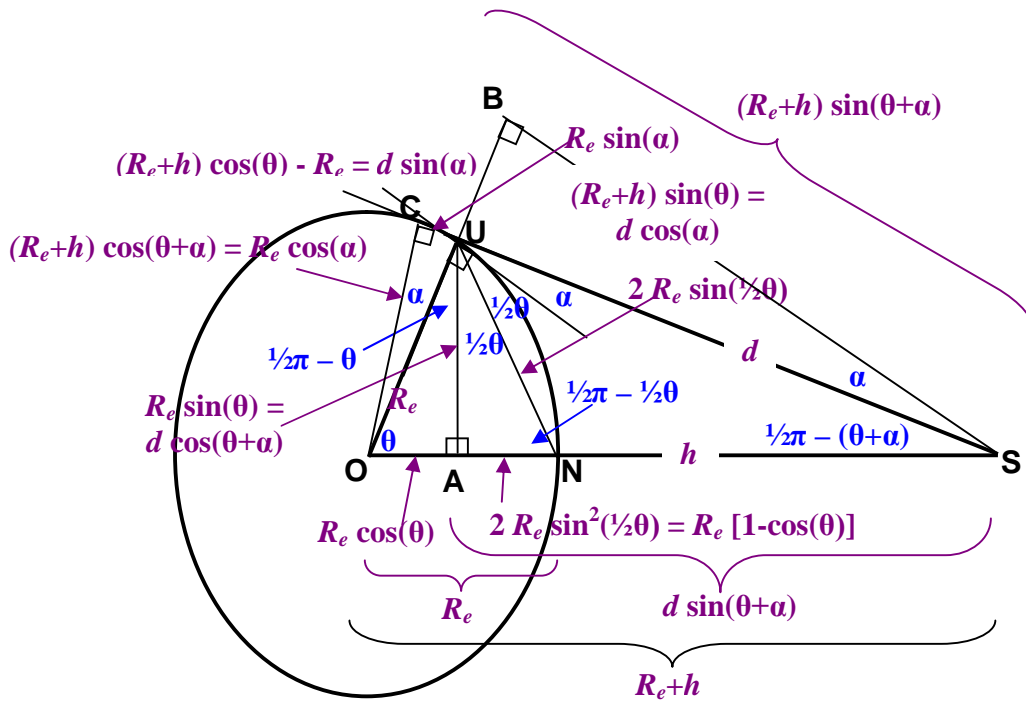


**Figure 8** Detailed Geometry for Vertical Plane Formulation

### 3.2 Computing Geocentric Angle

#### 3.2.1 Altitude and Elevation Angle Known – Basic Method

Manipulating Eq 5 yields

$$\begin{aligned}\theta &= -\alpha + \arccos\left(\frac{R_e}{R_e+h}\cos(\alpha)\right) \\ &= -\alpha + 2 \arcsin\left(\sqrt{\frac{R_e \sin^2\left(\frac{1}{2}\alpha\right) + \frac{1}{2}h}{R_e+h}}\right)\end{aligned}\quad \text{Eq 25}$$

Referring to Figure 8, the first line in Eq 25 can also be derived from the right triangle **AUS**, where the length of the adjacent side is  $R_e \sin(\theta)$  and the length of the hypotenuse is  $(R_e+h) \sin(\theta) / \cos(\alpha)$ .

The expressions on the right-hand sides of two lines in Eq 25 are analytically equivalent; however, the second is numerically better-conditioned when  $\theta$  is small.

Using Eq 13, the first line in Eq 25 can be approximated by

$$\begin{aligned}\theta &= -\alpha + \sqrt{2}\left(\frac{R_e}{2(R_e+h)}\alpha^2 + \frac{h}{R_e+h} - \frac{1}{24}\alpha^4\right)^{1/2} + \frac{\sqrt{2}}{12}\left(\frac{R_e}{2(R_e+h)}\alpha^2 + \frac{h}{R_e+h}\right)^{3/2} \\ &\text{to } O(\alpha^3) \quad \text{and} \quad O\left(\left(\frac{h}{R_e}\right)^{3/2}\right)\end{aligned}\quad \text{Eq 26}$$

When  $\alpha = 0$  (satellite/aircraft is on user's horizon),  $\theta$  achieves its maximum value for a visible target, which is given by

$$\theta_{\max \text{ vis}} = \arccos\left(\frac{R_e}{R_e+h}\right) = 2 \arcsin\left(\sqrt{\frac{\frac{1}{2}h}{R_e+h}}\right) \quad \text{for } \alpha = 0 \quad \text{Eq 27}$$

Since the interior angles of a planar triangle sum to  $\pi$ , it follows from Figure 1 that

$$\angle USO = \arcsin\left(\frac{R_e}{R_e+h}\cos(\alpha)\right) \quad \text{Eq 28}$$

In the satellite field, it is sometimes said that angle USO accounts for the parallax caused by the

satellite not being infinitely distant from the earth. The limiting values for angle USO are:

$$\begin{aligned} \angle USO &\rightarrow 0, & h \gg R_e \\ \angle USO &\rightarrow \frac{\pi}{2} - \alpha, & h \ll R_e \end{aligned} \quad \text{Eq 29}$$

### 3.2.2 Altitude and Elevation Angle Known – Alternative Method

An alternative expression for the geocentric angle can be found by starting with Eq 7 (which involves  $d$ ,  $h$  and  $\alpha$ ), then using Eq 4 to introduce  $\theta$  and eliminate  $d$ . The result is

$$\left[ \frac{R_e + h}{\cos(\alpha)} \right]^2 \sin^2(\theta) + [2R_e(R_e + h) \tan(\alpha)] \sin(\theta) - [h^2 + 2R_e h] = 0 \quad \text{Eq 30}$$

This is a quadratic equation in  $\sin(\theta)$ . Its solution is given by

$$\begin{aligned} \theta &= \arcsin(x) \\ x &= \frac{-B + \sqrt{B^2 - 4AC}}{2A} \\ A &= \left[ \frac{R_e + h}{\cos(\alpha)} \right]^2 \\ B &= 2R_e(R_e + h) \tan(\alpha) \\ C &= -h(h + 2R_e) \end{aligned} \quad \text{Eq 31}$$

### 3.2.3 Altitude and Slant Range Known

From Eq 6, the geocentric angle is given by

$$\begin{aligned} \theta &= \arccos\left(1 - \frac{1}{2} \frac{d-h}{R_e} \frac{d+h}{R_e+h}\right) \\ &= 2 \arcsin\left(\frac{1}{2} \sqrt{\frac{d-h}{R_e} \frac{d+h}{R_e+h}}\right) \\ &= \left(\frac{d-h}{R_e} \frac{d+h}{R_e+h}\right)^{1/2} + \frac{1}{24} \left(\frac{d-h}{R_e} \frac{d+h}{R_e+h}\right)^{3/2} + \text{etc.} \end{aligned} \quad \text{Eq 32}$$

Using Figure 8, the first line of Eq 32 can also be derived by applying Pythagoras's theorem to right triangle **UAS**. The second and third lines are numerically better-conditioned when  $\theta$  is small, and are preferred in such situations.

### 3.2.4 Elevation Angle and Slant Range Known

Eq 4 can be written

$$R_e \sin(\theta) = d \cos(\alpha) \cos(\theta) - d \sin(\alpha) \sin(\theta) \quad \text{Eq 33}$$

Thus

$$\begin{aligned} \theta &= \arctan\left(\frac{d \cos(\alpha)}{R_e + d \sin(\alpha)}\right) \\ &= \frac{\pi}{2} - \arctan\left(\tan(\alpha) + \frac{R_e}{d \cos(\alpha)}\right) \end{aligned} \quad \text{Eq 34}$$

The right-hand side of the first line in Eq 34 can also be derived from right triangle **OBS** in Figure 8. The second line is simply an alternative form, as the arc tangent function is not ill-conditioned for any value of its argument.

## 3.3 Computing Elevation Angle

### 3.3.1 Altitude and Geocentric Angle Known

Manipulating Eq 5 yields

$$\begin{aligned} \tan(\alpha) &= \frac{(R_e + h) \cos(\theta) - R_e}{(R_e + h) \sin(\theta)} = \frac{h \cos(\theta) - 2R_e \sin^2\left(\frac{1}{2}\theta\right)}{(R_e + h) \sin(\theta)} \\ &= \frac{h}{R_e + h} \cot(\theta) - \frac{R_e}{R_e + h} \tan\left(\frac{1}{2}\theta\right) \end{aligned} \quad \text{Eq 35}$$

The first expression on the right-hand side of Eq 35 can also be derived from right triangle **UBS** in Figure 8.

Special / limiting cases of Eq 35 are

$$\begin{aligned} \alpha &= -\frac{1}{2}\theta \quad \text{for } h = 0 \\ \alpha &\rightarrow \frac{h}{R_e + h} \frac{1}{\theta} - \frac{R_e}{R_e + h} \frac{\theta}{2} \quad \text{as } \theta \rightarrow 0 \\ h &= \left(\frac{1}{\cos(\theta)} - 1\right)R_e = \tan(\theta) \tan\left(\frac{1}{2}\theta\right)R_e \quad \text{for } \alpha = 0 \end{aligned} \quad \text{Eq 36}$$

The first line in Eq 36 describes how the satellite/aircraft elevation angle decreases as the satellite/aircraft moves away from the user along the surface of the earth. The last line gives the

altitude of the satellite/aircraft, as a function of distance, when the satellite/aircraft is on the horizon (ignoring refraction due to the earth's atmosphere).

### 3.3.2 Altitude and Slant Range Known

Manipulating Eq 7 yields

$$\begin{aligned} \sin(\alpha) &= \frac{h^2 + 2hR_e - d^2}{2dR_e} \\ &= \frac{1}{d} \left( h - \frac{(d-h)(d+h)}{2R_e} \right) \end{aligned} \quad \text{Eq 37}$$

Using Figure 8, the first line of Eq 37 can also be derived by applying Pythagoras's theorem to the right triangle **OBS**, with the length of the sides being  $R_e+h$  (hypotenuse),  $R_e+d \sin(\alpha)$  and  $d \cos(\alpha)$ . In the second line, the term in large parentheses is the perpendicular height of the satellite above the tangent plane at the user's location. It is interpreted as the altitude of the satellite minus a term which corrects for the curvature of the earth.

### 3.3.3 Geocentric Angle and Slant Range Known

Manipulating Eq 4 yields

$$\alpha = -\theta + \arccos\left(\frac{R_e}{d} \sin(\theta)\right) \quad \text{Eq 38}$$

Eq 38 can also be derived from right triangle **AUS** in Figure 8.

## 3.4 **Computing Slant Range**

### 3.4.1 Altitude and Geocentric Angle Known

From Eq 6, it follows that

$$\begin{aligned} d &= \sqrt{h^2 + 2R_e(R_e + h)(1 - \cos(\theta))} \\ &= \sqrt{h^2 + 4R_e(R_e + h)\sin^2\left(\frac{1}{2}\theta\right)} \\ &= 2R_e \sqrt{(1+u)\sin^2\left(\frac{1}{2}\theta\right) + \left(\frac{u}{2}\right)^2} \quad u \equiv \frac{h}{R_e} \end{aligned} \quad \text{Eq 39}$$

The first line in Eq 39 can also be derived by applying Pythagoras's theorem to right triangle **AUS** in Figure 8. The second and third lines are analytically equivalent to the first, but the ae

numerically better-conditioned when  $\theta$  is small, and preferred in such situations.

### 3.4.2 Altitude and Elevation Angle Known

Eq 7 can be written

$$d^2 + 2R_e d \sin(\alpha) - (h^2 + 2R_e h) = 0 \quad \text{Eq 40}$$

Its solution is

$d = -R_e \sin(\alpha) + \sqrt{(R_e)^2 \sin^2(\alpha) + 2hR_e + h^2}$	Eq 41
-----------------------------------------------------------------------	-------

Referring to Figure 8, Eq 41 can be interpreted as length(**CS**)-length(**CU**), where length(**CS**) is found by Pythagoras's theorem applied to right triangle **OCS**.

The minimum and maximum values for the slant range  $d$  (requiring the satellite is visible) are

$$\begin{aligned} d_{\min} &= h & \text{for} & \quad \alpha = \frac{1}{2}\pi \\ d_{\max \text{ vis}} &= \sqrt{h^2 + 2R_e h} & \text{for} & \quad \alpha = 0 \end{aligned} \quad \text{Eq 42}$$

As the satellite altitude approaches zero, the slant range converges as follows

$$d \rightarrow \frac{h}{\sin(\alpha)} \quad \text{as} \quad h \rightarrow 0 \quad \text{Eq 43}$$

### 3.4.3 Geocentric Angle and Elevation Angle Known

Eq 5 can be written

$d = R_e \frac{\sin(\theta)}{\cos(\alpha + \theta)}$	Eq 44
------------------------------------------------------	-------

Eq 44 is a manipulation of the two expressions for the length of **AU** in Figure 8. This equation is not ill-conditioned for any values of  $\theta$  and  $\alpha$ .

## 3.5 Computing Altitude

### 3.5.1 Slant Range and Geocentric Angle Known

Eq 6 can be written as a quadratic equation in  $R_e+h$ . Its solution is

$\begin{aligned} h &= -R_e (1 - \cos(\theta)) + \sqrt{d^2 - R_e^2 (1 - \cos^2(\theta))} \\ h &= -2R_e \sin^2\left(\frac{1}{2}\theta\right) + \sqrt{d^2 - R_e^2 \sin^2(\theta)} \end{aligned}$	Eq 45
-----------------------------------------------------------------------------------------------------------------------------------------------------------------------------------------------	-------

Referring to Figure 8, the first line in Eq 45 can be interpreted as length(**AS**)-length(**AN**), where length(**AS**) is found by Pythagoras’s theorem applied to right triangle **AUS**. The right-hand sides of the two lines are analytically equivalent. However, the right-hand side of the second line is numerically better-conditioned when  $\theta$  is small, and is preferred in such situations.

### 3.5.2 Slant Range and Elevation Angle Known

Rearranging Eq 7 yields

$$\begin{aligned}
 h &= -R_e + \sqrt{R_e^2 + d^2 + 2 R_e d \sin(\alpha)} \\
 &= R_e \left( \frac{x}{2} - \frac{x^2}{8} + \frac{x^3}{16} - \frac{5x^4}{128} + \frac{7x^5}{256} \pm \text{etc.} \right) \quad \text{when} \quad x = \frac{2 d \sin(\alpha)}{R_e} + \frac{d^2}{R_e^2} < 1
 \end{aligned}
 \tag{Eq 46}$$

Referring to Figure 8, the first line in Eq 46 can be interpreted as length(**OS**)-length(**ON**), where length(**OS**) is found by Pythagoras’s theorem applied to right triangle **OBS**.

As the satellite slant range approaches zero, the altitude converges as follows

$$h \rightarrow d \sin(\alpha) \quad \text{as} \quad d \rightarrow 0 \tag{Eq 47}$$

### 3.5.3 Elevation Angle and Geocentric Angle Known

Manipulating Eq 5 yields

$$h = \left( \frac{\cos(\alpha)}{\cos(\alpha + \theta)} - 1 \right) R_e \tag{Eq 48}$$

Eq 48 can also be derived by manipulating the equality of two expressions for the length of **OC** in Figure 8.

Setting  $\alpha = 0$  in Eq 48 yields Eq 49 for the “height of the user’s horizon”. Sometimes Eq 49 is replaced by a modified version that attempts to account for atmospheric refraction (bending of electromagnetic waves as a function of atmospheric density). This topic is partially addressed in the following section.

$$\begin{aligned}
 h_{horiz} &= \left( \frac{1}{\cos(\theta)} - 1 \right) R_e = \tan(\theta) \tan\left(\frac{1}{2}\theta\right) R_e \quad \text{for} \quad \alpha = 0 \\
 &= \left( \frac{1}{2}\theta^2 + \frac{5}{24}\theta^4 + \frac{61}{720}\theta^6 + \text{etc.} \right) R_e
 \end{aligned}
 \tag{Eq 49}$$

## 3.6 **Example Applications**

Three example applications are presented in this section, with the intent of providing a sense of

how the coordinate-free mathematical equations presented earlier in this chapter relate to a real problem. The examples are intended to illustrate that it is necessary to understand the application in order to utilize the equations properly and to interpret the results. Also, these examples suggest that, while providing useful information, the coordinate-free equations cannot answer some relevant question. For that reason, the same examples are re-visited again at the end of Chapter 4.

### 3.6.1 Example 1: En Route Radar Coverage

A traditional surveillance engineering task is predicting a radar installation's "coverage". There are two common problem formulations: Calculate either the minimum visible aircraft (a) Elevation MSL or HAT, for a known ground range from the radar; or (b) Ground range from the radar, for a known elevation or HAT.

For either case, the issues to be considered, and the approach taken herein, are:

- **Terrain Effects** — As stated in Chapter 1, blockage of electromagnetic waves by hills/mountains/structures is not addressed herein. These effects would be included in a more thorough analysis, and are particularly important in mountainous areas. However, terrain effects are handled numerically, rather than by an analytic model, and are thus outside the scope of this memorandum. The earth surrounding the radar is assumed to be smooth, although not necessarily at sea level.
- **Propagation Model** — Real sensors may not have the straight line propagation paths assumed by the equations earlier in Chapter 3. Relevant to this example: electromagnetic waves behave according to Snell's Law and refract (bend) towards the vertical as the atmospheric density increases at lower altitudes. Refraction effects are most pronounced for long, predominantly horizontal paths within the earth's atmosphere (all of which apply to en route ATC radars). A widely used model (employed herein), that approximates the effects of refraction and is compatible with the equations developed earlier in the chapter is the "four-thirds earth" model. According to Wikipedia (Ref. 7): "The 4/3 Earth radius rule of thumb is an average for the Earth's atmosphere assuming it is reasonably homogenized, absent of temperature inversion layers or unusual meteorological conditions."
- **Radar Antenna Height** — Three values are used for the height of the radar antenna phase center above the surrounding terrain,  $h_U$ : 50 ft, representative of the antenna height for a radar mounted on a tower; 500 ft, representative of the antenna height for a radar on top of a hill; and 5,000 ft, representative of the antenna height for a radar on top of a mountain.

Based on these considerations, the two known/independent variables are taken to be:

- (1) The satellite/aircraft elevation angle  $\alpha$  (provided it is equal to or greater than the minimum value for the associated antenna height  $h_U$ ); and
- (2) Either
  - (a) the geocentric angle  $\theta$  between the radar and satellite/aircraft (so the unknown/dependent variable is the aircraft altitude  $h_S$  above the terrain) — governed by Eq 48; or
  - (b) the aircraft altitude  $h_S$  (so the unknown/dependent variable is the geocentric angle  $\theta$ ) — governed by Eq 25.

Associating  $\mathbf{U}$  with the radar antenna location (because its elevation is known) and  $\mathbf{S}$  with

possible aircraft locations, the resulting equations are shown in Eq 50 below. For both cases (a) and (b), substitutions are made for the four-thirds earth model and to account for a non-zero user altitude (Subsection 2.3.1). Also, the equation for the minimum user altitude (Eq 24) is repeated.

$$\begin{aligned}
 (a) \quad h_S &= h_U + \left( \frac{\cos(\alpha)}{\cos\left(\alpha + \frac{3}{4}\theta\right)} - 1 \right) \left( \frac{4}{3}R_e + h_U \right) \quad \text{for } \alpha \geq \alpha_{min} \\
 (b) \quad \theta &= -\frac{4}{3}\alpha + \frac{8}{3} \arcsin \left( \sqrt{\frac{\left(\frac{4}{3}R_e + h_U\right) \sin^2\left(\frac{1}{2}\alpha\right) + \frac{1}{2}(h_S - h_U)}{\frac{4}{3}R_e + h_U}} \right) \quad \text{for } \alpha \geq \alpha_{min} \quad \text{Eq 50} \\
 \alpha_{min} &= -\frac{\pi}{2} + \arcsin \left( \frac{\frac{4}{3}R_e}{\frac{4}{3}R_e + h_U} \right)
 \end{aligned}$$

The results of exercising Eq 50 for case (a), when the geocentric angle is known, are shown in Figure 9. The maximum range depicted, 250 NM, is the specified value for current en route ATC radars (e.g., ARSR-4 and ATCBI-6). Curves are shown that correspond to the three radar HAT values at the theoretical minimum elevation angle for which targets are visible (blue) and for 1 deg larger than the minimum elevation angle (violet). Aircraft whose range/HAT combinations are above a given curve are visible to the radar; otherwise they are said to be “below the radar horizon”. If curves for the visibility of aircraft relative to mean sea level (altitude MSL) are needed, the elevation of the terrain is added to the HAT values in Figure 9.

**Sensitivity to radar antenna HAT** — Increasing the height of the radar’s antenna significantly decreases the minimum HAT at which aircraft are visible. In this example, raising the antenna HAT from 50 to 5,000 feet decreases the visible aircraft HAT by almost 21,000 feet — i.e., the ratio is greater than 4:1. This “leverage” can be appreciated by examining Figure 6. Line **US** acts like a lever arm with its fulcrum at **T**. Raising **U** lowers **S**, and since **T** is generally closer to **U** than **S**, the change in the elevation of **S** is greater than it is in **U**.

**Sensitivity to antenna elevation angle** — Increasing (possibly mistakenly) the elevation angle of the radar antenna above the minimum required to avoid blockage of the signal by the earth has a significant penalty. At the radar’s maximum range, a 1 degree increase in elevation angle corresponds to an increase in the minimum HAT at which targets are visible of approximately

$$\Delta\alpha \cdot d = (1 \text{ deg})(\pi \text{ rad}/180 \text{ deg})(250 \text{ NM})(6,076 \text{ ft/NM}) = 26,511 \text{ feet} \quad \text{Eq 51}$$

The resulting decrease in airspace under surveillance is more than is gained by raising the radar HAT to 5,000 feet. Thus aligning (often called “bore sighting”) the antenna is an important facet of a radar installation.

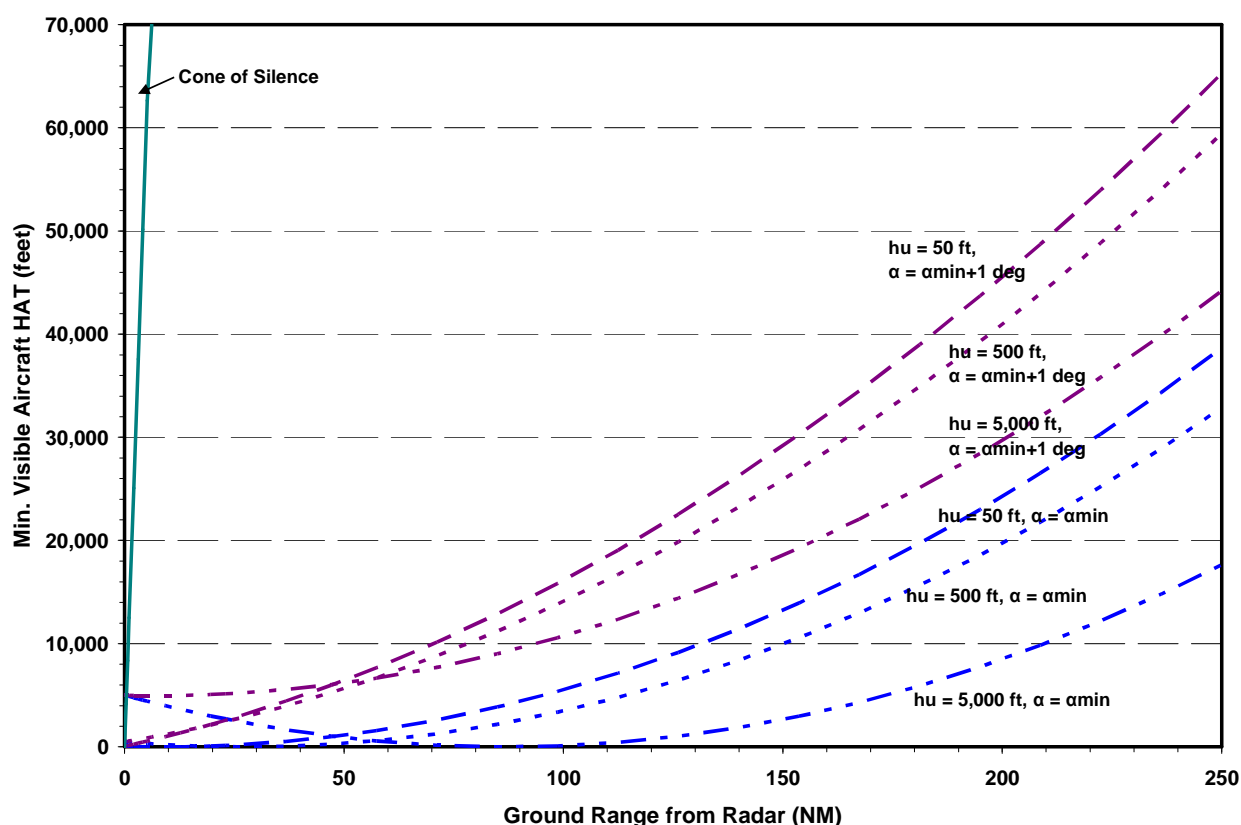


**Figure 9** Aircraft Minimum Visible HAT vs. Range for Three Radar HAT Values

**Cone of Silence** — “Visibility” is necessary for an aircraft to be detected by a radar. But it is not sufficient. Energy transmitted by the radar must reach the aircraft; then, energy scattered (primary radar) or transmitted (secondary radar) by the aircraft must return to the radar at a detectable level. When a radar performs well for most targets (the case here) and a target is visible, the determining factor for detectability is the antenna pattern. ATC radar antennas are designed to have their gain concentrated near the horizon, where most aircraft are. Conversely, ATC radars are not designed to detect aircraft almost directly above them (the “cone of silence”).

A “rule of thumb” for detecting a target by an ATC radar is that the target range be at least twice its height above the radar antenna — e.g., an aircraft at 10,000 ft above the antenna would not be detected when less than 20,000 ft or 3.3 NM from the radar (Ref. 8). Figure 9 includes the predicted cone of silence for an ATC radar antenna on the surface; larger antenna HAT values will result in slightly smaller cones of silence. Generally, the cone of silence is an issue to be aware of, but is not a major concern.

**Earth Model** — For either a normal-size or  $4/3^{\text{rds}}$  earth model, the minimum visible aircraft altitudes are small at short ranges. However, the minimum visible altitudes for the individual models (thus their differences) are substantial at longer ranges. For example, at a ground range of

250 NM, the predicted visible aircraft HAT for a 4/3<sup>rd</sup>s earth model is less than that for a normal-size earth by between 13.4 kft (for a radar antenna HAT of 50 ft) and 9.4 kft (for a radar antenna HAT of 5,000 ft).

### 3.6.2 Example 2: Aircraft Instrument Approach Procedure

Design of an Instrument Approach Procedure (IAP) is a straightforward application of the equations earlier in this chapter. The LPV approach\* to Kansas City International Airport (MCI) runway 19L is selected as an example — Figure 10 is the current approach plate.

The first consideration is that, since the navigation fixes on the approach plate quantify vertical height in terms of altitude MSL, the same metric must be used for procedure design. Second, the user location **U** is chosen as the point where aircraft crosses the runway threshold. The elevation above MSL of **U** is the sum of the elevation of the runway threshold (THRE = 978 ft) and the threshold crossing height (TCH = 59 ft); thus,  $h_U = 1,037$  ft.

In terms of the four variables defined in Subsection 3.1.1, the elevation angle  $\alpha$  is set equal to the specified glide path angle — i.e.,  $\alpha = 3.00$  deg — and constitutes one independent variable. The second independent variable describes movement along the approach route. Either  $\theta$  or  $h_S$  could be used; in this example,  $\theta$  is selected because it has fewer drawbacks. While its published precision (0.1 NM) is less than desired, the limits of its precision are known. Conversely, only lower bounds for  $h_S$  are specified on the approach plate; the amount that each is below the glide path angle is not known. (However, a positive, and one reason for selecting this example is that there are six positions along the approach where the minimum altitude MSL is stated.)

For this set of variables —  $\alpha$  and  $\theta$  known,  $h$  unknown — Subsection 3.5.3 provides the solution equation (Eq 48). After making substitutions for a non-zero user altitude  $h_U$  (Subsection 2.3.1), the result is Eq 52. Evaluating this equation (using the TERPS value for  $R_e$ ) yields Table 2.

$$h_S = h_U + \left( \frac{\cos(\alpha)}{\cos(\alpha + \theta)} - 1 \right) (R_e + h_U) \quad \text{Eq 52}$$

**Table 2** Specified and Computed Fix Altitudes for MCI Runway 19L LPV Approach

Fix Name	UMREW	FELUR	REMNS	ZASBO	YOVNU	GAYLY
Dist. from Threshold, NM (Figure 10)	1.9	4.9	6.2	9.3	12.4	15.5
Min. Altitude MSL, ft (Figure 10)	1,640	2,600	3,000	4,000	5,000	6,000
Glide Path Altitude MSL, ft (Eq 52)	1,645	2,619	3,046	4,075	5,122	6,187

---

\* LPV approaches utilize GPS and the Wide Area Augmentation System (WAAS) for lateral and vertical guidance, and are a current focus of FAA IAP activities. Their minimums are similar to those for ILS Category I procedures.

Because the computed altitudes on the last row of Table 2 are slightly larger than the published minimum altitudes on the row above, it is reasonable to conclude that the IAP design process described in the subsection closely replicates FAA process.

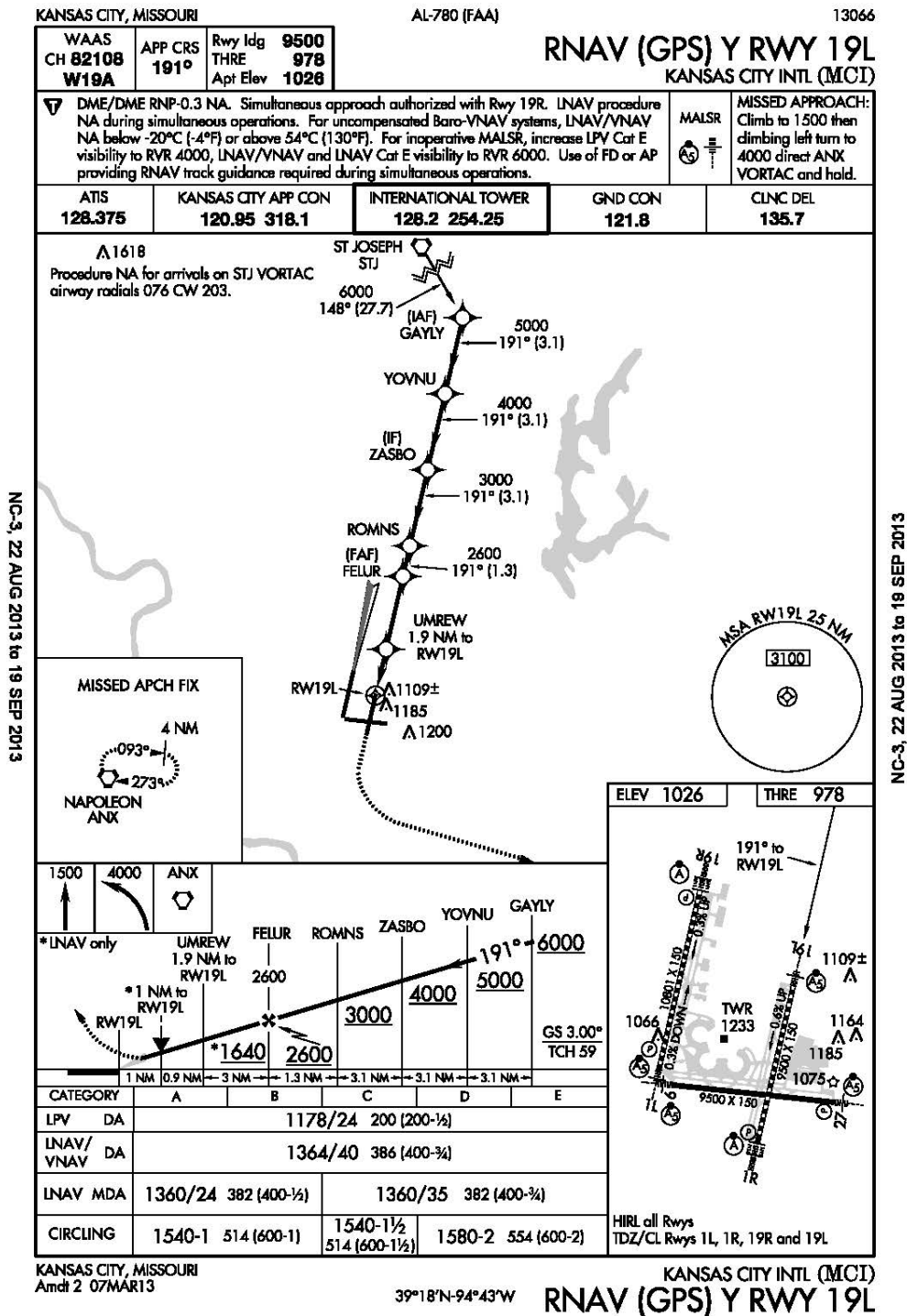


Figure 10 Approach Plate: LPV Procedure to MCI Runway 19L

### 3.6.3 Example 3: Satellite Visibility of/from Earth

A question that is readily addressed using the equations in this chapter is: What fraction of the earth's surface can see (and be seen by) a satellite at altitude  $h$ ? Clearly,  $h$  is one independent variable in such an analysis. The other independent variable is taken to be the minimum elevation angle  $\alpha$  (sometimes called the mask angle in this context) at which the satellite provides a usable signal. The quality of signals received at low elevation angles can be degraded due to multipath and attenuation by the atmosphere; and terrain blockage is an issue at low elevation angles. The dependent variable is taken to be  $\theta$ , the geocentric angle between the satellite nadir  $\mathbf{N}$  and the user  $\mathbf{U}$ . For this combination of variables, Subsection 3.2.1 provides an approach to the solution.

The remaining issue is whether to use a normal-size or 4/3 earth model. Normal-size is selected, because (unlike radar signals) satellite signals are outside of the earth's atmosphere over most of their propagation path. The earth's atmosphere extends to an altitude of approximately 5 NM, while satellite altitudes are at least several hundred nautical miles.

The basic equation to be evaluated is thus taken from Eq 25. As a way of visualizing the impact of satellite altitude on visibility, a modified version of Eq 15 is used. The results of exercising these equations (Eq 53) are shown in Figure 11.

$$\theta = -\alpha + 2 \arcsin \left( \sqrt{\frac{R_e \sin^2\left(\frac{1}{2}\alpha\right) + \frac{1}{2}h}{R_e + h}} \right) \quad \text{Eq 53}$$
$$\text{Fraction of Earth Visible} = \frac{1}{2}[1 - \cos(\theta)]$$

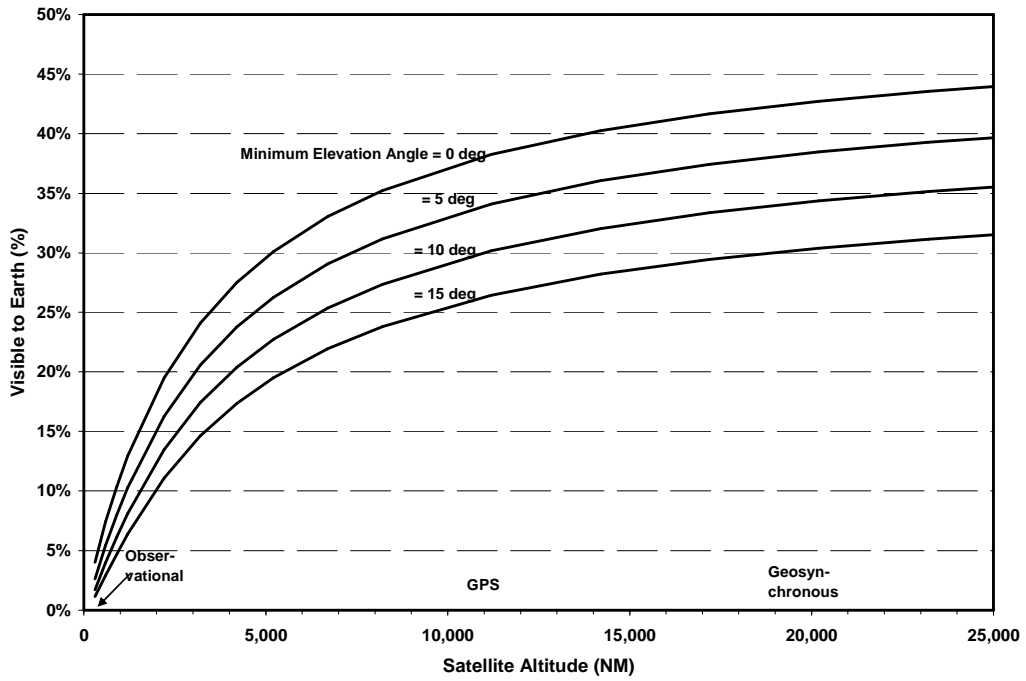


Figure 11 Fraction of Earth Visible vs. Satellite Altitude

## 4. SOLUTION TO SPHERICAL SURFACE FORMULATION

### 4.1 Basics of Spherical Trigonometry

#### 4.1.1 Historical Perspective

Spherical trigonometry deals with relationships among the sides and angles of spherical triangles, defined by intersecting great circles on a sphere (Figure 12). Spherical trigonometry originated over 2,000 years ago, largely motivated by two applications: maritime navigation (practical) and understanding the relationship of the earth to the “fixed stars” (intellectual). Early contributors were from classical Greece and medieval Islam (Persian and Arab). The subject was largely completed by Europeans in the 18<sup>th</sup> and 19<sup>th</sup> centuries. Until the 1950s, spherical trigonometry was a standard part of the mathematics curriculum in U.S. high schools — see Refs. 9 and 10.

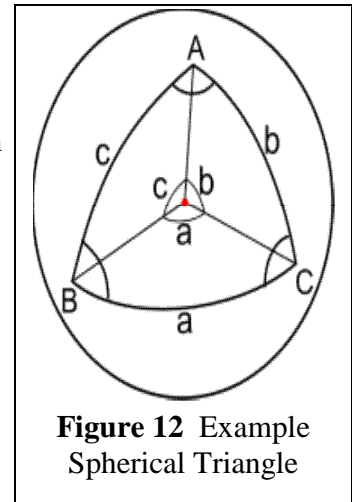


**Figure 12** Example Spherical Triangle

Although it has fallen into academic disfavor, the spherical trigonometric equations for points on the (spherical) earth’s surface are generally identical to, but simpler to derive than, those for the vector approach that is addressed in the following chapter.

Conversely, a drawback of spherical trigonometry is that it’s not well suited to problems involving locations at finite distances above the earth. Thus, it cannot be used to find the elevation angle of a satellite **S** with respect to the user **U**, or the user-satellite slant-range.

#### 4.1.2 Application to Navigation

Although similar, there are differences between spherical trigonometry and navigation on the surface of a spherical earth. In general, the vertices of a spherical triangle can be arbitrarily located on a sphere. However, for navigation analyses, one vertex is taken to be the North Pole, **P**<sup>\*</sup>. Such a spherical triangle is completed by the two endpoints of a navigation “leg” — e.g., points **U** and **S** in Figure 13.

For a spherical triangle employed for navigation analysis,

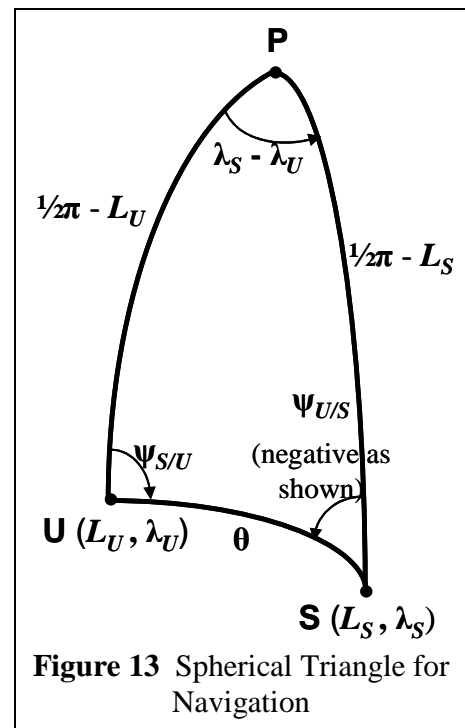


**Figure 13** Spherical Triangle for Navigation

\* While the North Pole is generally used in deriving navigation equations, the resulting expressions are valid for points in the southern hemisphere as well.

six triangular elements (requiring seven navigation variables) are involved:

- (a) Angular lengths of sides **PU** and **PS** — complements of the latitudes of points **U** and **S**, respectively;
- (b) Angle at **P** — the difference in the longitude of the points **U** and **S**;
- (c) Angular length of side **US** — the geocentric angle between the mission's start and end points; and
- (d) Angles at **U** and **S** — the azimuth (also called the bearing or course) angles of the leg joining **U** and **S** with respect to north.

Two differences relative to plane trigonometry are that the three angles of a spherical triangle do not sum to  $\pi$  and that right triangles do not play as prominent a role. Relative to item (b) above, if the path **US** crosses the  $\pm\pi$  line of longitude (idealized International Date Line), the difference between the east longitude and the west longitude may (depending upon the use) need to be adjusted by  $\pm 2\pi$ , so that the magnitude of the difference is less than or equal to  $\pi$ . Adjustment is not needed to use the difference as the argument of a trigonometric function, as all have a period of  $2\pi$ . However, if the longitude difference is computed and added to/subtracted from a known longitude to find an unknown longitude, the result may need to be adjusted by  $\pm 2\pi$ .

Figure 12 and Figure 13 can be misleading, in that all angles and sides are depicted as acute — i.e., in the range  $(0, \pi/2)$ . In reality, spherical trigonometric angles and sides are usually taken to be in the range  $(0, \pi)$ . In navigation there is a need to deal with angles having a wider range of values: latitude varies over  $[-\pi/2, \pi/2]$ , longitude varies over  $[-\pi, \pi]$ , geocentric angles vary over  $(0, \pi)$  and azimuths vary over  $[-\pi, \pi]$ . Thus, latitudes are usually found with the arc sine, longitudes with the two-argument arc tangent, geocentric angles with the arc cosine, and azimuths with the two-argument arc tangent. In order to use the two-argument arc tangent, there is usually the need to find expressions for both the sine and cosine on the angle.

On the surface of a sphere, point **S** to point **U** if is diametrically opposite to **U**; a line from **U** to **S** passes through the center of the sphere. **U** and **S** are antipodal if  $L_S = -L_U$  and  $\lambda_S = \lambda_U + \pi$ . When that is the case, the geocentric angle between **U** and **S** is  $\pi$ ; however, an infinite number of great circle paths connect **U** and **S**. As a result, many spherical trigonometry equations, and particularly those for azimuth angles, are indeterminate or fail for antipodal points.

#### 4.1.3 Resources Available on the Web

The worldwide web has many useful resources concerning spherical trigonometry. Examples that I'm familiar with, in approximate decreasing order of their complexity:

- I. Todhunter, *Spherical Trigonometry*, 5<sup>th</sup> Edition (Ref. 11) — Written by a British academic. Has been cited as the definitive work on the subject. Later editions were published but are not available without charge.

- W.M. Smart and R.M. Green, *Spherical Astronomy* (Ref. 12) — Also written by a British academics. Chapter 1 (24 pages of a 400+ page text) is devoted to spherical trigonometry. It has equations and their derivations (including more complex and useful ones) and associated narratives.
- Wikipedia, *Spherical Trigonometry* (Ref. 13) — A fine collection of equations and background information.
- Wolfram MathWorld (Ref. 14) — A good collection of equations
- Aviation Formulary (Ref. 15) — A website with equations similar to those in this chapter, without derivations. It also offers an Excel spreadsheet with formulas as macros.
- Spherical Trigonometry (Ref. 16) — An easily understood introduction to the topic.

#### 4.1.4 Key Formulas

In general (including herein) and without explicit statement otherwise, the labeling of the angles and sides of a spherical triangle is arbitrary. Thus, cyclic substitutions — i.e.,  $\mathbf{A} \rightarrow \mathbf{B}$ ,  $\mathbf{a} \rightarrow \mathbf{b}$ , etc. — can be made to derive two alternate versions of each identity. In addition to key formulas displayed below, there is a rich set of other spherical trigonometric identities that may be found in the literature.

Law of cosines for sides:

$$\cos(a) = \cos(b) \cos(c) + \sin(b) \sin(c) \cos(A) \quad \text{Eq 54}$$

The right-hand side of this law contains two sides (here,  $\mathbf{b}$  and  $\mathbf{c}$ ) and their included angle ( $\mathbf{A}$ ). The left-hand side contains the third side ( $\mathbf{a}$ ), which is opposite to the included angle.

Primary applications: (1) finding the third side of a triangle, given two sides and their included angle; and (2) finding any angle of a triangle (using cyclic substitution), given three sides.

Law of cosines for angles:

$$\cos(A) = -\cos(B) \cos(C) + \sin(B) \sin(C) \cos(a) \quad \text{Eq 55}$$

The right-hand side of this law contains two angles (here,  $\mathbf{B}$  and  $\mathbf{C}$ ) and their included side ( $\mathbf{a}$ ). The left-hand side contains the third angle ( $\mathbf{A}$ ), which is opposite to the included side.

Primary applications: (1) finding the third angle of a triangle, given the other two angles and their included side; and (2) finding any side of a triangle (using cyclic substitution) from the three angles.

Law of sines:

$$\frac{\sin(a)}{\sin(A)} = \frac{\sin(b)}{\sin(B)} = \frac{\sin(c)}{\sin(C)} \quad \text{Eq 56}$$

Primary application: finding a side (or angle) of triangle, given the opposite angle (or side) and

another opposite side-angle pair. The ambiguity of the arc sine function can be a concern.

Analogue of law of cosines for sides:

$$\begin{aligned}\sin(a) \cos(B) &= \cos(b) \sin(c) - \sin(b) \cos(c) \cos(A) \\ \sin(a) \cos(C) &= \cos(c) \sin(b) - \sin(c) \cos(b) \cos(A)\end{aligned}\tag{Eq 57}$$

The right-hand sides of both lines of the above equation have the same sides and included angle (and almost identical functions) as the right-hand side of the law of cosines for sides. However, whereas the law of cosines for sides has  $\cos(a)$  on the left-hand side, the analogue law has  $\sin(a) \cos(B)$  or  $\sin(a) \cos(C)$ , with  $B$  and  $C$  being the angles adjacent to side  $a$ .

Primary application: resolving ambiguities in situations where two sides and the included angle are known, and it is desired to find the other two angles directly from the known quantities.

Four-Part Cotangent Formula:

$$\begin{aligned}\cos(a) \cos(B) &= \sin(a) \cot(c) + \sin(B) \cot(C) && (cBaC) \\ \cos(a) \cos(C) &= \sin(a) \cot(b) + \sin(C) \cot(B) && (BaCb)\end{aligned}\tag{Eq 58}$$

The six elements of a triangle may be written in cyclic order as (aCbAcB). The four-part cotangent formula relates two sides and two angles forming four consecutive elements around a triangle. The side and angle at the ends of such a sequence appear once on each line in Eq 58, as the argument of a cotangent function, whereas the middle elements appear twice on a line.

Primary applications: (1) given two angles (here,  $B$  and  $C$ ) and their included side ( $a$ ), find the adjacent sides ( $b$  and  $c$ ); and (2) Given two sides ( $c$  and  $a$ , or  $a$  and  $b$ ) and their included angle ( $B$  or  $C$ ), find the adjacent angles ( $C$  and  $B$ ).

With same known quantities as the two cosine laws, the four-part cotangent formula provides solutions for the adjacent quantities that the cosine laws do not address. However, application (2) can also be accomplished by a combination of the law of sines and the analogue law (see solutions for longitude difference and azimuth angles below).

Napier's Analogies:

$$\begin{aligned}\tan \frac{1}{2}(A + B) &= \frac{\cos \frac{1}{2}(a - b)}{\cos \frac{1}{2}(a + b)} \cot \frac{1}{2}C && \tan \frac{1}{2}(a + b) = \frac{\cos \frac{1}{2}(A - B)}{\cos \frac{1}{2}(A + B)} \tan \frac{1}{2}c \\ \tan \frac{1}{2}(A - B) &= \frac{\sin \frac{1}{2}(a - b)}{\sin \frac{1}{2}(a + b)} \cot \frac{1}{2}C && \tan \frac{1}{2}(a - b) = \frac{\sin \frac{1}{2}(A - B)}{\sin \frac{1}{2}(A + B)} \tan \frac{1}{2}c\end{aligned}\tag{Eq 59}$$

Primary application: (1) given two sides (here,  $a$  and  $b$ ) and their opposite angles ( $A$  and  $B$ ), find the remaining side ( $c$ ) and remaining angle ( $C$ ).

Solving for Angles and Sides:

When solving for angles and sides after employing the above formulas, one must be aware of the possibility of ambiguous solutions to inverse trigonometric functions. In the realm of spherical trigonometry (versus navigation), where angles and sides are in the range  $(0, \pi)$ , the arc sine function and the law of sines are the primary source of concern, as two angles in the range  $(0, \pi)$  can have the same sine value. However, some problems do have two solutions; in these cases, neither result from the arc sine function is extraneous. Additional comments are provided concerning specific problems and equations below.

4.1.5 Taxonomy of Problems Involving Spherical Triangles

A spherical triangle is defined by six possible quantities. The case of five given elements is trivial, requiring only a single application of either cosine law or the sine law. For four given elements there is one non-trivial case. For three given elements there are six cases. Each of the total of seven cases is illustrated in Figure 14 and enumerated below (Ref. 17), along with a solution approach. Others solutions may also exist.

- (1) Three sides known — Eq 54, three times
- (2) Two sides and the included angle known — Eq 54 for  $a$ , Eq 56 and/or Eq 57 for  $B$  and  $C$
- (3) Two sides and a non-included angle known — Eq 56 for  $C$ , then follow case 7
- (4) Two angles and the included side known — Eq 55 for  $A$ , then Eq 56 or Eq 58  $b$  and  $c$
- (5) Two angles and a non-included side known — Eq 56 for  $b$ , then follow case 7
- (6) Three angles known — Eq 55, three times
- (7) Two sides and their opposite angles known — Eq 59 for  $A$  and  $a$ .

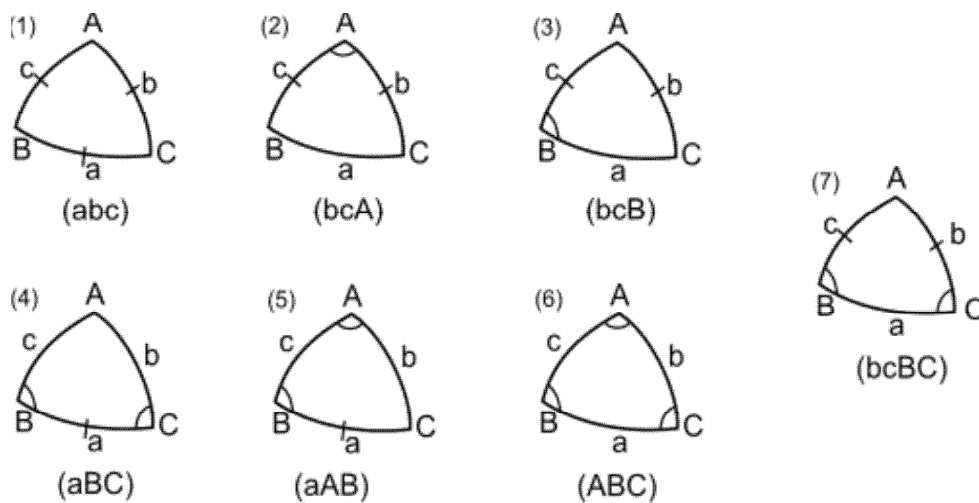


**Figure 14** Illustrating the Taxonomy of Spherical Triangle Problems

#### 4.1.6 Taxonomy of Spherical Surface Formulation Mathematical Problems

The spherical surface formulation introduced in Section 1.3 involves seven variables. For a full solution to a given situation, four variables must be known, from which three can be found. Thus, potentially, 35 mathematical problems and 105 solution equations could be involved. However, the spherical surface formulation is symmetric in **U** and **S**; interchanging **U** and **S** only flips the left and right sides in Figure 13 but does not change the underlying problem. Of the 35 possible mathematical problems, three are self-symmetric (the mathematical problem does not change if **U** and **S** are interchanged) and 16 have symmetric versions — see Table 3. Table 3 notes the 3 of 19 problems summarized (and 5 of the full 35) do not involve either longitude being known; thus the solution can only yield a longitude difference rather than an actual longitude. Table 3 also references the corresponding spherical triangle case (Subsection 4.1.5) and the cases that are addressed in the remainder of this chapter. All seven spherical triangle cases presented in Subsection 4.1.5 occur in Table 3

**Table 3** Taxonomy of Spherical Surface Formulation Mathematical Problems

Case #	$L_U$	$\lambda_U$	$\psi_{S/U}$	$L_S$	$\lambda_S$	$\psi_{U/S}$	$\theta$	SP <sup>1</sup>	SS <sup>2</sup>	No $\lambda$	ST Case <sup>3</sup>	Comment
1	X	X		X	X				X		2	Section 4.2
2	X	X	X	X				X			3	Section 4.5
3	X	X		X		X		X			3	Similar to #2
4	X	X		X			X	X			1	
5	X	X	X		X			X			4	Section 4.4
6	X	X			X	X		X			5	
7	X	X			X		X	X			3	
8	X	X	X			X		X			5	
9	X	X	X				X	X			2	Section 4.3
10	X	X				X	X	X			3	
11	X		X	X		X			X	X	7	
12	X		X	X			X	X		X	1, 2, +	Over-specified
13	X		X		X	X		X			5	Similar to #8
14	X		X		X		X	X			2	Similar to #9
15	X				X	X	X	X			3	
16	X		X			X	X	X		X	2, 4, +	Over-specified
17		X	X		X	X			X		6	
18		X	X		X		X	X			5	
19		X	X			X	X	X			4	

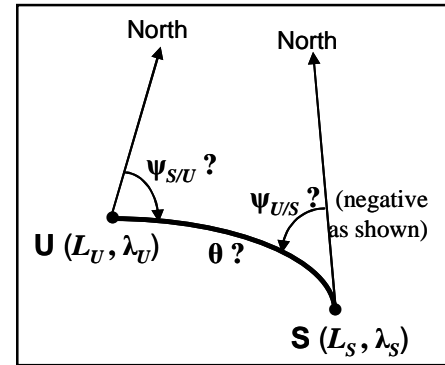
<sup>1</sup> Symmetric Problem exists

<sup>2</sup> Self-Symmetric problem

<sup>3</sup> Spherical Triangle Case (Subsection 4.1.5)

## 4.2 Solving the Indirect Problem of Geodesy

The indirect problem of geodesy is stated in Section 1.3 and illustrated on the right. In taxonomy of spherical triangles in Subsection 4.1.5, this problem falls under case (2). The known elements (and dimensions) are sides **PU** ( $\frac{1}{2}\pi - L_U$ ) and **PS** ( $\frac{1}{2}\pi - L_S$ ) and their included angle **UPS** ( $\lambda_S - \lambda_U$ ).



### 4.2.1 Computing the Geocentric Angle

Finding the geocentric angle between two locations on a spherical earth is a fundamental question, and apparently was a motivating factor in the creation of spherical trigonometry. Referring to Figure 13, the distance  $\theta$  between **U** and **S** is readily derived from the law of cosines for sides (Eq 54), treating the leg connecting **U** and **S** as the unknown quantity

$$\cos(\theta) = \cos(L_U)\cos(L_S)\cos(\lambda_U - \lambda_S) + \sin(L_U)\sin(L_S) \quad \text{Eq 60}$$

The right-hand side of Eq 60 should evaluate to a value in  $[-1, 1]$ ;  $\theta$  can then be found uniquely in  $[0, \pi]$ . Eq 60 was used by maritime navigators centuries ago, likely before 1,000 AD. However, when precision is limited (as it was for paper-and-pencil calculations using rudimentary trigonometry tables), the preceding equation is numerically ill-conditioned for small values of the geocentric angles  $\theta$  (which were the most frequently occurring). Also see Subsection 2.1.4.

To improve computational accuracy when the geocentric angle is small, over 1,000 years ago (Ref. 18) mathematicians defined the versine (in Latin, *sinus versus*) function as (Figure 15)

$$\text{vers}(\theta) \equiv 1 - \cos(\theta) = 2 \sin^2\left(\frac{\theta}{2}\right) \quad \text{Eq 61}$$

In early terminology, the familiar sine function was called *sinus rectus*, or vertical sine. Tables for the versine or the haversine (half of versine), and their inverses, date to the fourth century.

Using the haversine function, the geocentric angle can be found from what is sometimes called termed the “haversine formula”

$$\text{hav}(\theta) = \text{hav}(L_S - L_U) + \cos(L_S)\cos(L_U)\text{hav}(\lambda_S - \lambda_U) \quad \text{Eq 62}$$

The haversine formula eliminates the ill-conditioning of Eq 60 for small geocentric angles and requires only a few real-time (possibly, at sea) calculations.

Without explicitly utilizing the versine or haversine (which are less needed today, due to the

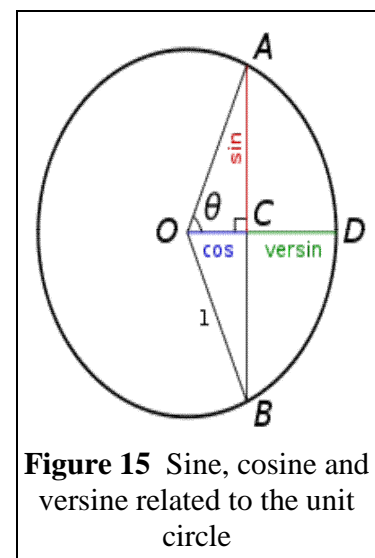


**Figure 15** Sine, cosine and versine related to the unit circle

availability of modern computational capabilities), an analytically equivalent version of the haversine formula is

$$\sin\left(\frac{\theta}{2}\right) = \sqrt{\sin^2\left(\frac{L_S - L_U}{2}\right) + \cos(L_S) \cos(L_U) \sin^2\left(\frac{\lambda_S - \lambda_U}{2}\right)} \quad \text{Eq 63}$$

The right-hand side of Eq 63 should evaluate to a value in [0, 1];  $\theta$  can then be found uniquely in  $[0, \pi]$ . The small latitude and longitude differences that occur when **U** and **S** are close only involve the sine function. This expression is reminiscent of Pythagoras’s formula for the hypotenuse of a plane triangle. In fact, it reduces to Pythagoras’s formula when the two points are close together and close to the equator.

A drawback of Eq 63 (although far less an issue than the problem it solves) is that it’s numerical ill-conditioned for angles near the antipodal point. One solution is to use the original equation (Eq 60) in these situations. Another is to use the following:

$$\cos\left(\frac{\theta}{2}\right) = \sqrt{\cos^2\left(\frac{L_S - L_U}{2}\right) - \cos(L_S) \cos(L_U) \sin^2\left(\frac{\lambda_S - \lambda_U}{2}\right)} = \frac{\sqrt{\cos\left(\frac{L_S - L_U}{2}\right) - \sqrt{\cos(L_S) \cos(L_U) \sin^2\left(\frac{\lambda_S - \lambda_U}{2}\right)}}}{\sqrt{\cos\left(\frac{L_S - L_U}{2}\right) + \sqrt{\cos(L_S) \cos(L_U) \sin^2\left(\frac{\lambda_S - \lambda_U}{2}\right)}}} \quad \text{Eq 64}$$

The previous two equations can be combined to create a form that is not ill-conditioned when executing an inverse trigonometric function

$$\tan\left(\frac{\theta}{2}\right) = \frac{\sqrt{\sin^2\left(\frac{L_S - L_U}{2}\right) + \cos(L_S) \cos(L_U) \sin^2\left(\frac{\lambda_S - \lambda_U}{2}\right)}}{\sqrt{\cos\left(\frac{L_S - L_U}{2}\right) - \sqrt{\cos(L_S) \cos(L_U) \sin^2\left(\frac{\lambda_S - \lambda_U}{2}\right)}}} \quad \text{Eq 65}$$

An expression for  $\sin(\theta)$  (vice for  $\sin(\frac{1}{2}\theta)$  in Eq 63) can be derived by vector analysis techniques, and is presented in Section 5.2 (Eq 114).

#### 4.2.2 Computing the Azimuth Angles of the Connecting Arc

Having solved for the geocentric angle, the remaining “part” of the indirect problem of geodesy is finding the azimuth angles at (the nadirs of) **U** and **S** of the great circle arc connecting these two points. This determination is slightly complicated by the fact that azimuth angles can vary over the range  $[-\pi, \pi]$ , so that a two-argument arc tangent function must be used.

First, the spherical trigonometry law of sines (Eq 56), applied to the angles at **P** and at **U** yields

$$\sin(\psi_{S/U}) = \frac{\cos(L_S) \sin(\lambda_S - \lambda_U)}{\sin(\theta)} \quad \text{Eq 66}$$

Second, the analogue to the law of cosines for sides (Eq 57) yields

$$\cos(\psi_{S/U}) = \frac{\sin(L_S) \cos(L_U) - \cos(L_S) \sin(L_U) \cos(\lambda_S - \lambda_U)}{\sin(\theta)} \quad \text{Eq 67}$$

Thus

$$\tan(\psi_{S/U}) = \frac{\cos(L_S) \sin(\lambda_S - \lambda_U)}{\sin(L_S) \cos(L_U) - \cos(L_S) \sin(L_U) \cos(\lambda_S - \lambda_U)} \quad \text{Eq 68}$$

Observe that, while Eq 66 and Eq 67 depend upon the geocentric angle  $\theta$  (which is not a “given” for the indirect problem), the solution (Eq 68) for  $\psi_{S/U}$  only depends upon the latitudes and longitudes of the great circle arc end points, which are “givens”. Thus, the solution for  $\psi_{S/U}$  does not “daisy chain” from the solution for  $\theta$ .

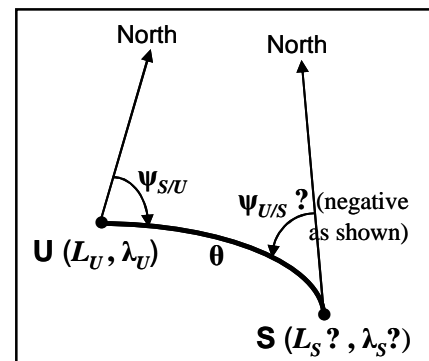
The spherical trigonometry method is symmetric with respect to the user and satellite, so

$$\tan(\psi_{U/S}) = \frac{\cos(L_U) \sin(\lambda_U - \lambda_S)}{\sin(L_U) \cos(L_S) - \cos(L_U) \sin(L_S) \cos(\lambda_U - \lambda_S)} \quad \text{Eq 69}$$

As mentioned previously, in navigation analyses it is useful to employ azimuths in the range  $[-\pi, \pi]$ , where negative values denote angles west of north. In some expositions, the azimuth angle at the second point is taken to be the angle the path would take if it were to continue — i.e., implicitly or explicitly, the first point is taken as the origin and the second as the destination of a trajectory. However, herein, the two points are on an equal basis and the azimuth angle at the second point is that for the great circle path toward the first point. Eq 68 and Eq 69 reflect these points of view.

### 4.3 Solving the Direct Problem of Geodesy

The direct problem of geodesy is stated in Section 1.3 and is illustrated on the right. In taxonomy of spherical triangles in Subsection 4.1.5, this problem falls under case (2). The known elements (and their dimensions) are sides **PU** ( $1/2\pi - L_U$ ) and **US** ( $\theta$ ) and their included angle **PUS** ( $\psi_{S/U}$ ).



#### 4.3.1 Computing the Satellite Latitude

Applying the spherical law of cosines for sides, where the unknown is the side **PS**, yields

$$\sin(L_S) = \sin(L_U) \cos(\theta) + \cos(L_U) \sin(\theta) \cos(\psi_{S/U}) \quad \text{Eq 70}$$

Note that latitude angles are restricted to the range  $[-\pi/2, \pi/2]$ , so in this context, the principal value of the arc sine function always yields the correct solution.

#### 4.3.2 Computing the Satellite Longitude

Finding the satellite longitude  $\lambda_S$  is more complex, as longitude angles are in the range  $[-\pi, \pi]$ .

First, apply the spherical law of sines to the angles at **P** and **U**

$$\sin(\lambda_S - \lambda_U) = \sin(\theta) \frac{\sin(\psi_{S/U})}{\cos(L_S)} \quad \text{Eq 71}$$

Then apply the analogue to the law of cosines for sides

$$\cos(\lambda_S - \lambda_U) = \frac{\cos(L_U) \cos(\theta) - \sin(L_U) \sin(\theta) \cos(\psi_{S/U})}{\cos(L_S)} \quad \text{Eq 72}$$

Thus the satellite longitude can be found from

$$\tan(\lambda_S - \lambda_U) = \frac{\sin(\theta) \sin(\psi_{S/U})}{\cos(L_U) \cos(\theta) - \sin(L_U) \sin(\theta) \cos(\psi_{S/U})} \quad \text{Eq 73}$$

The right-hand side of the above equation only depends upon “given” quantities for the direct problem, and not on the solution for  $L_S$ . After taking the arc tangent, the solution will yield a value of  $\lambda_S - \lambda_U$  in the range  $[-\pi, \pi]$ . If this is added to a value of  $\lambda_U$  (also in the range  $[-\pi, \pi]$ ), the result will be in the range  $[-2\pi, 2\pi]$ . Adjustments of  $\pm 2\pi$  must then be made to obtain a value of  $\lambda_S$  in the range  $(-\pi, \pi]$  — e.g., (1) If  $\lambda_S < 0$ , then  $\lambda_S = \lambda_S + 2\pi$ ; (2) If  $\lambda_S > \pi$ , then  $\lambda_S = \lambda_S - 2\pi$ .

Eq 70 and Eq 73 can be used to find a set of equally-spaced points on the trajectory from **U** to **S** by replacing  $\theta$  by  $k \cdot \theta / N$  and letting  $k = 1, \dots, N$ .

#### 4.3.3 Computing the Azimuth of the Connecting Arc at the Satellite

After  $L_S$  and  $\lambda_S$  have been found, the direct problem solution can be completed by finding the azimuth of the great circle arc at the satellite’s location,  $\psi_{U/S}$ , using Eq 69. An alternative, preferred approach that does not daisy chain solutions is to first apply the law of sines,

$$\sin(\psi_{U/S}) = -\frac{\cos(L_U) \sin(\psi_{S/U})}{\cos(L_S)} \quad \text{Eq 74}$$

A minus sign is introduced in the above equation to cause the two azimuth angles to have opposite signs.

Then apply the analogue to the law of cosines for sides

$$\cos(\psi_{U/S}) = \frac{\sin(L_U)\sin(\theta) - \cos(L_U)\cos(\theta)\cos(\psi_{S/U})}{\cos(L_S)} \quad \text{Eq 75}$$

Thus

$\tan(\psi_{U/S}) = \frac{-\cos(L_U)\sin(\psi_{S/U})}{\sin(L_U)\sin(\theta) - \cos(L_U)\cos(\theta)\cos(\psi_{S/U})} \quad \text{Eq 76}$
------------------------------------------------------------------------------------------------------------------------------------------

Eq 69 and Eq 76 have identical computational burdens.

#### 4.4 Solving a Modified Version of the Direct Problem: Satellite Longitude Known

In this modification to the direct problem, the longitude of **S**,  $\lambda_S$ , is known, and the geocentric angle,  $\theta$ , between **U** and **S** is unknown (the opposite of the assumptions for these quantities in unmodified problem). In taxonomy of spherical triangles in Subsection 4.1.5, this problem falls under case (4). The known elements (and dimensions) are angles **UPS** ( $\lambda_S - \lambda_U$ ) and **SUP** ( $\psi_{S/U}$ ) and their included side **UP** ( $1/2\pi - L_U$ ).

This is a well-posed problem, as every great circle crosses line of longitude exactly once. Also, the solutions presented below do not require daisy-chaining of one solution to another.

##### 4.4.1 Computing the Satellite Latitude

The latitude  $L_S$  is found from the four-part cotangent formula (Eq 58)

$\tan(L_S) = \frac{\sin(L_U)\cos(\lambda_S - \lambda_U) - \sin(\lambda_S - \lambda_U)\cot(\psi_{S/U})}{\cos(L_U)} \quad \text{Eq 77}$
---------------------------------------------------------------------------------------------------------------------------------------

In computing  $L_S$  from Eq 77, observe that, using the arc tangent function, it can be unambiguously found in  $[-\pi/2, \pi/2]$ .

##### 4.4.2 Computing the Geocentric Angle

The geocentric angle  $\theta$  is found from the four-part cotangent formula (Eq 58)

$\cot(\theta) = \frac{\sin(L_U)\cos(\psi_{S/U}) - \sin(\psi_{S/U})\cot(\lambda_S - \lambda_U)}{\cos(L_U)} \quad \text{Eq 78}$
-------------------------------------------------------------------------------------------------------------------------------

In computing  $\theta$  from Eq 78, observe that, using the arc cotangent function, it can be unambiguously found in  $[0, \pi]$ .

#### 4.4.3 Computing the Azimuth of the Connecting Arc at the Satellite

The azimuth angle  $\psi_{U/S}$  is found from the law of cosines for angles (Eq 55)

$$\cos(\psi_{U/S}) = -\cos(\psi_{S/U}) \cos(\lambda_S - \lambda_U) + \sin(\psi_{S/U}) \sin(\lambda_S - \lambda_U) \sin(L_U) \quad \text{Eq 79}$$

In computing  $\psi_{U/S}$  from Eq 79, observe that, using the arc cosine function, it can be unambiguously found in either  $[0, \pi]$  or  $[-\pi, 0]$ . The former is employed when **S** is west of **U**; the latter is employed when **S** is east of **U**.

### 4.5 Solving a Modified Version of the Direct Problem: Satellite Latitude Known

In this modification to the direct problem, the latitude of **S**,  $L_S$ , is known, and the geocentric angle,  $\theta$ , between **U** and **S** is unknown (the opposite of the assumptions for these quantities in unmodified problem). In the taxonomy of spherical triangle problems described in Subsection 4.1.5, this situation falls into case (3). The known elements (and their dimensions) are sides **PU** ( $\frac{1}{2}\pi - L_U$ ) and **PS** ( $\frac{1}{2}\pi - L_S$ ) and adjacent angle **PUS** ( $\psi_{S/U}$ ).

The problem posed may have zero, one or two solutions — because every great circle, except a meridian, has a maximum latitude  $L_{\max}$  and minimum latitude  $-L_{\max}$ . Section 0 contains the formula for  $L_{\max}$ , but is not needed here. Unlike the previous three sections, I am not aware of an analysis that avoids daisy-chaining solutions to this problem.

#### 4.5.1 Computing the Azimuth of the Connecting Arc at the Satellite

The approach begins by applying the law of sines to finding  $\psi_{U/S}$

$$\sin(\psi_{U/S}) = -\frac{\cos(L_U) \sin(\psi_{S/U})}{\cos(L_S)} \quad \text{Eq 80}$$

Consistent with the convention used herein, a minus sign is introduced on the right-hand side of the above equation, causing the two azimuth angles to have opposite signs.

The absolute value of the right-hand side of Eq 80 can be: (a) greater than unity (in which case there is no solution, as  $|L_S| > L_{\max}$ ); (b) equal to unity (in which case there is one solution, as  $|L_S| = L_{\max}$ ); and (c) less than unity (in which case there are two solutions, as  $|L_S| < L_{\max}$ ). If (a) is true, there's nothing more to be done. If (b) is true, refer to Section 0. If (c) is true, label the solutions  $\psi_{U/S,1}$  and  $\psi_{U/S,2}$  and proceed.

#### 4.5.2 Computing the Satellite Longitude

The longitude  $\lambda_S$  is found using one of Napier's Analogies (Eq 59) and using the solutions for  $\psi_{S/U}$  found with Eq 80

$$\tan \frac{1}{2}(\lambda_{S,i} - \lambda_U) = \frac{\cos \frac{1}{2}(L_U - L_S)}{\sin \frac{1}{2}(L_U + L_S)} \cot \frac{1}{2}(\psi_{S/U} - \psi_{U/S,i}) \quad \text{Eq 81}$$

In computing  $\lambda_{S,i}$  ( $i = 1, 2$ ) from Eq 81 using the arc tangent function, each solution can be unambiguously found in  $[\lambda_U - \pi, \lambda_U + \pi]$ .

Eq 81 is indeterminate when  $L_U = -L_S$  (the sine term and the cotangent term are both zero). In this case, an alternate equation can be used:

$$\tan \frac{1}{2}(\lambda_{S,i} - \lambda_U) = \frac{\sin \frac{1}{2}(L_U - L_S)}{\cos \frac{1}{2}(L_U + L_S)} \cot \frac{1}{2}(\psi_{S/U} + \psi_{U/S,i}) \quad \text{Eq 82}$$

Eq 82 is indeterminate when  $L_U = L_S$  (the sine term is zero and the cotangent term is infinite).

#### 4.5.3 Computing the Geocentric Angle

The geocentric angle  $\theta$  is also from Napier's Analogies (Eq 59) using the solutions for  $\psi_{S/U}$  found with Eq 80

$$\tan \frac{1}{2}\theta_i = \frac{\cos \frac{1}{2}(\psi_{S/U} - \psi_{U/S,i})}{\cos \frac{1}{2}(\psi_{S/U} + \psi_{U/S,i})} \cot \frac{1}{2}(L_U + L_S) \quad \text{Eq 83}$$

In computing  $\theta_i$  ( $i = 1, 2$ ) from Eq 83 using the arc tangent function, each solution can be unambiguously found in  $[0, \pi]$ .

Eq 83 is indeterminate when  $L_U = -L_S$  (the cosine term in the numerator is zero and the cotangent term is infinite). In this case, an alternate equation can be used:

$$\tan \frac{1}{2}\theta_i = \frac{\sin \frac{1}{2}(\psi_{S/U} - \psi_{U/S,i})}{\sin \frac{1}{2}(\psi_{S/U} + \psi_{U/S,i})} \tan \frac{1}{2}(L_U - L_S) \quad \text{Eq 84}$$

Eq 84 is indeterminate when  $L_U = L_S$ .

#### 4.6 Latitude Extremes of a Great Circle

A special case of Clairaut's equation\* applies to full great circles (circling the earth), and can be simply derived using the law of sines applied to the angles at two end points of a navigation leg — **U** and **S**, in this case. If both azimuth angles are treated as positive

$$\cos(L_U) \sin(\psi_{S/U}) = \cos(L_S) \sin(\psi_{U/S}) \quad \text{Eq 85}$$

Using the trigonometric identity  $\sin(\psi) = \sin(\pi - \psi)$  yields the interpretation

$\cos(L) \sin(\psi) = C$	Eq 86
--------------------------	-------

Thus all points on a given great circle have the same value, **C**, for the product  $\cos(L) \sin(\psi)$ . Clearly,  $|C| \leq 1$  and is positive for eastward routes and negative for westward routes. Satisfying Eq 86 is a necessary, but not sufficient, condition for the path to be a great circle — e.g., a counterexample is a constant-latitude route.

A common application of Eq 86 is finding the northern- and southern-most latitudes of a great circle. At those points,  $\sin(\psi) = \pm 1$ , so  $\cos(L_{\max}) = |C|$ . The geometric interpretation of a great circle is the intersection of a plane and the surface of the earth, where the plane contains locations **U** and **S** and center of the earth **O**.  $L_{\max}$  is the angle between that plane and the equatorial plane (and  $|C|$  is the cosine of that angle). It follows from Eq 66 that

$\cos(L_{\max}) =  \cos(L_U) \sin(\psi_{S/U})  = \left  \frac{\cos(L_U) \cos(L_S) \sin(\lambda_S - \lambda_U)}{\sin(\theta)} \right $	Eq 87
---------------------------------------------------------------------------------------------------------------------------------------	-------

The longitude  $\lambda(L_{\max})$  corresponding to  $L_{\max}$  can be found using the methodology in Section 4.5. At  $L_{\max}$ , the azimuth  $\psi$  is  $\pm\pi/2$ , where the sign is opposite of the sign of  $\psi_{S/U}$ . Thus from Eq 82

$\tan \frac{1}{2}(\lambda(L_{\max}) - \lambda_U) = \frac{\sin \frac{1}{2}(L_U - L_{\max})}{\cos \frac{1}{2}(L_U + L_{\max})} \cot \frac{1}{2} \left( \psi_{S/U} - \text{sgn}(\psi_{S/U}) \frac{\pi}{2} \right)$	Eq 88
-----------------------------------------------------------------------------------------------------------------------------------------------------------------------------------------------------------------	-------

$\lambda(-L_{\max})$  will occur at  $\lambda(L_{\max}) \pm \pi$ . Eq 88 is derived from the solution to the direct problem of geodesy. An alternate expression for  $\lambda(L_{\max})$ , derived by vector analysis and based on the indirect problem of geodesy, is presented in Chapter 5 (Eq 122).

As stated in Section 4.5, not all great circle routes connecting **U** and **S** or pass through  $L_{\max}$  and  $\lambda(L_{\max})$  or its Southern Hemisphere equivalent. Stated informally, to pass through  $L_{\max}$  and  $\lambda(L_{\max})$  — or  $-L_{\max}$ ,  $\lambda(-L_{\max})$  — a route between **U** and **S** must have enough of a change in

---

\* Alexis Claude de Clairaut (or Clairault) (1713 –1765) was a prominent French mathematician, astronomer and geophysicist.

longitude to bend towards a pole.

Mathematically, a route will pass through  $L_{\max}$  and  $\lambda(L_{\max})$  if the azimuth angles at **U** and **S** are both acute

$$|\psi_{S/U}| < \frac{\pi}{2} \quad \text{and} \quad |\psi_{U/S}| < \frac{\pi}{2} \quad \text{Eq 89}$$

In this situation, the route will achieve larger latitude (pass closer to the North Pole) than either **U** or **S**. Alternatively both azimuth angles may be obtuse

$$|\psi_{S/U}| > \frac{\pi}{2} \quad \text{and} \quad |\psi_{U/S}| > \frac{\pi}{2} \quad \text{Eq 90}$$

In this case, the route will pass closer to the South Pole than either **U** or **S**.

## 4.7 Example Applications

The example applications presented at the end of Chapter 3 are extended in the first three subsections below, to demonstrate the capabilities of spherical trigonometry to provide more complete solutions to relevant technical issues. A fourth application example is added concerning planning a route of flight — a problem which cannot even partially be addressed by the plane trigonometry methodology of Chapter 3.

### 4.7.1 Example 1, Continued: En Route Radar Coverage

Predictions of radar visibility of aircraft as a function of the aircraft's range and altitude, like those in Subsection 3.6.1, are useful. However, for a specific radar installation, a more valuable analysis product is a depiction of the radar's altitude coverage overlaid on a map. As an example, the ARSR-4/ATCBI-6 installation at North Truro, MA (FAA symbol: QEA) is selected. Its coordinates are  $L_U = 42.034531$  deg and  $\lambda_U = -70.054272$  deg, and its antenna elevation is  $h_U = 224$  ft MSL. It is assumed that the terrain elevation in the coverage area is 0 ft MSL, which is correct for the nearby ocean and a bit optimistic (in terms of coverage) for the nearby land.

The sequence of calculations is as follows:

1. Using Eq 50 (third line), the radar's minimum usable elevation angle is found to be  $\alpha_{min} = -0.230$  deg
2. Aircraft altitudes  $h_S$  of 3,000 ft, 10,000 ft and 25,000 ft MSL are selected for the contours to be depicted.
3. Using Eq 50 (second line), the geocentric angles  $\theta$  corresponding to the selected altitudes are found; the associated ground ranges are 85.7 NM, 141.2 NM and 212.6 NM, respectively.

4. Using Eq 50 (first line), the minimum visible aircraft altitude at the maximum ground range (250 NM) is found to be  $h_S = 35,590$  ft.
5. For each contour, using special cases of Eq 63, four  $(L_S, \lambda_S)$  points on the contour — those at the same latitude or the same longitude as the radar — are found as follows:

$$\begin{aligned}
 L_S = L_U \quad \lambda_S = \lambda_U - 2 \arcsin \left( \frac{\sin\left(\frac{1}{2}\theta\right)}{\cos(L_U)} \right) \\
 L_S = L_U \quad \lambda_S = \lambda_U + 2 \arcsin \left( \frac{\sin\left(\frac{1}{2}\theta\right)}{\cos(L_U)} \right) \\
 L_S = L_U - \theta \quad \lambda_S = \lambda_U \\
 L_S = L_U + \theta \quad \lambda_S = \lambda_U
 \end{aligned}
 \tag{Eq 91}$$

6. With a graphics program, the remaining points for each contour are found by “interpolation” using a circle/ellipse.

An alternative to steps 5 and 6 is to compute four sets of points (one set for each contour) using Eq 63, by assuming values for  $L_S$ , and solving for  $\lambda_S$ .

The result of carrying out steps 1-6 for the North Truro radar system is shown in Figure 16. The significance of the contour values is that: (a) Inside a contour, all aircraft having altitudes greater than the contour value are visible to the radar (and aircraft closer to the radar are visible at lower altitudes); and (b) Outside the contour, all aircraft having altitudes less than the contour value are not visible to the radar.

**Consistency Check** — The primary purposes of QEA are (1) surveillance of higher altitude airspace, for use by ARTCC controllers; and (2) surveillance of much of the New England off shore airspace, for use by the Department of Defense (DoD) in their air defense mission. A third purpose is backup surveillance of the Boston TRACON airspace; horizontally, this airspace is a circle centered on Logan Airport with a radius of 60 NM. I have been told by Boston TRACON controllers they consider QEA coverage to extend upward from an altitude of 3,000 ft MSL. Figure 16 is consistent with that statement.

**Cone of Silence** — As discussed in Subsection 3.6.1, ATC radars usually have a cone of silence directly above the antenna; targets within the relatively small cone of silence cannot be detected. Following the usual practice, contours for QEA’s cone of silence are not shown in Figure 16.

The U.S. has an extensive ATC radar infrastructure. Generally, one radar’s cone of silence will be covered by nearby radar(s). In the case of QEA, the Boston ARTCC also receives feeds from

the Nantucket, MA, terminal radar, which covers QEA's cone of silence down to low altitudes (46.5 NM between the two).

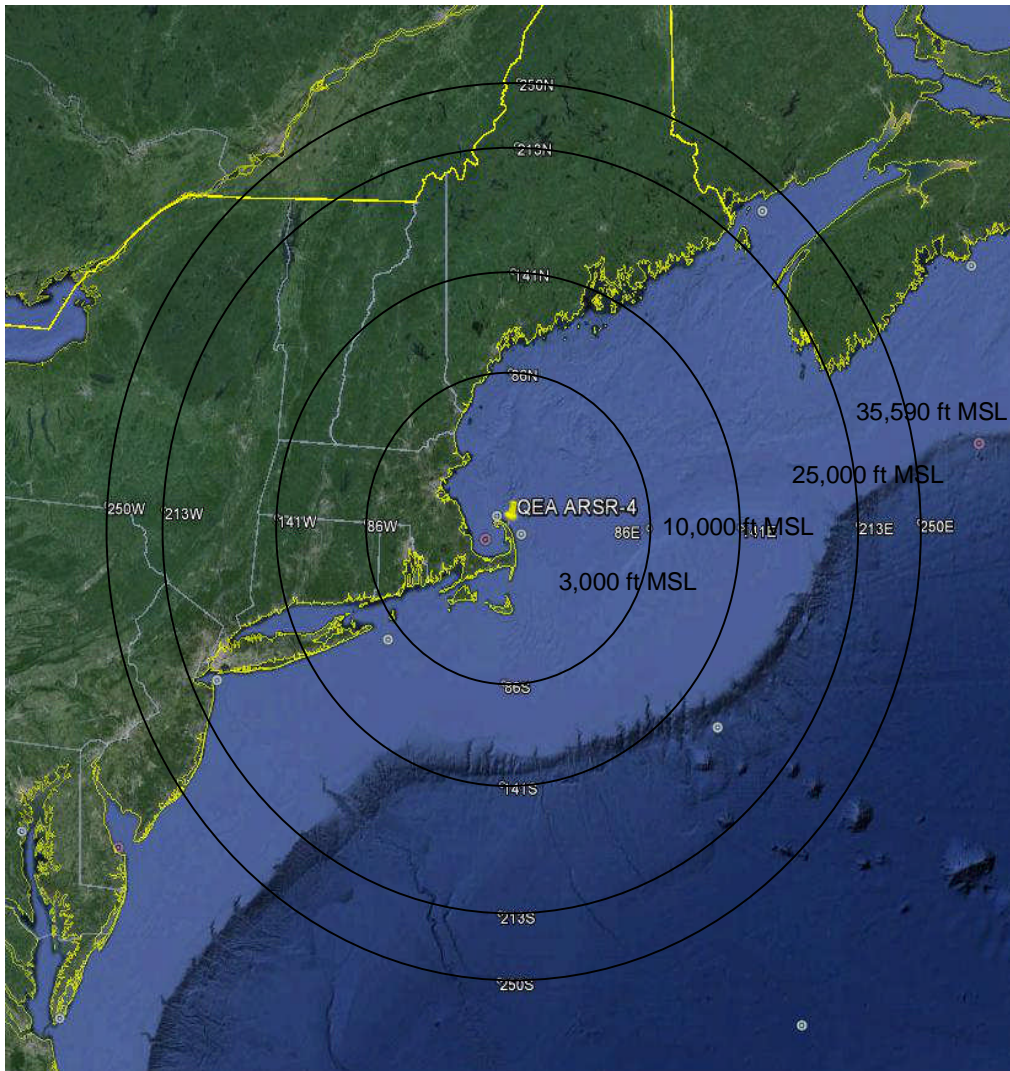


**Figure 16** Aircraft Altitude Visibility Contours for the North Truro, MA, Radar System

#### 4.7.2 Example 2, Continued: Aircraft Instrument Approach Procedure

Subsection 3.6.2 demonstrates computation of the flight profile (altitude vs. distance from threshold) for an aircraft instrument approach procedure. However, for the procedure to be used operationally, the coordinates of the fixes are needed by ATC personnel. Computing them is a straightforward application of spherical geometry.

The sequence of calculations is as follows:

1. Using the website AirNav (Ref. 19), the latitudes and longitudes of the ends of KMCI runway 19L / 1R are obtained.

2. Associating **U** with the 1R end and **S** with the 19L end of the runway, the azimuth of the approach course in the direction away the 19R end is computed, using Eq 68, to be  $\psi_{SU} = 12.89$  deg
3. Associating **U** with the 19R end of the runway and **S** with the fix locations, the coordinates of the fixes are found using Eq 70 and Eq 73.

The results of carrying out steps 1-3 are shown in Table 4.

**Table 4** Computed Fix Coordinates for MCI Runway 19L LPV Approach

Fix Name	UMREW	FELUR	REMNS	ZASBO	YOVNU	GAYLY
Range from Threshold, NM	1.9	4.9	6.2	9.3	12.4	15.5
Latitude, deg	39.337737	39.386470	39.407586	39.457940	39.508292	39.558642
Longitude, deg	-94.692345	-94.677907	-94.671645	-94.656696	-94.641725	-94.626732

#### 4.7.3 Example 3, Continued: Satellite Visibility of/from Earth

Extending the analysis in Subsection 3.6.3 to calculating the latitude/longitude coordinates of the footprint of a geostationary satellite is a good example of the application of the equations in this chapter. Geostationary satellites have circular orbits. They are positioned directly above the earth's equator, and their altitude is selected so that their orbital speed matches the earth's rotation rate. Thus, from the earth, they appear to be stationary. Many communications satellites, including those used for television, are geostationary.

The Wide Area Augmentation System (WAAS) satellites (which augment the Global Positioning System (GPS)) are chosen for this example. The FAA operates three geostationary WAAS satellites (Ref. 20) in order to satisfy the needs of the most demanding civil aviation operations or functions — e.g., guidance for low-visibility approaches or along narrow, obstacle-constrained routes. The parameters used in this calculation are:

- Altitude,  $h = 35,786,000$  m = 19,323 NM
- Mask angle,  $\alpha = 5$  deg
- Radius of the earth,  $R_e = 6,378,137$  m = 3,444 NM (WGS-84 equatorial radius)

Substituting these values into the top line of Eq 53 yields  $\theta = 76.3$  deg. Thus the user's position **U** can be up to 76.3 deg (in terms of the geocentric angle) away from the satellite nadir **N** and satellite will be visible. Since geostationary satellites are directly above the equator, the maximum user latitudes with visibility are  $\pm 76.3$  deg if the user is at the same longitude as the satellite. Similarly, if the user is on the equator, the longitude extremes at which the satellite is visible are  $\pm 76.3$  deg from the satellite longitude.

Obtaining the coordinates of perimeter of the visible region (satellite footprint) involves solving the following modified version of Eq 63:

$$\lambda_U = \lambda_S \pm 2 \arcsin \left( \sqrt{\frac{\sin^2\left(\frac{\theta}{2}\right) - \sin^2\left(\frac{L_U}{2}\right)}{\cos(L_U)}} \right) \tag{Eq 92}$$

A set values is assumed for  $L_U$  in the interval  $[-\theta, \theta]$ , and the corresponding two sets of values for  $\lambda_U$  are computed (which are symmetrically located about  $\lambda_S$ ).

The WAAS satellite labels and longitudes are: AMR, -98 deg; CRE, -107.3 deg; and CRW, -133 deg. When these calculations are carried out, the resulting footprints are depicted in Figure 17. To provide context, the locations of a few airports are also shown in Figure 17. As a check on the calculations herein, Ref. 20 has a page, “WAAS GEO Footprint”, that is very similar to Figure 17.

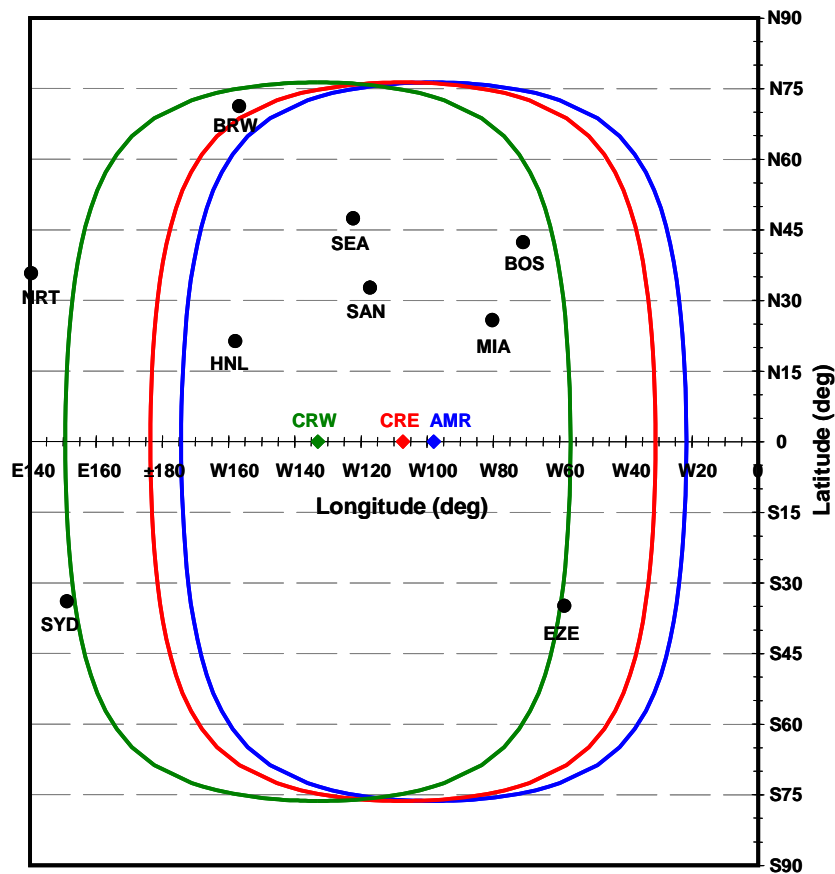


Figure 17 WAAS Satellite Visibility Contours for 5 deg Mask Angle

#### 4.7.4 Example 4: Great Circle Flight Route

For many reasons — e.g., siting of ground-based communications, navigation and surveillance equipment; estimation of fuel consumption; positioning of search and rescue assets; and analysis

of over-flight paths — there is a need to be able to calculate great circle routes between any two places on the earth. Such calculations are a straightforward application of the equations presented earlier in this chapter. The basic approach is: first solve the indirect problem of geodesy (Section 4.2), so that geocentric angle and the azimuth angle of the path starting point are known; then divide the path into equal-length segments and solve the direct problem of geodesy (Section 4.3) for each segment, starting at one end of the path and progressing to the other.

The sequence of calculations is:

1. The latitudes and longitudes,  $(L_U, \lambda_U)$  and  $(L_S, \lambda_S)$ , are obtained for the path end points. The calculation starting point,  $\mathbf{U}$ , may be assigned to either end.
2. The full-path geocentric angle  $\theta$  and starting point azimuth angle  $\psi_{S/U}$  are found from Eq 63 and Eq 68, respectively.
3. The flight path is divided into equal-length segments, which are labeled 1 to N; the points at the ends of the segments are labeled from 0 to N, where  $\mathbf{U}$  has coordinates  $(L_0, \lambda_0)$  and  $\mathbf{S}$  has coordinates  $(L_N, \lambda_N)$ . The starting azimuth angle is  $\psi_{1/0} = \psi_{S/U}$ .
4. For  $i = 1$  to N,
  - (a) the coordinates  $(L_i$  and  $\lambda_i)$  of the end point of the current segment are found using Eq 70 and Eq 73, where the geocentric angle employed is  $\theta/N$  and starting point azimuth angle is  $\psi_{i/i-1}$ ;
  - (b) the azimuth angle at the segment end point  $\psi_{i-1/i}$  is found using Eq 76; and
  - (c) the starting azimuth angle for the next segment is found using  $\psi_{i+1/i} = \psi_{i-1/i} \pm \pi$ .

The result of carrying out steps 1-4 for the route between Boston Logan (BOS) and Tokyo Narita (NRT) airports — using coordinates from Table 5 and Table 6 in Chapter 6 and with  $N = 50$  — is shown in Figure 18.

In addition to showing the predicted BOS-NRT flight path for a spherical earth model (green curve), Figure 18 also shows the predicted path for an ellipsoidal earth model using Vincenty's algorithm (Subsection 2.2.3). Qualitatively, there is close agreement between the two models' predictions. For the scales and line thickness employed, the only perceptible separation between the curves is at the highest latitudes. Chapter 6 addresses quantitative differences between a spherical earth model and Vincenty's algorithm.

For this route the computed geocentric angle is  $\theta = 1.689$  rad, which is 53.8% of  $\pi$  rad ( $\pi$  rad corresponding to the longest possible great circle route). The associated computed distance (using the earth radius defined by Eq 21) is 5,807 NM. Using equations from Section 0, the trajectory's northern-most latitude is N71.7 deg (from Eq 87), which occurs at a longitude of W143.42 deg. If the earth were sliced in half by a plane passing through BOS, NRT and the center of the earth, that plane would make an angle of 71.7 deg with the plane of the equator. The plane would intersect the equator at  $W143.42 \text{ deg} \pm 90 \text{ deg} = W53.42 \text{ deg}$  and  $E126.58 \text{ deg}$ . Using equations from Section 4.5, the trajectory crosses the Arctic Circle (N67 deg latitude) at

the longitudes W104.7 deg and E177.9 deg. Although it appears to be larger, because the convergence of longitude lines at the North Pole is not depicted, 29.2% of the trajectory is within the Arctic Circle.

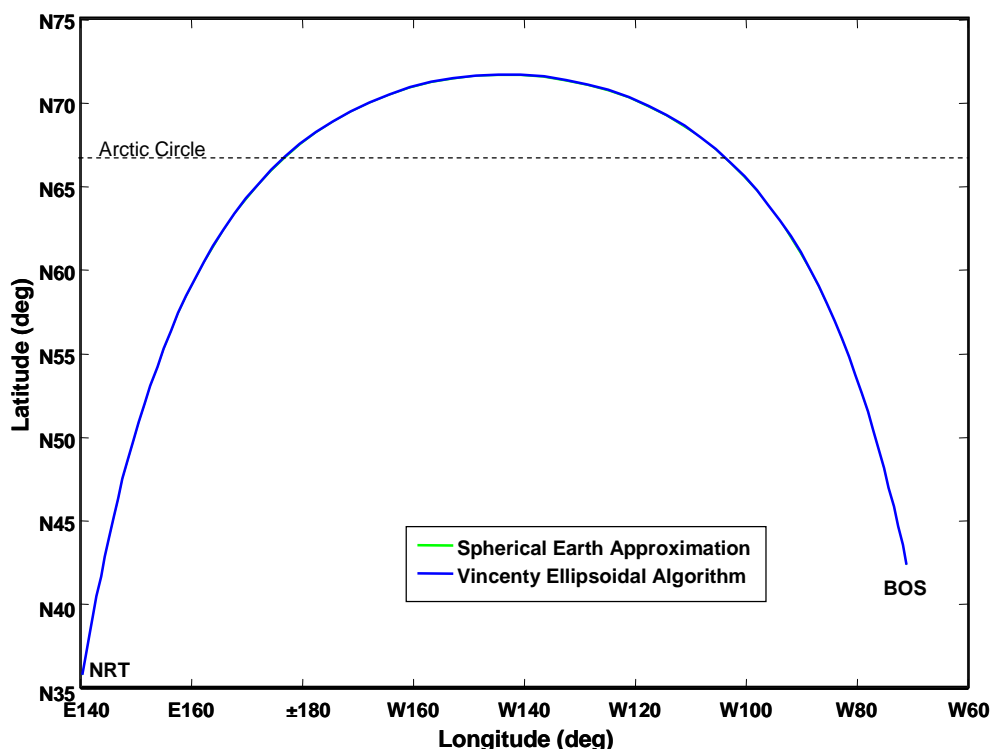


**Figure 18** Latitude/Longitude Coordinates of Paths Connecting BOS and NRT for Spherical-Earth Approximation and Vincenty's Ellipsoidal-Earth Algorithm

#### 4.7.5 Example 5: Radar Display Coordinate Transformations

In this subsection, an ATC radar is associated with the user **U** and an aircraft under surveillance with the satellite **S**. The radar's installation information will include:

- $L_U$  – Radar latitude
- $\lambda_U$  – Radar longitude
- $h_U$  – Radar antenna elevation above sea level

For each radar scan (revolution), a secondary surveillance radar provides three quantities concerning an aircraft:

- $\psi_{S/U}$  – Aircraft azimuth relative to North (from antenna direction)
- $d$  – Slant range between the aircraft and the radar (determined from interrogation-reply time)
- $h_S$  – Aircraft barometric elevation above sea level (reported by transponder)

Some long-range radars may correct for propagation phenomena (e.g., refraction), but those capabilities are not addressed here.

The first goal in ATC radar display is to accurately depict the horizontal separation between aircraft. When two aircraft are only separated vertically (i.e., are at the same latitude and longitude) then their screen icons should overlay each other — or at least be close in comparison to the minimum allowable separation. Figure 19 shows the effect of directly displaying the slant range of two aircraft with only vertical separation (although it exaggerates the effect). Without altitude or elevation angle information, this may be the best that can be done — e.g., for an aircraft without Mode C altitude-reporting capability. Busy airspace typically requires Mode C capability. Generally, the display processing methodology depends upon the radar’s maximum range. Two situations are addressed.

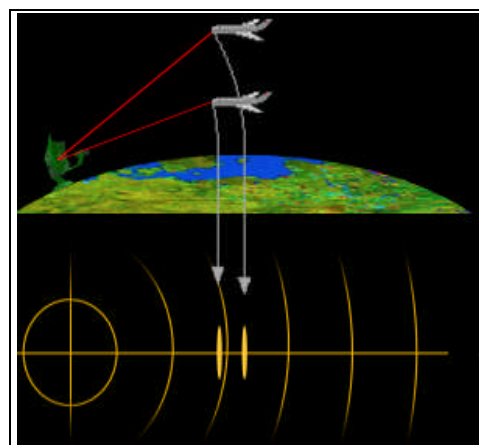


**Figure 19** Effect of Displaying a Target’s Slant Range

**Tangent Plane Display** — This method displays targets on a plane that is tangent to the earth at the radar’s latitude/longitude and sea level. Locations on the plane can be computed in Cartesian (east/north) or polar (range/azimuth) coordinates. The steps in the calculation are:

1. The aircraft elevation angle,  $\alpha$ , is found using Eq 37, modified to account for the radar antenna elevation:

$$\alpha = \arcsin \left( \frac{(h_S - h_U)^2 + 2(h_S - h_U)(R_e + h_U) - d^2}{2d(R_e + h_U)} \right) \quad \text{Eq 93}$$

2. The aircraft range along the tangent plane, **TPRng**, is found (sometimes called the slant-range correction)

$$TPRng = d \cos(\alpha) \quad \text{Eq 94}$$

3. If needed, **TPRng** can be resolved into east and north components

$$\begin{aligned} TPEast &= TPRng \sin(\psi_{S/U}) \\ TPNorth &= TPRng \cos(\psi_{S/U}) \end{aligned} \quad \text{Eq 95}$$

If the earth were flat, this method would be error-free, but it does not fully account for the earth’s curvature. Figure 20 shows the slant range correction error (difference in computed **TPRng** values for two aircraft at the same latitude/longitude but different altitudes) for ranges/altitudes characteristic of a terminal radar. The maximum error is approximately 250 ft. This value should be contrasted with the terminal area separation standard of 3 NM and the en route separation standard of 5 NM (which pertains to aircraft entering terminal airspace from the en route domain). Thus the maximum display processing error is less than 1.5% (terminal) and less than 1% (en route) of the relevant separation standards. This is acceptable for engineering work.

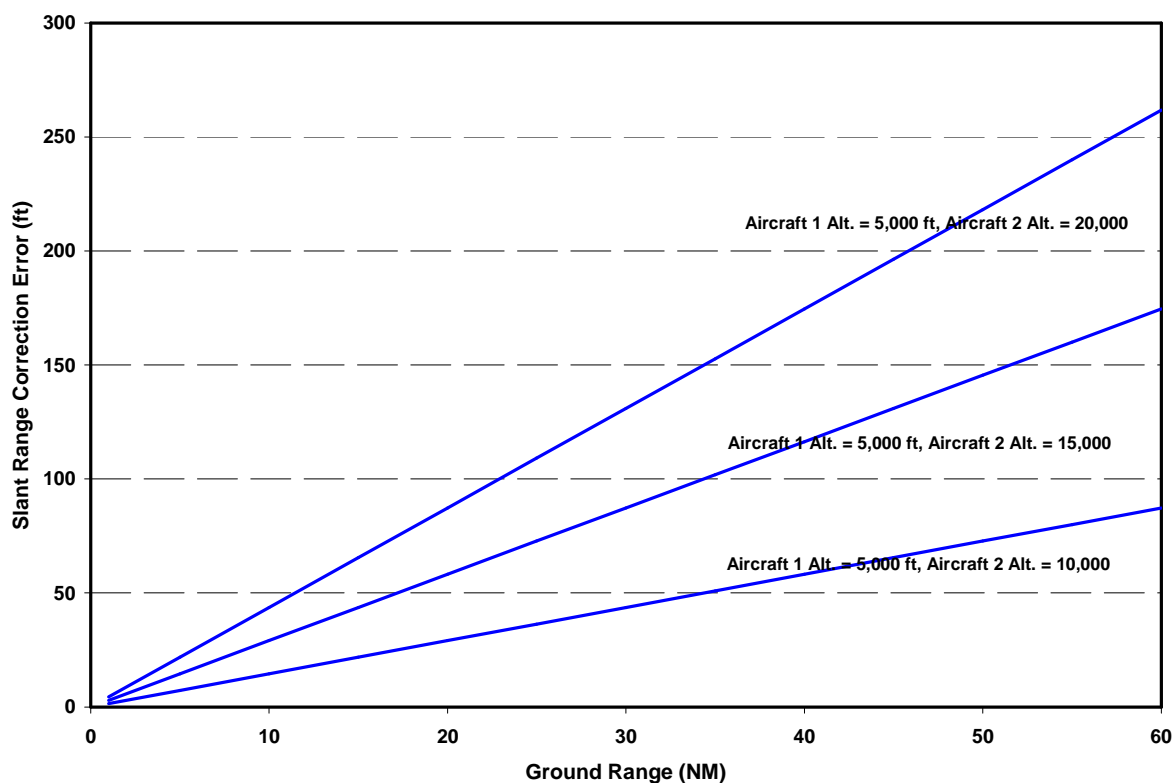


**Figure 20** Separation (Slant Range Correction) Error for Tangent Plane Radar Display

**Latitude/Longitude Display** — Because errors for a tangent plane display increase with the ranges and altitude differences of targets, en route radars use a more accurate method that fully accounts for the earth’s curvature.

1. The target’s geocentric angle relative to the radar is found using Eq 32, modified to account for the radar’s elevation:

$$\theta = 2 \arcsin \left( \frac{1}{2} \sqrt{\frac{d - (h_S - h_U)}{R_e + h_U} \frac{d + (h_S - h_U)}{R_e + h_S}} \right) \quad \text{Eq 96}$$

2. The target’s latitude/longitude are found from Eq 70 and Eq 73, repeated here:

$$L_S = \arcsin(\sin(L_U) \cos(\theta) + \cos(L_U) \sin(\theta) \cos(\psi_{S/U}))$$

$$\lambda_S = \lambda_U + \arctan \left( \frac{\sin(\theta) \sin(\psi_{S/U})}{\cos(L_U) \cos(\theta) - \sin(L_U) \sin(\theta) \cos(\psi_{S/U})} \right) \quad \text{Eq 97}$$

3. The target’s latitude and longitude are converted to the coordinates of a map projection (e.g., Lambert conformal conic) for display to a controller.

En route radar coverage area will include multiple airports, and possibly several major ones. It’s advantageous to display targets relative to the airport locations.

## 5. VECTOR APPROACH TO A UNIFIED 3D SOLUTION

Section 5.1 immediately below provides definitions of the vectors and coordinate frames needed to analyze the geometry of an earth-based user and aircraft or satellite. Section 5.2 addresses the classic indirect problem of geodesy, and provides vector versions of the key equations in Section 4.2. Section 5.3 returns to the problem illustrated by Figure 1. It demonstrates that for some combinations of known and unknown variables, vector analysis provides an alternative method of deriving solutions found in Chapter 3. Section 5.5 addresses the direct problem of geodesy, and shows that, to a significant extent, the equations in Section 4.3 can be found by vector analysis. Lastly, Section 5.3 shows how vector analysis can be used to find the highest latitude of a trajectory.

A list of software packages which generally utilize the vector approach can be found at Ref. 21.

### 5.1 Vector and Coordinate Frame Definitions

#### 5.1.1 Earth-Centered Earth-Fixed (ECEF) Coordinate Frame

The coordinates of the locations of interest on the earth's surface are:

- User position: latitude  $L_U$  and longitude  $\lambda_U$
- Satellite position: latitude  $L_S$ , longitude  $\lambda_S$ , and altitude  $h$

Define the earth-centered earth-fixed (ECEF) coordinate frame  $e$  by (see Figure 21, where the figure's  $\phi$  is our  $L$ ):

- x-axis: lies in the plane of the equator and points toward Greenwich meridian
- y-axis: completes the right-hand orthogonal system
- z-axis: lies along the earth's spin axis.

The location of the user and satellite in the  $e$ -frame are

$$\underline{\mathbf{r}}_{OU}^e = \begin{bmatrix} r_{OU,x}^e \\ r_{OU,y}^e \\ r_{OU,z}^e \end{bmatrix} = \underline{\mathbf{1}}_{OU}^e R_e = \begin{bmatrix} 1_{OU,x}^e \\ 1_{OU,y}^e \\ 1_{OU,z}^e \end{bmatrix} R_e = \begin{bmatrix} \cos(L_U) \cos(\lambda_U) \\ \cos(L_U) \sin(\lambda_U) \\ \sin(L_U) \end{bmatrix} R_e \quad \text{Eq 98}$$

and

$$\underline{\mathbf{r}}_{OS}^e = \begin{bmatrix} r_{OS,x}^e \\ r_{OS,y}^e \\ r_{OS,z}^e \end{bmatrix} = \underline{\mathbf{1}}_{OS}^e (R_e + h) = \begin{bmatrix} 1_{OS,x}^e \\ 1_{OS,y}^e \\ 1_{OS,z}^e \end{bmatrix} (R_e + h) = \begin{bmatrix} \cos(L_S) \cos(\lambda_S) \\ \cos(L_S) \sin(\lambda_S) \\ \sin(L_S) \end{bmatrix} (R_e + h) \quad \text{Eq 99}$$

Here  $\underline{\mathbf{1}}_{OU}^e$  and  $\underline{\mathbf{1}}_{OS}^e$  are unit vectors associated with  $\underline{\mathbf{r}}_{OU}^e$  and  $\underline{\mathbf{r}}_{OS}^e$ , respectively.

Given  $\underline{\mathbf{r}}_{OU}^e$ , the user's latitude and longitude can be found from

$$L_U = \arctan\left(\frac{r_{OU,z}^e}{\sqrt{(r_{OU,x}^e)^2 + (r_{OU,y}^e)^2}}\right) = \arcsin\left(\frac{r_{OU,z}^e}{R_e}\right) \quad \text{Eq 100}$$

$$\lambda_U = \arctan(r_{OU,y}^e, r_{OU,x}^e)$$

Similarly, given,  $\underline{\mathbf{r}}_{OS}^e$ , the satellite's latitude and longitude can be found from

$$L_S = \arctan\left(\frac{r_{OS,z}^e}{\sqrt{(r_{OS,x}^e)^2 + (r_{OS,y}^e)^2}}\right) = \arcsin\left(\frac{r_{OS,z}^e}{R_e + h}\right) \quad \text{Eq 101}$$

$$\lambda_S = \arctan(r_{OS,y}^e, r_{OS,x}^e)$$

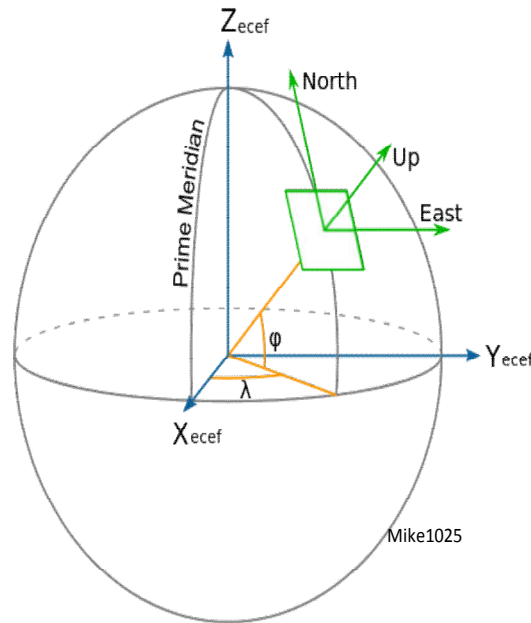


**Figure 21** Vector Technique Coordinate Frames of Interest

### 5.1.2 Local-Level Coordinate Frame at User's Position

Define a local-level coordinate frame  $u$  corresponding to the user's position

- e-axis point east
- n-axis points north
- u-axis points up (away from earth's center).

The direction cosine matrix which rotates the  $e$ -frame into the  $u$ -frame is

$$\mathbf{C}_e^u = \mathbf{T} \mathbf{T}_2(-L_U) \mathbf{T}_3(\lambda_U) \quad \text{Eq 102}$$

where  $\mathbf{T}_i(\xi)$  denotes the rotation matrix about axis  $i$  by angle  $\xi$ .

$$\begin{aligned}\mathbf{T}_1(\xi) &= \begin{bmatrix} 1 & 0 & 0 \\ 0 & \cos(\xi) & \sin(\xi) \\ 0 & -\sin(\xi) & \cos(\xi) \end{bmatrix} \\ \mathbf{T}_2(\xi) &= \begin{bmatrix} \cos(\xi) & 0 & -\sin(\xi) \\ 0 & 1 & 0 \\ \sin(\xi) & 0 & \cos(\xi) \end{bmatrix} \\ \mathbf{T}_3(\xi) &= \begin{bmatrix} \cos(\xi) & \sin(\xi) & 0 \\ -\sin(\xi) & \cos(\xi) & 0 \\ 0 & 0 & 1 \end{bmatrix}\end{aligned}\tag{Eq 103}$$

and  $\mathbf{T}$  denotes the axis-permutation matrix

$$\mathbf{T} = \begin{bmatrix} 0 & 1 & 0 \\ 0 & 0 & 1 \\ 1 & 0 & 0 \end{bmatrix}\tag{Eq 104}$$

Thus

$$\mathbf{C}_e^u = \begin{bmatrix} -\sin(\lambda_U) & \cos(\lambda_U) & 0 \\ \sin(-L_U)\cos(\lambda_U) & \sin(-L_U)\sin(\lambda_U) & \cos(-L_U) \\ \cos(-L_U)\cos(\lambda_U) & \cos(-L_U)\sin(\lambda_U) & -\sin(-L_U) \end{bmatrix}\tag{Eq 105}$$

### 5.1.3 User and Satellite Positions in User's Local-Level Frame

The positions of the user and satellite in the  $u$ -frame are, respectively

$$\underline{\mathbf{r}}_{OU}^u = \mathbf{C}_e^u \begin{bmatrix} r_{OU,x}^e \\ r_{OU,y}^e \\ r_{OU,z}^e \end{bmatrix} = \begin{bmatrix} r_{OU,e}^u \\ r_{OU,n}^u \\ r_{OU,u}^u \end{bmatrix} = \begin{bmatrix} 0 \\ 0 \\ 1 \end{bmatrix} R_e\tag{Eq 106}$$

and

$$\underline{\mathbf{r}}_{OS}^u = \mathbf{C}_e^u \begin{bmatrix} r_{OS,x}^e \\ r_{OS,y}^e \\ r_{OS,z}^e \end{bmatrix} = \begin{bmatrix} r_{OS,e}^u \\ r_{OS,n}^u \\ r_{OS,u}^u \end{bmatrix} = \begin{bmatrix} \cos(L_S)\sin(\lambda_S - \lambda_U) \\ -\cos(L_S)\sin(L_U)\cos(\lambda_S - \lambda_U) + \sin(L_S)\cos(L_U) \\ \cos(L_S)\cos(L_U)\cos(\lambda_S - \lambda_U) + \sin(L_S)\sin(L_U) \end{bmatrix} (R_e + h)\tag{Eq 107}$$

Thus, using Eq 106 and Eq 107, the vector from  $\mathbf{U}$  to  $\mathbf{S}$  is

$$\underline{\mathbf{r}}_{US}^u = \underline{\mathbf{r}}_{OS}^u - \underline{\mathbf{r}}_{OU}^u = \begin{bmatrix} r_{US,e}^u \\ r_{US,n}^u \\ r_{US,u}^u \end{bmatrix} = \begin{bmatrix} (R_e + h) \cos(L_U) \sin(\lambda_S - \lambda_U) \\ -(R_e + h) \cos(L_S) \sin(L_S) \cos(\lambda_S - \lambda_U) + (R_e + h) \sin(L_S) \cos(L_U) \\ (R_e + h) \cos(L_S) \cos(L_U) \cos(\lambda_S - \lambda_U) + (R_e + h) \sin(L_S) \sin(L_U) - R_e \end{bmatrix} \quad \text{Eq 108}$$

The horizontal and vertical components of  $\underline{\mathbf{r}}_{US}^u$  can be expressed as

$$r_{US,horiz}^u = \sqrt{(r_{US,e}^u)^2 + (r_{US,n}^u)^2} = (R_e + h) \sin(\theta) \quad \text{Eq 109}$$

$$r_{US,vert}^u = r_{US,u}^u = (R_e + h) \cos(\theta) - R_e$$

Eq 109 can be found from Figure 1 by inspection. It can also be derived analytically from Eq 108 using Eq 60.

Two angles associated with  $\underline{\mathbf{r}}_{US}^u$  are of interest

- $\Psi_{S/U}$  – The azimuth angle of the horizontal component of  $\underline{\mathbf{r}}_{US}^u$ , measured clockwise from north
- $\alpha$  – The elevation angle of  $\underline{\mathbf{r}}_{US}^u$ , measured from the horizontal plane

$$\Psi_{S/U} = \arctan(r_{US,e}^u, r_{US,n}^u) \quad \text{Eq 110}$$

$$\alpha = \arctan\left(\frac{r_{US,u}^u}{\sqrt{(r_{US,e}^u)^2 + (r_{US,n}^u)^2}}\right) \quad \text{Eq 111}$$

The two-argument arc tangent function is used in Eq 110 because azimuth angles lie in the range  $(-\pi, \pi]$ .

The length  $d$  of  $\underline{\mathbf{r}}_{US}^u$  is also of interest

$$d = \sqrt{(r_{US,e}^u)^2 + (r_{US,n}^u)^2 + (r_{US,u}^u)^2} \quad \text{Eq 112}$$

## 5.2 Solving the Indirect Problem of Geodesy

### 5.2.1 Geocentric Angle from Latitudes and Longitudes, by Vector Dot Product

The vectors  $\underline{\mathbf{r}}_{OU}^e$  and  $\underline{\mathbf{r}}_{OS}^e$  meet at the earth's center, in geocentric angle  $\theta$ . The dot product of these vectors, normalized by the product of their lengths, yields

$$\begin{aligned}
 \underline{\mathbf{1}}_{OU}^e \bullet \underline{\mathbf{1}}_{OS}^e &= \underline{\mathbf{1}}_{OU,x}^e \underline{\mathbf{1}}_{OS,x}^e + \underline{\mathbf{1}}_{OU,y}^e \underline{\mathbf{1}}_{OS,y}^e + \underline{\mathbf{1}}_{OU,z}^e \underline{\mathbf{1}}_{OS,z}^e \\
 &= \cos(L_U) \cos(L_S) \cos(\lambda_U - \lambda_S) + \sin(L_U) \sin(L_S) \\
 &= \cos(\theta)
 \end{aligned}
 \tag{Eq 113}$$

Eq 113 demonstrates that if one forms the vector dot product indicated on the first line, the result will be the same as if one performed the scalar operations indicated on the second line, which in turn is equal to the equation for  $\cos(\theta)$  found by spherical trigonometry (Eq 60).

### 5.2.2 Geocentric Angle from Latitudes and Longitudes, by Vector Cross Product

The cross product of vectors  $\underline{\mathbf{r}}_{OU}^e$  and  $\underline{\mathbf{r}}_{OS}^e$ , normalized by the product of their lengths, yields another expression for the geocentric angle:

$$\begin{aligned}
 \sin(\theta) &= \frac{|\underline{\mathbf{1}}_{OU}^e \times \underline{\mathbf{1}}_{OS}^e|}{|\underline{\mathbf{1}}_{OU}^e| |\underline{\mathbf{1}}_{OS}^e|} \\
 &= \sqrt{\cos^2(L_U) \sin^2(L_S) + \cos^2(L_S) \sin^2(L_U) + \cos^2(L_U) \cos^2(L_S) \sin^2(\lambda_S - \lambda_U) \dots} \\
 &\quad \dots - 2 \cos(L_U) \sin(L_U) \cos(L_S) \sin(L_S) \cos(\lambda_S - \lambda_U)
 \end{aligned}
 \tag{Eq 114}$$

Since  $\theta$  lies in  $[0, \pi]$ , solving Eq 114 for  $\theta$  using the arc sine function yields both the correct angle and an extraneous solution. Another source of information, such as Eq 113, also must be used.

### 5.2.3 Path Azimuth Angles, from Latitudes and Longitudes

By substituting two elements of  $\underline{\mathbf{r}}_{US}^u$  from Eq 108 into Eq 110,  $\psi_{S/U}$  is found to be equal to

$$\psi_{S/U} = \arctan(r_{US,e}^u, r_{US,n}^u) = \arctan\left(\frac{\cos(L_S) \sin(\lambda_S - \lambda_U)}{\sin(L_S) \cos(L_U) - \cos(L_S) \sin(L_U) \cos(\lambda_S - \lambda_U)}\right)
 \tag{Eq 115}$$

Eq 115 demonstrates that if one computes  $\psi_{S/U}$  using the arc tangent function with two elements of the vector  $\underline{\mathbf{r}}_{US}^u$  as arguments, the result will be the same as if one computed  $\psi_{S/U}$  using the arc tangent indicated on the right-hand side. The latter is equal to the equation for  $\psi_{S/U}$  found by spherical trigonometry (Eq 68).

The labeling of the points **U** and **S** in Eq 115 can be reversed, yielding

$$\psi_{U/S} = \arctan\left(\frac{\cos(L_U) \sin(\lambda_U - \lambda_S)}{\sin(L_U) \cos(L_S) - \cos(L_U) \sin(L_S) \cos(\lambda_U - \lambda_S)}\right)
 \tag{Eq 116}$$

While the arguments on right-hand sides of Eq 115 and Eq 116 are shown (for convenience) as ratios, the azimuth angles should be computed using a two-argument arc tangent function.

Eq 116 is derived by vector analysis (rather than by spherical trigonometry). However, it not a vector equation *per se* — i.e., it does not make use of vectors or the components of vectors. The vector equation for  $\psi_{U/S}$  is

$$\psi_{U/S} = \arctan(r_{SU,e}^s, r_{SU,n}^s) \quad \text{Eq 117}$$

Vector  $\underline{\mathbf{r}}_{SU}^s$  is found from

$$\underline{\mathbf{r}}_{SU}^s = \underline{\mathbf{r}}_{OU}^s - \underline{\mathbf{r}}_{OS}^s = \mathbf{C}_e^s(\underline{\mathbf{r}}_{OU}^e - \underline{\mathbf{r}}_{OS}^e) \quad \text{Eq 118}$$

where  $\underline{\mathbf{r}}_{OU}^e$  and  $\underline{\mathbf{r}}_{OS}^e$  are given by Eq 98 and Eq 99, respectively, and (interpreting Eq 105)

$$\mathbf{C}_e^s = \begin{bmatrix} -\sin(\lambda_S) & \cos(\lambda_S) & 0 \\ \sin(-L_S)\cos(\lambda_S) & \sin(-L_S)\sin(\lambda_S) & \cos(-L_S) \\ \cos(-L_S)\cos(\lambda_S) & \cos(-L_S)\sin(\lambda_S) & -\sin(-L_S) \end{bmatrix} \quad \text{Eq 119}$$

### 5.3 Corollaries of the Indirect Problem Solution

#### 5.3.1 Latitude Extremes of a Great Circle

I am not aware of a vector form of Clairaut's equation as used herein (Eq 86), or in general. However, the most useful application of Clairaut's equation, determining the northern- and southern-most latitudes of a great circle, is readily found by vector analysis. The cross product of unit vectors  $\underline{\mathbf{1}}_{OU}^e$  (Eq 98) and  $\underline{\mathbf{1}}_{OS}^e$  (Eq 99) is normal to the plane of the great circle containing **U** and **S**.

$$\begin{aligned} \underline{\mathbf{1}}_{OU}^e \times \underline{\mathbf{1}}_{OS}^e &= \begin{bmatrix} (\underline{\mathbf{1}}_{OU}^e \times \underline{\mathbf{1}}_{OS}^e)_x \\ (\underline{\mathbf{1}}_{OU}^e \times \underline{\mathbf{1}}_{OS}^e)_y \\ (\underline{\mathbf{1}}_{OU}^e \times \underline{\mathbf{1}}_{OS}^e)_z \end{bmatrix} = \begin{bmatrix} \underline{1}_{OU,y}^e \underline{1}_{OS,z}^e - \underline{1}_{OU,z}^e \underline{1}_{OS,y}^e \\ \underline{1}_{OU,z}^e \underline{1}_{OS,x}^e - \underline{1}_{OU,x}^e \underline{1}_{OS,z}^e \\ \underline{1}_{OU,x}^e \underline{1}_{OS,y}^e - \underline{1}_{OU,y}^e \underline{1}_{OS,x}^e \end{bmatrix} \\ &= \begin{bmatrix} \cos(L_U)\sin(L_S)\sin(\lambda_U) - \sin(L_U)\cos(L_S)\sin(\lambda_S) \\ \sin(L_U)\cos(L_S)\cos(\lambda_S) - \cos(L_U)\sin(L_S)\cos(\lambda_U) \\ \cos(L_U)\cos(L_S)\sin(\lambda_S - \lambda_U) \end{bmatrix} \end{aligned} \quad \text{Eq 120}$$

When  $\underline{\mathbf{1}}_{OU}^e \times \underline{\mathbf{1}}_{OS}^e$  is adjusted to unit length (Eq 114), its z-component is equal to the cosine of the latitude of the highest (and lowest) point on the great circle that includes the route in question (projection of a unit vector onto the earth's spin axis). Thus,

$$\cos(L_{\max}) = \left| \frac{\cos(L_U)\cos(L_S)\sin(\lambda_S - \lambda_U)}{\sin(\theta)} \right| \quad \text{Eq 121}$$

Eq 121 is identical to Eq 87, demonstrating that manipulating the components of  $\underline{\mathbf{1}}_{OU}^e$  and  $\underline{\mathbf{1}}_{OS}^e$

yields the same result as Clairaut's equation.

The longitude where the highest latitude is achieved can be found from the x- and y-components of vector  $\underline{\mathbf{1}}_{\text{OU}}^e \times \underline{\mathbf{1}}_{\text{OS}}^e$  (from Eq 120).

$$\lambda(L_{\max}) = \arctan\left(\frac{(\underline{\mathbf{1}}_{\text{OU}}^e \times \underline{\mathbf{1}}_{\text{OS}}^e)_y}{(\underline{\mathbf{1}}_{\text{OU}}^e \times \underline{\mathbf{1}}_{\text{OS}}^e)_x}\right) = \arctan\left(\frac{\sin(L_U)\cos(L_S)\cos(\lambda_S) - \cos(L_U)\sin(L_S)\cos(\lambda_U)}{\cos(L_U)\sin(L_S)\sin(\lambda_U) - \sin(L_U)\cos(L_S)\sin(\lambda_S)}\right) \quad \text{Eq 122}$$

The statements found at the end of Section 4.4 are valid here as well. Not all great circle routes between two points on the earth's surface, **U** and **S**, will contain one of the points where the full great circle passes closest to the North or South Poles. Criteria for when a route will include a point closest to either pole are given in Section 4.4.

### 5.3.2 Locus of Points on a Great Circle

From Eq 98, it follows that any point **X** on the earth has the *e*-frame coordinates  $\underline{\mathbf{r}}_{\text{OX}}^e$

$$\underline{\mathbf{r}}_{\text{OX}}^e = \begin{bmatrix} r_{\text{OX},x}^e \\ r_{\text{OX},y}^e \\ r_{\text{OX},z}^e \end{bmatrix} = \underline{\mathbf{1}}_{\text{OX}}^e R_e = \begin{bmatrix} 1_{\text{OX},x}^e \\ 1_{\text{OX},y}^e \\ 1_{\text{OX},z}^e \end{bmatrix} R_e = \begin{bmatrix} \cos(L_X) \cos(\lambda_X) \\ \cos(L_X) \sin(\lambda_X) \\ \sin(L_X) \end{bmatrix} R_e \quad \text{Eq 123}$$

Here  $L_X$  and  $\lambda_X$  are the latitude and longitude of **X**, respectively. In order for **X** to be on the great circle containing **U** and **S**, the vector  $\underline{\mathbf{r}}_{\text{OX}}^e$  must be orthogonal to the vector  $\underline{\mathbf{1}}_{\text{OU}}^e \times \underline{\mathbf{1}}_{\text{OS}}^e$  — that is, the dot product of these two vectors must be zero. One can then solve for  $L_X$  in terms of  $\lambda_X$  and the coordinates of **U** and **S**.

$$\tan(L_X) = -\frac{(\underline{\mathbf{1}}_{\text{OU}}^e \times \underline{\mathbf{1}}_{\text{OS}}^e)_x \cos(\lambda_X) + (\underline{\mathbf{1}}_{\text{OU}}^e \times \underline{\mathbf{1}}_{\text{OS}}^e)_y \sin(\lambda_X)}{(\underline{\mathbf{1}}_{\text{OU}}^e \times \underline{\mathbf{1}}_{\text{OS}}^e)_z} \quad \text{Eq 124}$$

Solving for  $\lambda_X$  in terms of  $L_X$  and the coordinates of **U** and **S** is more complicated. This is a consequence of the fact that while every great circle crosses every line of longitude exactly once, a great circle may cross a line of latitude zero, one or two times. Section 4.5 addresses this issue using spherical trigonometry.

## 5.4 Computing Satellite Elevation Angle and Slant Range

Section 5.2 shows that, if the latitude/longitude of locations **U** and **S** on the surface are known, the vector method can be used to find the three angles  $\theta$ ,  $\psi_{S/U}$  and  $\psi_{U/S}$ . However, the equations in Section 5.2 do not include **h**, **d** or **a**. (all of which are related to the height of the aircraft/

satellite above the earth's surface). The two subsections immediately below show that if  $h$  and  $\theta$  are known, then  $d$  and  $\alpha$  can be found by the vector method. Moreover, the expressions that are derived are identical to those found in Chapter 3 using the coordinate-free method.

The four other possible equations associated with an aircraft or satellite above the earth when the geocentric angle is known — finding  $h$  or  $d$  from  $\alpha$  and  $\theta$ , and finding  $h$  or  $\alpha$  from  $d$  and  $\theta$  — are not pursued. For these variable combinations, the solutions for the unknown variables will involve manipulation of the scalar components of  $\underline{\mathbf{r}}_{US}^u$ . That being the case, one may as well utilize the scalar equations derived in Chapter 3.

#### 5.4.1 Solution for Elevation Angle from Altitude and Geocentric Angle

As shown in Eq 111 the satellite elevation angle can be found from the components of  $\underline{\mathbf{r}}_{US}^u$ . Using Eq 109, Eq 111 can be expanded as

$$\tan(\alpha) = \frac{(R_e + h)\cos(\theta) - R_e}{(R_e + h)\sin(\theta)} = \frac{h \cos(\theta) - 2R_e \sin^2\left(\frac{1}{2}\theta\right)}{(R_e + h)\sin(\theta)} \quad \text{Eq 125}$$

The right-hand side of Eq 125 is identical to the first line of Eq 35, demonstrating that manipulating the components of  $\underline{\mathbf{r}}_{US}^u$  can yield the same value for  $\alpha$  as the scalar methodology used in Chapter 3.

#### 5.4.2 Solution for Slant Range from Altitude and Geocentric Angle

The user-satellite slant range can be found by substituting both lines of Eq 109 into Eq 112, yielding:

$$d = \sqrt{h^2 + 4R_e(R_e + h)\sin^2\left(\frac{1}{2}\theta\right)} \quad \text{Eq 126}$$

Eq 126 is identical to the second line of Eq 39. This demonstrates that applying Pythagoras's theorem to the components of  $\underline{\mathbf{r}}_{US}^u$  (Eq 112) yields the same value for  $d$  as the scalar methodology used in Chapter 3.

### 5.5 *Solving the Direct Problem of Geodesy*

The approach used to finding  $L_S$  and  $\lambda_S$  is to form  $\underline{\mathbf{r}}_{OS}^e$  and utilize its components. Then,  $\psi_{U/S}$  can be addressed utilizing  $L_S$  and/or  $\lambda_S$ .

Given  $L_U$ ,  $\lambda_U$ ,  $\theta$  and  $\psi_{S/U}$ ,  $\mathbf{N}$  is constrained but  $\mathbf{S}$  is not. Consequently, form right triangle **OUS** with right angle at **U** and sides  $R_e$ ,  $d$  and hypotenuse  $(R_e + h)$ , where

$$d = R_e \tan(\theta)$$

$$R_e + h = \frac{R_e}{\cos(\theta)} \quad \text{Eq 127}$$

Then  $\underline{\mathbf{r}}_{US}^u$  is given by

$$\underline{\mathbf{r}}_{US}^u = \begin{bmatrix} r_{US,e}^u \\ r_{US,n}^u \\ r_{US,u}^u \end{bmatrix} = \begin{bmatrix} \tan(\theta) \sin(\psi_{S/U}) \\ \tan(\theta) \cos(\psi_{S/U}) \\ 0 \end{bmatrix} R_e \quad \text{Eq 128}$$

Utilizing Eq 98 and Eq 105 yields

$$\underline{\mathbf{r}}_{OS}^e = \underline{\mathbf{r}}_{OU}^e + \underline{\mathbf{r}}_{US}^e = \underline{\mathbf{r}}_{OU}^e + (\mathbf{C}_e^u)^T \underline{\mathbf{r}}_{US}^u = \begin{bmatrix} r_{OS,x}^e \\ r_{OS,y}^e \\ r_{OS,z}^e \end{bmatrix} \quad \text{Eq 129}$$

$$= \begin{bmatrix} \cos(L_U) \cos(\lambda_U) - \sin(\lambda_U) \tan(\theta) \sin(\psi_{S/U}) + \sin(-L_U) \cos(\lambda_U) \tan(\theta) \cos(\psi_{S/U}) \\ \cos(L_U) \sin(\lambda_U) + \cos(\lambda_U) \tan(\theta) \sin(\psi_{S/U}) + \sin(-L_U) \sin(\lambda_U) \tan(\theta) \cos(\psi_{S/U}) \\ \sin(L_U) + \cos(-L_U) \tan(\theta) \cos(\psi_{S/U}) \end{bmatrix} R_e$$

From Eq 101 and Eq 129 it follows that

$$L_S = \arcsin(\sin(L_U) \cos(\theta) + \cos(L_U) \sin(\theta) \cos(\psi_{S/U}))$$

$$\lambda_S = \arctan\left(\frac{\cos(L_U) \sin(\lambda_U) + \cos(\lambda_U) \tan(\theta) \sin(\psi_{S/U}) - \sin(L_U) \sin(\lambda_U) \tan(\theta) \cos(\psi_{S/U})}{\cos(L_U) \cos(\lambda_U) - \sin(\lambda_U) \tan(\theta) \sin(\psi_{S/U}) - \sin(L_U) \cos(\lambda_U) \tan(\theta) \cos(\psi_{S/U})}\right) \quad \text{Eq 130}$$

While the right-hand side of the second line of Eq 130 involves a ratio,  $\lambda_S$  should be computed using a two-argument arc tangent function. Eq 130 can be used to find a set of equally-spaced points on the trajectory from  $\mathbf{U}$  to  $\mathbf{S}$  by replacing  $\theta$  by  $k \cdot \theta / N$  and letting  $k = 1, \dots, N$ .

Once  $L_S$  and  $\lambda_S$  have been found,  $\psi_{U/S}$  can be computed using Eq 116.

It's of interest to compare the equations in this section to those for the same/similar quantities developed using spherical trigonometry in Section 4.3. First, the expressions in Eq 130 for  $L_S$  and  $\lambda_S$  only involve known quantities — i.e., there is no “daisy chaining” of the solution for one unknown quantity to determine the other. The equations for  $L_S$  in Eq 130 and Eq 70 are identical. A difference is that Eq 130 is a solution for  $\lambda_S$  while Eq 73 is a solution for  $\lambda_S - \lambda_U$ ; thus, the right-hand sides of these equations are necessarily different. In terms of the azimuth angle  $\psi_{U/S}$ , Eq 116 in this chapter daisy chains from the solutions for  $L_S$  and  $\lambda_S$  in Eq 130, while Eq 76 in Chapter 5 does not involving daisy chaining of solutions.

## 6. SPHERICAL EARTH APPROXIMATION ACCURACY

### 6.1 Evaluation Methodology and Scenarios

To analyze the accuracy of the spherical earth approximation, a set of fourteen airports were selected. This set is intended to be representative of current aviation activity. However, in terms of frequency of operations, these airports over-emphasize longer routes — e.g., some routes are too long for commercial transport aircraft at this time. The result is a total of 91 possible paths between airport pairs. For each pair, estimates of the length of the shortest path are computed for:

- WGS-84 ellipsoidal earth model utilizing Vincenty's algorithm (Subsection 2.2.3);
- Spherical approximation of the earth utilizing a constant radius; and
- Spherical representation of the earth utilizing several methods for tailoring the radius of curvature (RoC) to the path involved.

The airports employed for this analysis were partitioned into two groups of seven each — CONUS (Table 5) and International (Table 6). The CONUS group essentially spans the CONUS land area. It includes paths of various lengths and orientations (e.g., predominately east-west and predominately north-south). The International airport group, which includes one each in Alaska and Hawaii, provides additional pairs with greater separation but also with varying orientations. Airports near the Arctic Circle and south of the Equator are included. HNL-JNB is the longest path (10,365 NM). As a point of interest, the current longest scheduled commercial flight route is 8,285 NM, between Newark and Singapore.

**Table 5** CONUS Airports Used in Analysis

Airport Name (IATA Code)	Lat. (deg)	Lon. (deg)	Major City Served
Gen. Edward Lawrence Logan International (BOS)	42.3629722	-71.0064167	Boston, MA
Ronald Reagan Washington National (DCA)	38.8522	-77.0378	Washington, DC
O'Hare International (ORD)	41.9786	-87.9047	Chicago, IL
Miami International (MIA)	25.7933	-80.2906	Miami, FL
San Diego International (SAN)	32.7336	-117.1897	San Diego, CA
Dallas/Fort Worth International (DFW)	32.8969	-97.0381	Dallas/Fort Worth, TX
Seattle–Tacoma International (SEA)	47.4489	-122.3094	Seattle, WA

**Table 6** International Airports Used in Analysis

Airport Name (IATA Code)	Lat. (deg)	Lon. (deg)	Major City Served
Wiley Post–Will Rogers Memorial (BRW)	71.2848889	-156.7685833	Barrow, Alaska
Honolulu International (HNL)	21.318681	-157.9224287	Honolulu, Hawaii
London Heathrow (LHR)	51.4775	-0.4614	London, England
Narita International (NRT)	35.7647	140.3864	Tokyo, Japan
Ministro Pistarini International (EZE)	-34.8222	-58.5358	Buenos Aires, Argentina

Airport Name (IATA Code)	Lat. (deg)	Lon. (deg)	Major City Served
Oliver Reginald Tambo International (JNB)	-26.1392	28.246	Johannesburg, South Africa
Sydney (SYD)	-33.946111	151.177222	Sydney, Australia

Because the ellipsoidal earth model is symmetric with respect to the equator, the signs of all the above airport latitudes can be reversed without changing any computed airport-pair distance. Also, all airport longitudes can be adjusted by adding the same arbitrary value to them without changing any airport-pair computed distance. Thus the spherical-earth characterizations presented below are more widely applicable than it might initially appear.

### 6.2 Spherical Earth Model Azimuth Error

For 14 airports, there are  $(14 \times 13) / 2 = 91$  interconnecting paths. Each path has a beginning and ending azimuth angle, resulting in a total of 182 angles to be considered. Statistical characterizations of the difference between the ellipsoidal- and spherical-model predictions for these azimuth angles are shown below, in Table 7 and Figure 22. For 177 angles (97.3%), the difference in computed angles for the two models is less than 0.25 deg. For three angles (1.7%), the difference is between 0.25 and 0.5 deg. For the path between HNL and JNB, the difference in the beginning and computed azimuth angles (1.1%) is between 1.5 and 2.0 deg. This path, which is long and crosses the equator at a shallow angle, appears to be a near worst-case for the spherical earth model in terms of predicting azimuth angles.

**Table 7** Absolute Value of Difference in Calculated Airport-Airport Path Azimuth Angles for Spherical and Ellipsoidal Earth Models

Airport Pair Characterization	No. of Angles	Angle Dif. (deg)	
		Ave	Max
CONUS-CONUS	42	0.070	0.118
CONUS-International	98	0.099	0.339
International-International	42	0.162	1.873
<b>All Combinations</b>	<b>182</b>	<b>0.101</b>	<b>1.873</b>

### 6.3 Methodology for Determining Spherical Earth Model Distance Error

The primary accuracy metric used herein is the relative difference in the calculated lengths for the shortest path connecting two airports using ellipsoidal and spherical earth models.

$$RelDif = \frac{\theta_{sph} R_{eff} - \rho_{Vin}}{\rho_{Vin}} \tag{Eq 131}$$

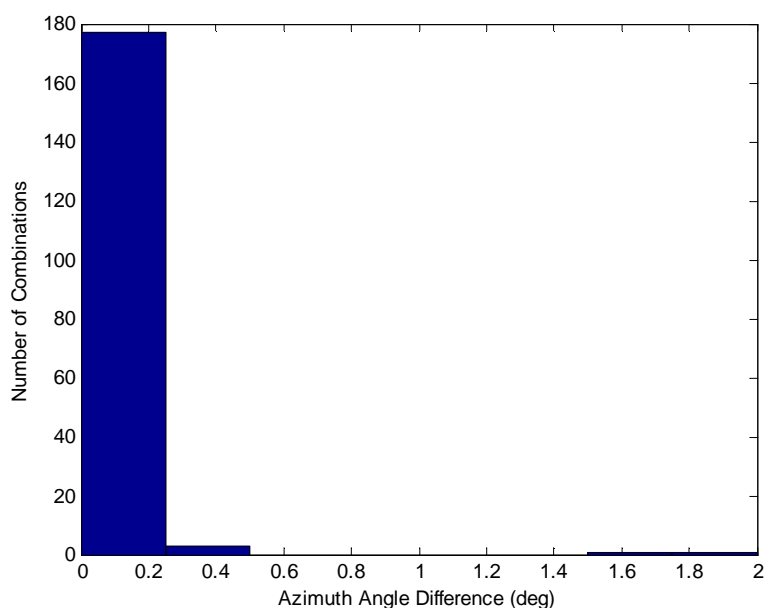


**Figure 22** Histogram of Differences in Airport-Airport Azimuth Angles between Spherical and Ellipsoidal Earth Models

In Eq 131,

$\rho_{vin}$  = Distance along an geodesic arc connecting the latitudes/longitudes of two airports on an ellipsoid, calculated using Vincenty’s algorithm

$\theta_{sph}$  = Spherical earth geocentric angle encompassing the radials to the same airport latitudes/longitudes

$R_{eff}$  = Effective RoC of the earth.

Tailoring  $R_{eff}$  to a specific path or application will be most accurate for (1) paths along a meridian, and (2) “short” paths. Paths along a meridian have (a) the same ground tracks for the ellipsoidal and spherical earth models, and (b) the same great circle angles (latitude differences) for the ellipsoidal spherical earth models. Thus, along a meridian, by tailoring the effective RoC based on the latitude of the path, the spherical earth model can be used to determine an ellipsoidal path length to any degree of accuracy.

The accuracy of the spherical earth model for estimating the lengths of “short” paths is based on the fact that  $R_{ns}$  and  $R_{ew}$  do not change rapidly with latitude (Figure 5), so a single value for  $R_{eff}$  can be quite accurate. The next two sections quantify a “short” path for various methods of determining  $R_{eff}$ .

Tailoring  $R_{eff}$  to a specific path or application will be least accurate for paths that are primarily east-west in orientation and “long”. For such routes, the ground tracks for the two earth models are different. For example, for a route between two airports at the same latitude, the spherical earth model will predict a path that passes further from the nearer pole than will the ellipsoidal

earth model. Thus a strategy based on tailoring  $R_{eff}$  to a spherical-earth ground track generally will not converge to the ellipsoidal/geodesic path length between the airports. However, it can provide improvement over a single, global value for the effective RoC.

### 6.4 Distance Errors for Three Methods of Computing the Effective RoC

Calculations are made using three methods for determining the effective RoC to be used with a spherical earth model determination of the geocentric angle between two locations.

$R_{eff,0}$  = Global radius of curvature, independent of the airport end points involved, found using the arithmetic mean of the ellipsoids three semi-axes (Eq 21)

$R_{eff,1}$  = Radius of curvature corresponding to the latitude and azimuth of the mid-point of the great circle joining the starting and end points involved, found using Eq 18 and Eq 19

$R_{eff,3,NN}$  = Effective RoC, computed as the weighted sum of the RoCs corresponding to the latitudes and azimuths of the starting point (denoted by U), mid-point (denoted by M) and end point (denoted by S) of the great circle joining U and S. A nearest neighbor (NN) weighting method is used — each point along the path is assigned the RoC of the nearest computed RoC

$$R_{eff,3,NN} = 0.25R_{e,U} + 0.5R_{e,M} + 0.25R_{e,S} \tag{Eq 132}$$

Statistics for the relative differences in calculated distances between pairs of the airports listed in Table 5 and Table 6 are shown in Table 8 below. For the global radius of curvature, the accuracy is in the range 0.17% (average) to 0.43% (maximum), that are consistent with the assumption that the spherical earth approximation’s accuracy is comparable to the earth’s flattening, 0.3%.

**Table 8** Absolute Value of Relative Difference in Calculated Distances (Percent) for Spherical-Earth Model and Three Methods of Determining the Effective RoC

Airport Pair Characterization	Number of Pairs	$R_{eff,0}$		$R_{eff,1}$		$R_{eff,3,NN}$	
		Ave	Max	Ave	Max	Ave	Max
CONUS-CONUS	21	0.176	0.271	0.005	0.018	0.003	0.009
CONUS-International	49	0.171	0.406	0.085	0.186	0.029	0.066
International-International	21	0.165	0.433	0.106	0.212	0.033	0.069
<b>All Combinations</b>	<b>91</b>	<b>0.171</b>	<b>0.433</b>	<b>0.071</b>	<b>0.212</b>	<b>0.024</b>	<b>0.069</b>

In Table 8, there is a significant progressive decrease in the relative distance error as the number of points used to compute the effective RoC is increased. When only the mid-point of the path is used to compute the effective RoC, the overall average relative error in the length of the paths between airports and the maximum relative error are both reduced by approximately a factor of two from their values for the global radius of curvature. When the effective radius of curvature is based on the two end points and the midpoint of the path, with nearest-neighbor weighting, the

overall average and maximum relative errors are both reduced by a further factor of three, to less than 0.03% and 0.07% respectively.

In Table 8, the primary distinction among the three airport groups is that the relative path length errors are significantly smaller for the CONUS-CONUS routes when at least one path point is used to estimate the effective RoC. For the same number of computed RoC values, the CONUS-International and International-International routes have comparable errors.

The scatter plot immediately below (Figure 23) depicts the error in calculated airport-airport path lengths using a spherical-earth model, when three points with NN weighting are used to determine the effective RoC. For path lengths less than 2,300 NM, which includes all CONUS-CONUS paths, the error is always less than 0.2 NM (or 0.009%). For paths lengths between approximately 2,000 NM and 6,000 NM, the length error increases monotonically, reaching a maximum of approximately 4.5 NM (0.08%). For path lengths greater than approximately 6,000 NM, the errors become unstructured but do not increase.

Table 9 below lists the paths having the ten greatest errors in calculated length when the spherical earth approximation is used with three points and NN weights used for determining the effective RoC. The two paths having the largest error in calculated distance EZE-SYD and HNL-LHR are depicted in Figure 24 below (Ref. 22). All ten paths are longer than 5,800 NM; consequently, they generally involve passage close to a pole or have large longitude changes.

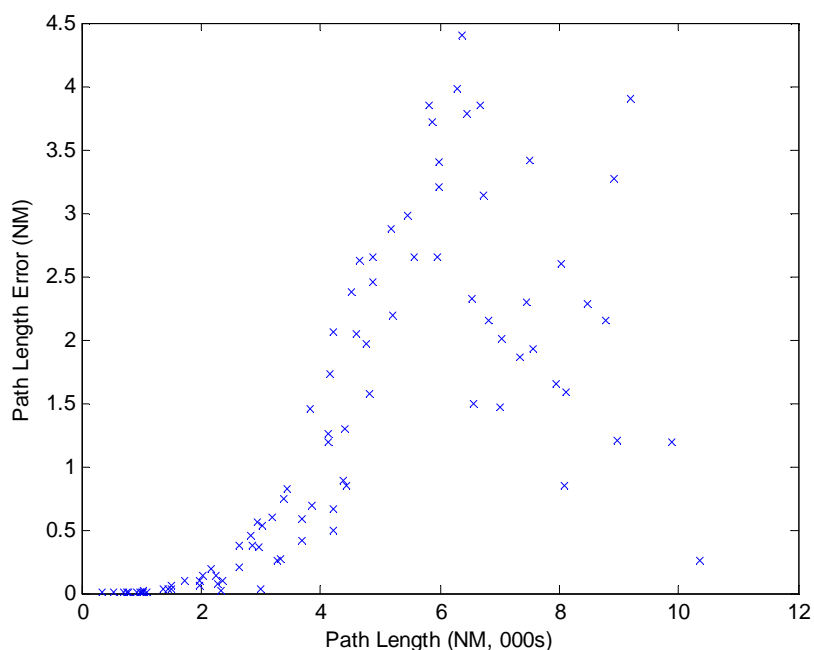


**Figure 23** Path Length Errors for Spherical-Earth Model vs. Actual Path Lengths, for Three-Point NN Determination of Effective RoC

**Table 9** Ten Airport Pairs Having the Largest Error in Calculated Path Length, for a Spherical-Earth Model and Three-Point NN Determination of the Effective RoC

Airport 1	Airport 2	Length (NM)	Error (NM)	Error (%)
EZE	SYD	6,366	4.41	0.069
HNL	LHR	6,289	3.98	0.063
LHR	SYD	9,188	3.90	0.042
BRW	SYD	6,675	3.85	0.058
BOS	NRT	5,823	3.84	0.066
MIA	NRT	6,462	3.78	0.059
DCA	NRT	5,883	3.72	0.063
BRW	EZE	7,515	3.42	0.046
LHR	EZE	5,999	3.40	0.057
SEA	JNB	8,919	3.27	0.037
<b>Average</b>		<b>6,912</b>	<b>3.76</b>	<b>0.056</b>

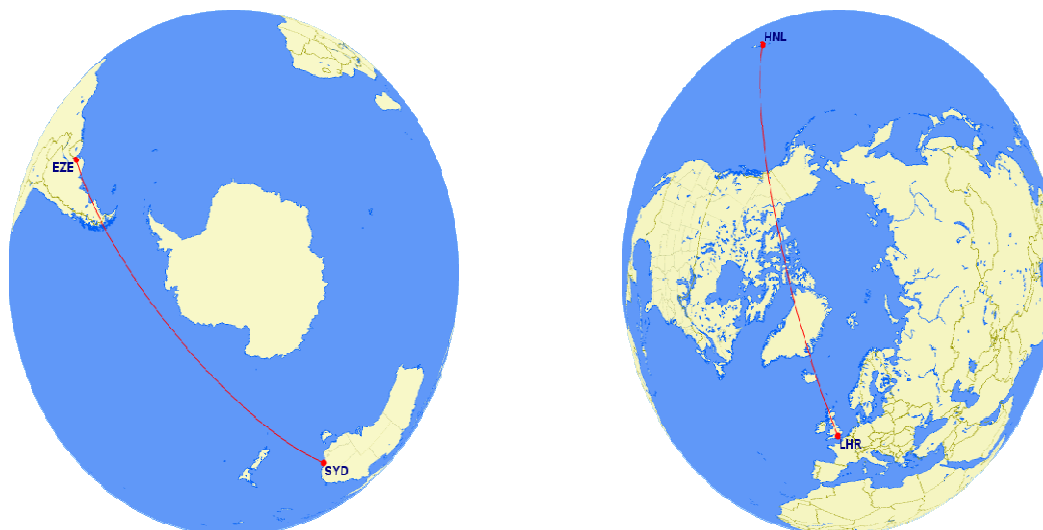


**Figure 24** Airport-Airport Great-Circle Paths Having the Largest Errors in Calculated Lengths, for a Spherical-Earth Model and Three-Point NN Determination of the Effective RoC

### 6.5 Improving the Effective RoC by a 3-Point Parabolic Fit

Spherical-earth effective RoCs using values calculated at the path’s beginning, middle and end points, with nearest-neighbor weights, are satisfactory for many applications. However, there is always interest in improving accuracy. One obvious approach to improving estimation accuracy, discussed subsequently, is to increase the number of points where the RoC is computed.

An alternative, computationally cheaper, approach is to adjust the weights for the three calculated RoCs. The alternative employed here is to fit a parabola to the three computed RoC values, then use the parabola’s average value over the path as the effective RoC. This approach thus employs

an interpolating curve that better matches the behavior of the actual RoC over a path, which is continuous and has a continuous derivative. The resulting alternative to Eq 132 is

$$R_{eff,3,PF} = (1/6)R_{e,U} + (2/3)R_{e,M} + (1/6)R_{e,S} \tag{Eq 133}$$

This method is equivalent to Simpson’s (earlier, Kepler’s) rule for numerical integration.

For the same set of 91 airport-airport paths, Table 10 below contrasts the results for parabolic-fit (PF) weights to the results for NN weights. For CONUS-CONUS paths, there is little difference. For the longer paths involving International airports, the PF weights reduce the path-length error to approximately half the value for the NN weights. For PF weights, the overall average path length error is less than 0.01%, and the maximum error is less than 0.05%.

**Table 10** Percentage Error in Calculated Airport-Airport Path Lengths, for Spherical-Earth Model and Two Methods of Weighting Three Computed RoCs

Airport Pair Characterization	Number of Pairs	$R_{eff,3,NN}$		$R_{eff,3,PF}$	
		Ave	Max	Ave	Max
CONUS-CONUS	21	0.003	0.009	0.003	0.006
CONUS-International	49	0.029	0.066	0.010	0.036
International-International	21	0.033	0.069	0.014	0.044
<b>All Combinations</b>	<b>91</b>	<b>0.024</b>	<b>0.069</b>	<b>0.009</b>	<b>0.044</b>

Figure 25 below is a scatter plot of the path length error versus latitude change experienced over a path for the PF weights. Use of the PF weights reduces path-length errors significantly for paths with a latitude change of less than 40 deg. Moreover, for latitude changes of more than 40 deg, the errors appear to be better structured than those in Figure 23, indicating that the calculation technique is better aligned with the underlying physics.

Table 11 below lists the paths having the ten largest errors in calculated length when the spherical earth approximation is used with three points and PF weights for determining the effective RoC. When contrasted with Table 9 (which has the same information for the NN weights), the paths in Table 11 are longer (averages: 8,397 NM vs. 6,912 NM) and have smaller errors (averages: 2.56 NM vs. 3.76 NM).

The first nine of the ten paths listed in Table 11 cross the equator, generally at a shallow angle — i.e., the paths are primarily east-west in orientation. Figure 26 (Ref. 22) below illustrates the path with the largest error, NRT-EZE. The tenth path listed, EZE-SYD, is the one exception; it happens to be the path with the largest error for NN-weighting of the three calculated RoCs, and is shown in Figure 24.

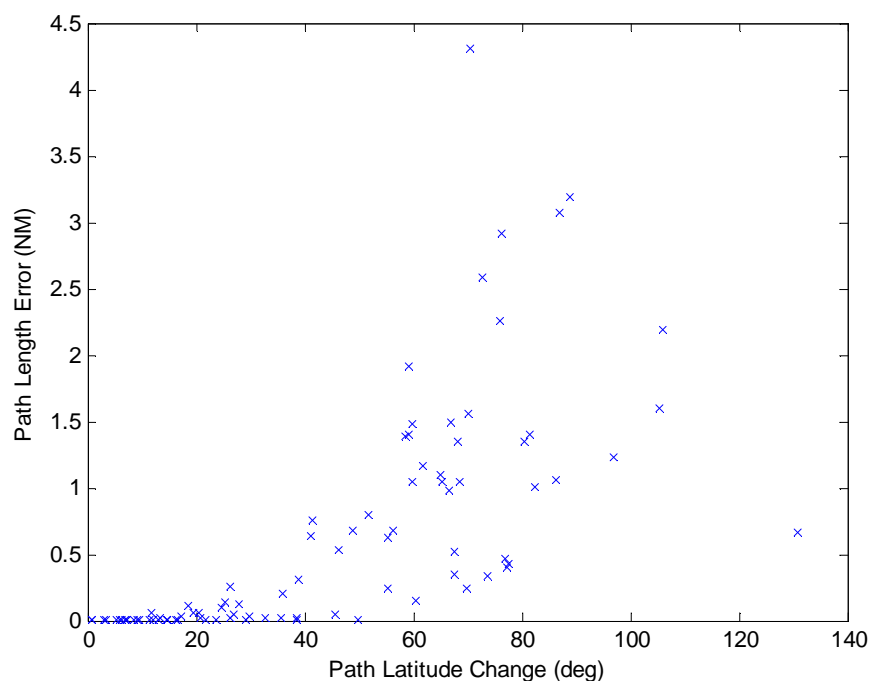


**Figure 25** Airport-Airport Calculated Path Length Error for Spherical-Earth Model vs. Latitude Change over the Path, for Three-Point PF Determination of the Effective RoC

**Table 11** Ten Airport Pairs Having the Largest Error in Calculated Path Length, for a Spherical-Earth Model and Three-Point PF Determination of the Effective RoC

Airport #1	Airport #2	Length (NM)	Error (NM)	Error (%)
NRT	EZE	9,884	4.31	0.043
SEA	JNB	8,919	3.19	0.036
HNL	JNB	10,364	3.07	0.030
BOS	SYD	8,774	2.92	0.033
DCA	SYD	8,485	2.59	0.031
ORD	SYD	8,022	2.25	0.028
BRW	EZE	7,515	2.19	0.029
SAN	JNB	8,969	1.92	0.021
BRW	SYD	6,675	1.60	0.024
EZE	SYD	6,366	1.56	0.025
<b>Average</b>		<b>8,397</b>	<b>2.56</b>	<b>0.030</b>

As observed earlier, tailoring of the effective RoC to a path is least effective for long paths having a primarily east-west orientation. The results in Table 11 are consistent with that observation, and suggest that determining the RoC at the start, mid-point and end of a path, combined with using PF weights to calculate the effective RoC, may be approaching the limit on path-length accuracy that can be achieved using a spherical earth model.

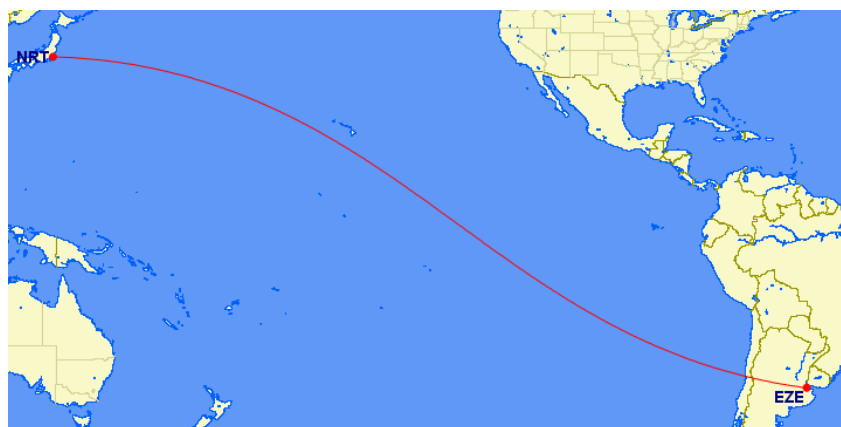


**Figure 26** Great-Circle Path Having the Largest Error in Calculated Length, for a Spherical-Earth Model and Three-Point PF Determination of the Effective RoC

## 6.6 Experiments in Further Improving Path Length Accuracy

Several hypotheses were explored with the intent that they might lead to further improvements in path length determination accuracy based on a spherical earth model and a tailored effective RoC:

- Isolating trans-equatorial paths having (a) both airports at least 15 deg from the equator, and (b) the airport longitude difference at least twice as large as their latitude difference; then using the nearest neighbor algorithm
- Utilizing five points to calculate the RoC and fitting a cubic spline to these points
- Utilizing nine points to calculate the RoC and fitting a cubic spline to these points

In exploring the first hypothesis, seven airport-pairs were found to satisfy the criteria and the associated error statistics were computed. The overall 91-path average error was slightly reduced, from 0.009% to 0.008%. The reduction in the maximum fractional error was a bit more, from 0.044% to 0.037%. The most dramatic change was in the path having the largest length error, which was reduced by more than one nautical mile, from 4.31 NM to 3.28 NM. However, the overall effect was not comparable to the change observed previously when transitioning from one to three computed RoC values or from NN to PF weighting of three computed RoC values.

Figure 27 below is a scatter plot of the path length error for three methods of determining the effective RoC: (1) parabolic fit to three calculated RoC values (blue “x”), (2) cubic spline fit to five calculated RoC values (green “o”), and (3) cubic spline fit to nine calculated RoC values (red “+”). There are quantitative variations, but qualitatively, the three-point parabolic fit is at least as accurate as the two other methods for longer paths. This figure tends to confirm the observation (at the end of Section 6.5) that determining the RoC at the start, mid-point and end of a path, combined with using PF weights to calculate the effective RoC, appears to be approaching the limit on path-length accuracy that can be achieved using a spherical earth model.

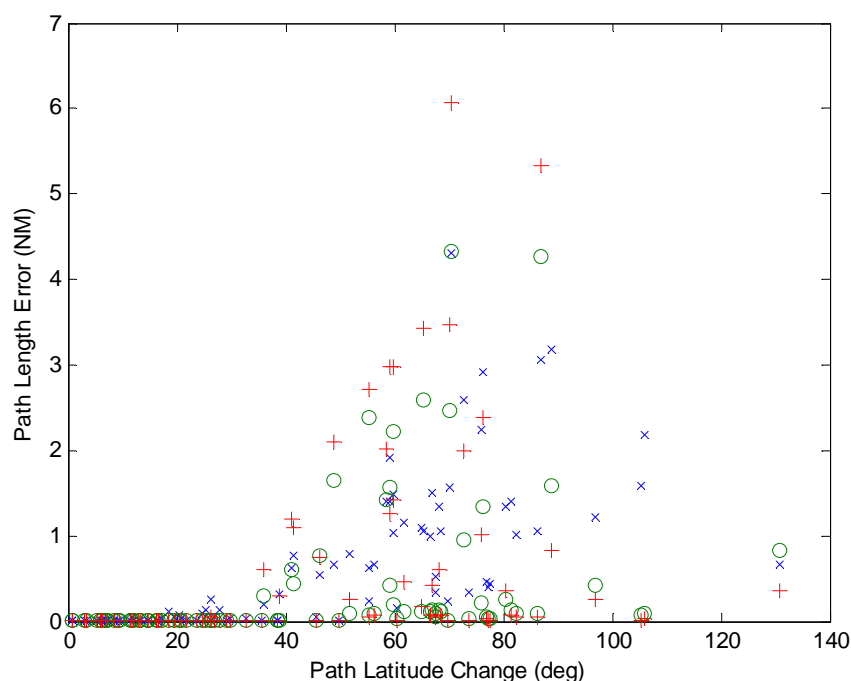


**Figure 27** Airport-Airport Calculated Path Length Errors for Spherical-Earth Model vs. Latitude Change over the Path, for Three Methods of Determining the Effective RoC

To elaborate further, the following two tables illustrate the error characteristics for a spherical earth model for five north-south and five east-west routes, respectively. In Table 12, for north-south routes, the path azimuth angle is essentially constant, as the change in direction is less than 10 deg for all five paths. More pertinently, the relative path length determination error decreases monotonically to a few parts per million as more calculated RoC values are utilized.

**Table 12** Error Statistics for Five Airport Pairs Having Predominately North-South Paths for Spherical-Earth Model and Three Methods of Determining the Effective RoC

Airport #1	Airport #2	Dist (NM)	Mid Az (deg)	Az Chg (deg)	Error 3pt (%)	Error 5pt (%)	Error 9pt (%)
BOS	EZE	4,666	172.3	1.1	0.0085	0.0005	0.0001
DCA	EZE	4,523	167.9	0.8	0.0076	0.0006	0.0003
BRW	HNL	2,999	-179.3	0.9	0.0000	0.0000	0.0000
LHR	JNB	4,884	163.8	8.2	0.0089	0.0008	0.0004
NRT	SYD	4,211	172.3	0.2	0.0058	0.0004	0.0001
<b>Average</b>		<b>4,257</b>	—	—	<b>0.0062</b>	<b>0.0005</b>	<b>0.0002</b>

In contrast, in Table 13 for east-west routes, the paths fall into two subcategories — those with both airports on both sides of the equator (BOS-NRT, EZE-SYD and JNB-SYD) and those with airports on opposites sides of the equator (MIA-SYD and NRT-EZE). The former have large (on the order of 100 deg) changes in the path azimuth angle, as the paths “bow” towards the nearer pole; the latter have small changes in azimuth angle.. More pertinently, for these five paths, the

relative path length determination error does not decrease (and in fact increases) as more calculated RoC values are utilized.

**Table 13** Error Statistics for Five Airport Pairs Having Predominately East-West Paths for Spherical-Earth Model and Three Methods of Determining the Effective RoC

Airport #1	Airport #2	Dist (NM)	Mid Az (deg)	Az Chg (deg)	Error 3pt (%)	Error 5pt (%)	Error 9pt (%)
BOS	NRT	5,823	-100.8	132.0	0.0180	0.0443	0.0589
MIA	SYD	8,113	-123.0	19.3	0.0182	0.0023	0.0176
NRT	EZE	9,884	125.7	6.9	0.0436	0.0437	0.0615
EZE	SYD	6,366	-88.7	129.7	0.0245	0.0386	0.0544
JNB	SYD	5,963	97.0	85.4	0.0127	0.0075	0.0183
<b>Average</b>		<b>7,230</b>	<b>—</b>	<b>—</b>	<b>0.0234</b>	<b>0.0273</b>	<b>0.0421</b>

## 7. REFERENCES

1. Order 8260.3B: Change 25; *United States Standard for Terminal Instrument Procedures (TERPS)*; FAA Flight Standards Service; March 9, 2012.
2. Order 8260.58: *United States Standard for Performance Based Navigation (PBN) Instrument Procedure Design*; FAA Flight Standards Service; September 21, 2012.
3. [http://en.wikipedia.org/wiki/Inverse\\_trigonometric\\_functions](http://en.wikipedia.org/wiki/Inverse_trigonometric_functions)
4. Christopher Jekeli; *Geometric Reference Systems in Geodesy*; Ohio State University; July 2006.
5. Thaddeus Vincenty: "Direct and Inverse Solutions of Geodesics on the Ellipsoids with Applications of Nested Equations", *Survey Review*; XXIII, Number 176; April 1975.
6. C. M. Thomas and W. E. Featherstone: "Validation of Vincenty's Formulas for the Geodesic Using a New Fourth-Order Extension of Kivioja's Formula"; *Journal of Surveying Engineering*, American Society of Civil Engineers; February 2005.
7. [http://en.wikipedia.org/wiki/Non-line-of-sight\\_propagation](http://en.wikipedia.org/wiki/Non-line-of-sight_propagation), retrieved Sept. 1, 2013.
8. <http://www.radartutorial.eu/18.explanations/ex47.en.html>
9. [http://en.wikipedia.org/wiki/History\\_of\\_trigonometry](http://en.wikipedia.org/wiki/History_of_trigonometry)
10. [http://en.wikipedia.org/wiki/Mathematics\\_in\\_medieval\\_Islam](http://en.wikipedia.org/wiki/Mathematics_in_medieval_Islam)
11. I. Todhunter; *Spherical Trigonometry*; MacMillan; 5<sup>th</sup> edition, 1886.
12. W.M. Smart and R.M. Green: *Spherical Astronomy*; Cambridge University Press; Sixth Edition, 1977.
13. [http://en.wikipedia.org/wiki/Spherical\\_trigonometry](http://en.wikipedia.org/wiki/Spherical_trigonometry)
14. <http://mathworld.wolfram.com/SphericalTrigonometry.html>
15. <http://williams.best.vwh.net/avform.htm>
16. <http://www.krysstal.com/sphertrig.html>
17. [http://en.wikipedia.org/wiki/File:Spherical\\_trigonometry\\_triangle\\_cases.svg](http://en.wikipedia.org/wiki/File:Spherical_trigonometry_triangle_cases.svg)
18. <http://en.wikipedia.org/wiki/Versine>
19. <http://www.airnav.com/airport/KMCI>
20. <http://www.nstb.tc.faa.gov/index.htm>
21. <http://www3.sympatico.ca/craymer/geodesy/gps.html#matlab>
22. <http://www.gcmap.com>